



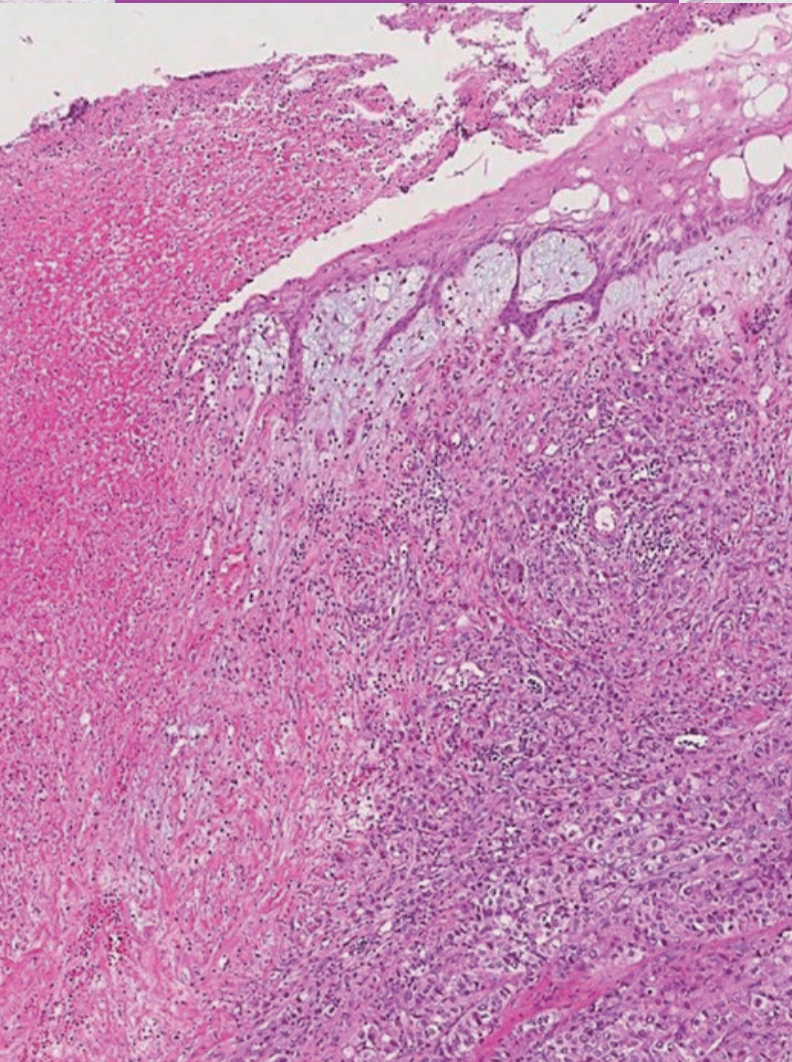
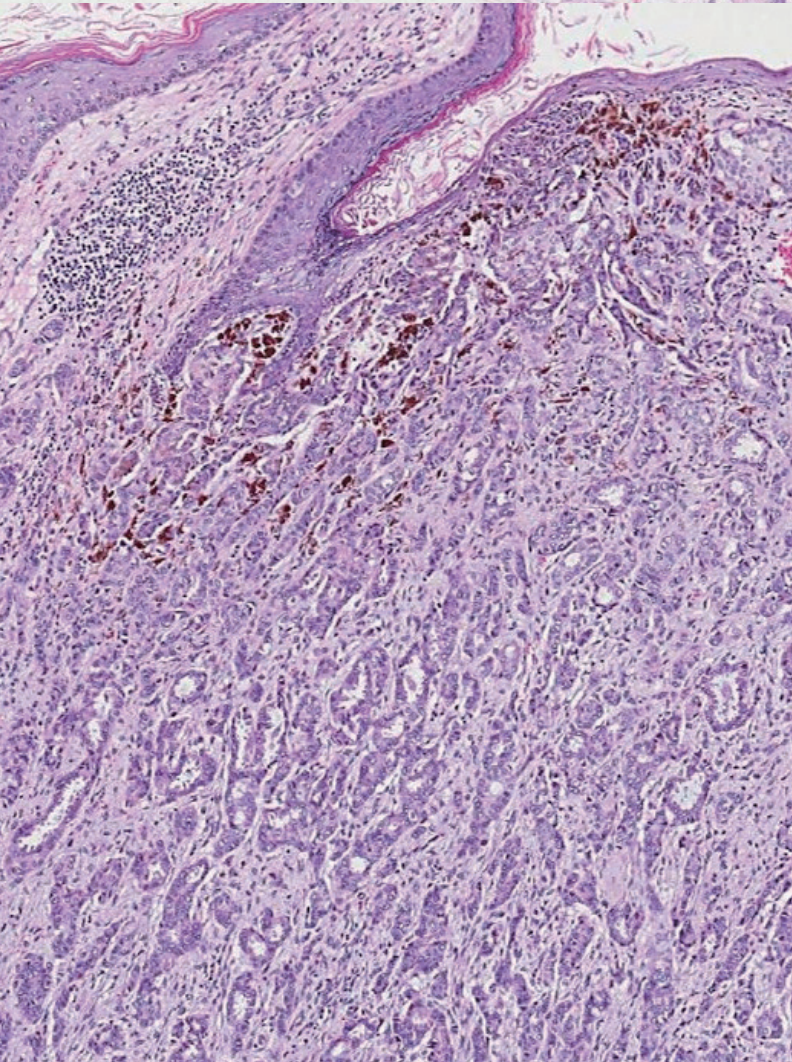
# JPTM

Journal of **P**athology  
and **T**ranslational **M**edicine

January 2021  
Vol. 55 / No.1  
jpatholtm.org  
pISSN: 2383-7837  
eISSN: 2383-7845



*Standardized Pathology*  
*Report for Breast Cancer*





## Aims & Scope

The *Journal of Pathology and Translational Medicine* is an open venue for the rapid publication of major achievements in various fields of pathology, cytopathology, and biomedical and translational research. The Journal aims to share new insights into the molecular and cellular mechanisms of human diseases and to report major advances in both experimental and clinical medicine, with a particular emphasis on translational research. The investigations of human cells and tissues using high-dimensional biology techniques such as genomics and proteomics will be given a high priority. Articles on stem cell biology are also welcome. The categories of manuscript include original articles, review and perspective articles, case studies, brief case reports, and letters to the editor.

## Subscription Information

To subscribe to this journal, please contact the Korean Society of Pathologists/the Korean Society for Cytopathology. Full text PDF files are also available at the official website (<https://jpathol.tml.org>). *Journal of Pathology and Translational Medicine* is indexed by Emerging Sources Citation Index (ESCI), PubMed, PubMed Central, Scopus, KoreaMed, KoMCI, WPRIM, Directory of Open Access Journals (DOAJ), and CrossRef. Circulation number per issue is 50.

## Editors-in-Chief

Jung, Chan Kwon, MD (*The Catholic University of Korea, Korea*) <https://orcid.org/0000-0001-6843-3708>  
Park, So Yeon, MD (*Seoul National University, Korea*) <https://orcid.org/0000-0002-0299-7268>

## Senior Editors

Hong, Soon Won, MD (*Yonsei University, Korea*) <https://orcid.org/0000-0002-0324-2414>  
Kim, Chong Jai, MD (*University of Ulsan, Korea*) <https://orcid.org/0000-0002-2844-9446>

## Associate Editors

Shin, Eunah, MD (*Yongin Severance Hospital, Yonsei University, Korea*) <https://orcid.org/0000-0001-5961-3563>  
Kim, Haeryoung, MD (*Seoul National University, Korea*) <https://orcid.org/0000-0002-4205-9081>

## Editorial Board

Avila-Casado, Maria del Carmen, MD (*University of Toronto, Toronto General Hospital UHN, Canada*)

Bae, Young Kyung, MD (*Yeungnam University, Korea*)

Bongiovanni, Massimo, MD (*Lausanne University Hospital, Switzerland*)

Bychkov, Andrey, MD (*Chulalongkorn University, Thailand Kameda Medical Center, Japan Nagasaki University Hospital, Japan*)

Choi, Yeong-Jin, MD (*The Catholic University of Korea, Korea*)

Chong, Yo Sep, MD (*The Catholic University of Korea, Korea*)

Chung, Jin-Haeng, MD (*Seoul National University, Korea*)

Fadda, Guido, MD (*Catholic University of Rome-Foundation Agostino Gemelli University Hospital, Italy*)

Gong, Gyungyub, MD (*University of Ulsan, Korea*)

Ha, Seung Yeon, MD (*Gachon University, Korea*)

Han, Jee Young, MD (*Inha University, Korea*)

Jain, Deepali, MD (*All India Institute of Medical Sciences, India*)

Jang, Se Jin, MD (*University of Ulsan, Korea*)

Jeong, Jin Sook, MD (*Dong-A University, Korea*)

Jun, Sun-Young, MD (*The Catholic University of Korea, Korea*)

Kang, Gyeong Hoon, MD (*Seoul National University, Korea*)

Kim, Aeree, MD (*Korea University, Korea*)

Kim, Jang-Hee, MD (*Ajou University, Korea*)

Kim, Jung Ho, MD (*Seoul National University, Korea*)

Kim, Kyu Rae, MD (*University of Ulsan, Korea*)

Kim, Se Hoon, MD (*Yonsei University, Korea*)

Kim, Woo Ho, MD (*Seoul National University, Korea*)

Ko, Young Hye, MD (*Sungkyunkwan University, Korea*)

Koo, Ja Seung, MD (*Yonsei University, Korea*)

Lai, Chiung-Ru, MD (*Taipei Veterans General Hospital, Taiwan*)

Lee, C. Soon, MD (*University of Western Sydney, Australia*)

Lee, Hye Seung, MD (*Seoul National University, Korea*)

Liu, Zhiyan, MD (*Shandong University, China*)

Lkhagvadorj, Sayamaa, MD (*Mongolian National University of Medical Sciences, Mongolia*)

Moon, Woo Sung, MD (*Jeonbuk University, Korea*)

Paik, Jin Ho, MD (*Seoul National University, Korea*)

Park, Chan-Sik, MD (*University of Ulsan, Korea*)

Park, Young Nyun, MD (*Yonsei University, Korea*)

Shahid, Pervez, MD (*Aga Khan University, Pakistan*)

Song, Joon Seon, MD (*University of Ulsan, Korea*)

Sung, Chang Ohk, MD (*University of Ulsan, Korea*)

Tan, Puay Hoon, MD (*National University of Singapore, Singapore*)

Than, Nandor Gabor, MD (*Semmelweis University, Hungary*)

Tse, Gary M., MD (*The Chinese University of Hong Kong, Hong Kong*)

Yatabe, Yasushi, MD (*Aichi Cancer Center, Japan*)

Yoon, Sun Och, MD (*Yonsei University, Korea*)

Zhu, Yun, MD (*Jiangsu Institution of Nuclear Medicine, China*)

## Consulting Editors

Huh, Sun, MD (*Hallym University, Korea*)

Kakudo, Kennichi, MD (*Kindai University, Japan*)

Ro, Jae Y., MD (*Cornell University, The Methodist Hospital, U.S.A.*)

## Ethic Editor

Choi, In-Hong, MD (*Yonsei University, Korea*)

## Statistics Editors

Kim, Dong Wook (*National Health Insurance Service Ilsan Hospital, Korea*)

Lee, Hye Sun (*Yonsei University, Korea*)

## Manuscript Editor

Chang, Soo-Hee (*InfoLumi Co., Korea*)

## Layout Editor

Kim, Haeja (*iMiS Company Co., Ltd., Korea*)

## Website and JATS XML File Producers

Cho, Yoonsang (*M2Community Co., Korea*)

Im, Jeonghee (*M2Community Co., Korea*)

## Administrative Assistants

Jung, Ji Young (*The Korean Society of Pathologists*)

Jeon, Annmi (*The Korean Society for Cytopathology*)

## Contact the Korean Society of Pathologists/the Korean Society for Cytopathology

**Publishers:** Cho, Nam Hoon, MD, Gong, Gyungyub, MD

**Editors-in-Chief:** Jung, Chan Kwon, MD, Park, So Yeon, MD

**Published by the Korean Society of Pathologists/the Korean Society for Cytopathology**

## Editorial Office

Room 1209 Gwanghwamun Officia, 92 Saemunan-ro, Jongno-gu, Seoul 03186, Korea

Tel: +82-2-795-3094 Fax: +82-2-790-6635 E-mail: [office@jpathol.tml.org](mailto:office@jpathol.tml.org)

#1508 Renaissancetower, 14 Mallijae-ro, Mapo-gu, Seoul 04195, Korea

Tel: +82-2-593-6943 Fax: +82-2-593-6944 E-mail: [office@jpathol.tml.org](mailto:office@jpathol.tml.org)

## Printed by iMiS Company Co., Ltd. (JMC)

Jungang Bldg. 18-8 Wonhyo-ro 89-gil, Yongsan-gu, Seoul 04314, Korea

Tel: +82-2-717-5511 Fax: +82-2-717-5515 E-mail: [ml@smileml.com](mailto:ml@smileml.com)

## Manuscript Editing by InfoLumi Co.

210-202, 421 Pangyo-ro, Bundang-gu, Seongnam 13522, Korea

Tel: +82-70-8839-8800 E-mail: [infolumi.chang@gmail.com](mailto:infolumi.chang@gmail.com)

Front cover image: Extensive intraductal component and skin involvement in invasive breast carcinoma (p6, p7).

© Copyright 2021 by the Korean Society of Pathologists/the Korean Society for Cytopathology

© Journal of Pathology and Translational Medicine is an Open Access journal under the terms of the Creative Commons Attribution Non-Commercial License (<https://creativecommons.org/licenses/by-nc/4.0>).

© This paper meets the requirements of KS X ISO 9706, ISO 9706-1994 and ANSI/NISO Z.39.48-1992 (Permanence of Paper).



## CONTENTS

---

### REVIEWS

- 1     **Standardized pathology report for breast cancer**  
Soo Youn Cho, So Yeon Park, Young Kyung Bae, Jee Yeon Kim, Eun Kyung Kim, Woo Gyeong Kim, Youngmee Kwon, Ahwon Lee, Hee Jin Lee, Ji Shin Lee, Jee Young Park, Gyungyub Gong, Hye Kyoung Yoon
- 16    **Imaging features of breast cancer molecular subtypes: state of the art**  
Nariya Cho
- 26    **DNA-protein biomarkers for immunotherapy in the era of precision oncology**  
Binnari Kim, So Young Kang, Kyoung-Mee Kim

### ORIGINAL ARTICLES

- 33     **Automated immunohistochemical assessment ability to evaluate estrogen and progesterone receptor status compared with quantitative reverse transcription-polymerase chain reaction in breast carcinoma patients**  
Taesung Jeon, Aeree Kim, Chungyeul Kim
- 43     **Interobserver diagnostic reproducibility in advanced-stage endometrial carcinoma**  
Ho Jin Jung, Soo Yeon Lee, Jin Hwa Hong, Yi Kyeong Chun
- 53     **A comparative prognostic performance of definitions of Crohn-like lymphoid reaction in colorectal carcinoma**  
Younghoon Kim, Jeong Mo Bae, Jung Ho Kim, Nam-Yun Cho, Gyeong Hoon Kang
- 60     **Causes of necrotic features in fine-needle aspirates from cervical lymph nodes**  
Young Jin Seo, Hyeongchan Shin, Hye Won Lee, Hye Ra Jung

### CASE REPORTS

- 68     **A case of cribriform carcinoma of the skin: a newly described rare condition**  
Hyun Lee, Chong-Hyun Won, Chan-Sik Park



- 
- 75    Fibrocartilaginous mesenchymoma with an unusual location in the rib

Sun-Ju Oh

- 79    *EGFR*-mutated pulmonary adenocarcinoma with concurrent *PIK3CA* mutation, and with acquired *RET* fusion and *EGFR* T790M mutation after afatinib therapy

Minhye Kim, Ji Min Na, Gyeong-Won Lee, Seung Jun Lee, Jong Duk Kim, Jung Wook Yang

**Instructions for Authors** for *Journal of Pathology and Translational Medicine* are available at <http://jpathol.tn.org/authors/authors.php>



## Standardized pathology report for breast cancer

Soo Youn Cho<sup>1</sup>, So Yeon Park<sup>2</sup>, Young Kyung Bae<sup>3</sup>, Jee Yeon Kim<sup>4</sup>, Eun Kyung Kim<sup>5</sup>, Woo Gyeong Kim<sup>6</sup>, Youngmee Kwon<sup>7</sup>, Ahwon Lee<sup>8</sup>, Hee Jin Lee<sup>9</sup>, Ji Shin Lee<sup>10</sup>, Jee Young Park<sup>11</sup>, Gyungyub Gong<sup>9</sup>, Hye Kyoung Yoon<sup>12</sup>

<sup>1</sup>Department of Pathology and Translational Genomics, Samsung Medical Center, Sungkyunkwan University School of Medicine, Seoul;

<sup>2</sup>Department of Pathology, Seoul National University Bundang Hospital, Seoul National University College of Medicine, Seongnam;

<sup>3</sup>Department of Pathology, Yeungnam University College of Medicine, Daegu;

<sup>4</sup>Department of Pathology, Pusan National University Yangsan Hospital, Pusan National University College of Medicine, Yangsan;

<sup>5</sup>Department of Pathology, Eulji University College of Medicine, Seoul;

<sup>6</sup>Department of Pathology, Inje University Haeundae Paik Hospital, Busan;

<sup>7</sup>Department of Pathology, National Cancer Center, Goyang;

<sup>8</sup>Department of Hospital Pathology, Seoul St. Mary's Hospital, College of Medicine, The Catholic University of Korea, Seoul;

<sup>9</sup>Department of Pathology, Asan Medical Center, University of Ulsan College of Medicine, Seoul;

<sup>10</sup>Department of Pathology, Chonnam National University Medical School, Gwangju;

<sup>11</sup>Department of Pathology, School of Medicine, Kyungpook National University, Kyungpook National University Chilgok Hospital, Daegu;

<sup>12</sup>Department of Pathology, Busan Paik Hospital, Inje University, Busan, Korea

Given the recent advances in management and understanding of breast cancer, a standardized pathology report reflecting these changes is critical. To meet this need, the Breast Pathology Study Group of the Korean Society of Pathologists has developed a standardized pathology reporting format for breast cancer, consisting of 'standard data elements,' 'conditional data elements,' and a biomarker report form. The 'standard data elements' consist of the basic pathologic features used for prognostication, while other factors related to prognosis or diagnosis are described in the 'conditional data elements.' In addition to standard data elements, all recommended issues are also presented. We expect that this standardized pathology report for breast cancer will improve diagnostic concordance and communication between pathologists and clinicians, as well as between pathologists inter-institutionally.

**Key Words:** Breast neoplasms; Diagnosis; Pathology report

**Received:** October 23, 2020 **Revised:** November 19, 2020 **Accepted:** November 20, 2020

**Corresponding Author:** Hye Kyoung Yoon, MD, PhD, Department of Pathology, Busan Paik Hospital, Inje University, 75 Bokji-ro, Busanjin-gu, Busan 47392, Korea  
Tel: +82-51-890-6628, Fax: +82-51-890-5825, E-mail: pathyoon@inje.ac.kr

This article has been published jointly, with consent, in both *Journal of Pathology and Translational Medicine* and *Journal of Breast Cancer*.

In Korea, the incidence of breast cancer has steadily increased partly due to an increase in screening mammography and to changes in lifestyle [1]. Breast cancer has become the most common cancer in women in Korea [1]. Thus, pathologists are encountering more breast cancer specimens in daily practice. Furthermore, as our understanding of breast cancer biology deepens and treatment strategies for breast cancer rapidly progress, including advances in neoadjuvant therapy, targeted therapy, and immunotherapy, the role of pathologists in evaluation of breast specimens is changing [2]. Therefore, it would be useful to provide pathologists with a standard reporting format for reference and recent updates in the field of breast cancer diagnosis.

A committee for standardization of breast cancer reporting

was formed in the Breast Pathology Study Group of the Korean Society of Pathologists. The 'Standardized Pathology Report for Breast Cancer' was developed after several committee meetings. The report form refers to the College of American Pathologists (CAP) Cancer Protocols [3], the American Joint Committee on Cancer (AJCC) 8th edition [4], and the World Health Organization (WHO) Classification of Breast Tumors, 5th edition [5], and was modified by the Breast Pathology Study Group of the Korean Society of Pathologists.

The purpose of this report form is to enable standardized pathologic diagnosis of breast cancer and to improve communication between clinicians and pathologists, as well as between pathologists inter-institutionally. The basic pathologic features



for prognostication are described in the “standard data elements” section, and other factors related to prognosis or diagnosis are described in the ‘conditional data elements’ section. Finally, descriptions on biomarkers essential for breast cancer diagnosis and treatment are included.

## STANDARD DATA ELEMENTS

All essential standard data elements for the report form are summarized in Table 1. In addition, all data elements including recommended issues as well as standard data elements can be found in Supplementary Table S1.

### Breast specimen types

Breast specimen types can be roughly divided into wide exci-

sion and total mastectomy. Wide excision is defined as removal of only part of the breast tissue, with or without axillary contents, and includes specimens designated as excisional biopsy, segmental or partial mastectomy, lumpectomy, or quadrantectomy. Total mastectomy refers to removal of all breast tissue, which may include skin, nipple, or areola, with or without axillary contents, and includes simple mastectomy (total mastectomy without axillary node removal), skin-sparing mastectomy (total mastectomy with removal of the nipple and a narrow surrounding rim of skin), nipple-sparing mastectomy (total mastectomy without removal of skin or nipple), modified radical mastectomy (total mastectomy with axillary node dissection and with occasional removal of a small portion of the pectoralis muscle), and radical mastectomy (total mastectomy with pectoralis muscle removal and axillary node dissection) [6].

**Table 1.** Standard data element

<b>Breast specimen type</b>	
<input type="checkbox"/>	Wide excision (specify)
<input type="checkbox"/>	Total mastectomy (specify)
<b>Specimen laterality</b>	
<input type="checkbox"/>	Right
<input type="checkbox"/>	Left
<input type="checkbox"/>	Unspecified
<b>Tumor location</b>	
<input type="checkbox"/>	UOQ
<input type="checkbox"/>	LOQ
<input type="checkbox"/>	UIQ
<input type="checkbox"/>	LIQ
<input type="checkbox"/>	Central
<input type="checkbox"/>	Unspecified
<b>Histologic type</b>	
<input type="checkbox"/>	Invasive breast carcinoma of no special type (specify for special morphological patterns)
<input type="checkbox"/>	Invasive lobular carcinoma (specify for subtype)
<input type="checkbox"/>	Tubular carcinoma
<input type="checkbox"/>	Cribriform carcinoma
<input type="checkbox"/>	Mucinous carcinoma
<input type="checkbox"/>	Invasive micropapillary carcinoma
<input type="checkbox"/>	Carcinoma with apocrine differentiation
<input type="checkbox"/>	Metaplastic carcinoma (specify for subtype)
<input type="checkbox"/>	Other rare subtype (specify)
<b>Tumor focality</b>	
<input type="checkbox"/>	Unifocal
<input type="checkbox"/>	Multifocal
<b>Tumor size</b>	
____ × ____ × ____ cm	
<b>Histologic grade</b>	
<input type="checkbox"/>	Grade I (Low)
<input type="checkbox"/>	Grade II (Intermediate)
<input type="checkbox"/>	Grade III (High)
<b>Ductal carcinoma in situ (DCIS)</b>	
<input type="checkbox"/>	Not identified
<input type="checkbox"/>	Present ( <input type="checkbox"/> EIC-positive, <input type="checkbox"/> EIC-negative)

(Continued to the next page)



Table 1. Continued

*Nuclear grade*

- ☐ Grade I (Low)  
☐ Grade II (Intermediate)  
☐ Grade III (High)

*Necrosis*

- ☐ Not identified  
☐ Present (☐ focal, ☐ central)

*Extent of DCIS (for EIC-positive case)*

Estimated size:        x        cm  
 No. of blocks with DCIS/No. of blocks examined:        /

**Lobular carcinoma in situ** (in case of invasive lobular carcinoma)

- ☐ Not identified  
☐ Present (☐ classic type, ☐ pleomorphic type)

**Tumor extension***Skin*

- ☐ Not present  
☐ Present (☐ uninvolved, ☐ involved, without skin ulceration/ with skin ulceration/with satellite skin nodule)

*Skeletal muscle*

- ☐ Not present  
☐ Present (☐ uninvolved, ☐ involved in pectoralis muscle, ☐ involved in pectoralis muscle and chest wall)

**Resection margin**

- ☐ Cannot be assessed  
☐ Positive for carcinoma  
     Location (specify): invasive carcinoma/DCIS/invasive carcinoma and DCIS (unifocal, multifocal, extensive)  
☐ Uninvolved by invasive carcinoma and/or DCIS  
     Distance from closest margin : \_\_\_\_\_ mm from \_\_\_\_\_ margin

**Regional lymph node metastasis**

Total number of lymph nodes examined:  
 Number of lymph nodes involved with metastases:  
 (sentinel node:        /        , nonsentinel node:        /        )  
 Size of largest metastasis:        mm  
 Extranodal extension: Not identified/Present

**Lymphovascular invasion**

- ☐ Not identified  
☐ Present

**Pathologic stage classification (pTNM, AJCC 8th edition)**

TNM descriptors: ☐ m   ☐ r   ☐ y  
 Primary tumor (pT):  
 Regional lymph nodes (pN):

UOQ, upper outer quadrant; LOQ, lower outer quadrant; UIQ, upper inner quadrant; LIQ, lower inner quadrant; EIC, extensive intraductal component; AJCC, American Joint Committee on Cancer.

**Histological type**

The histopathologic classification of breast tumors in this paper is based on the WHO Classification of Breast Tumors, 5th edition [5] (Supplementary Table S2). The term “invasive breast carcinoma (IBC) of no special type (NST)” defines a large and heterogeneous group of IBCs that cannot be classified morphologically as any of the special histological types. The terms “invasive breast carcinoma, not otherwise specified (NOS),” “invasive ductal carcinoma,” or “infiltrating ductal carcinoma” are also acceptable; however, invasive mammary carcinoma of NST is not

recommended.

IBC-NST encompasses a wide spectrum of histological patterns, including some special morphological patterns. Oncocytic, lipid-rich, glycogen-rich, clear cell, and sebaceous carcinomas; carcinoma with medullary pattern; invasive carcinoma with neuroendocrine differentiation; and carcinomas with pleomorphic and choriocarcinomatous patterns are considered wide morphological patterns of IBC-NST regardless of the extent of differentiation or pattern. Breast carcinomas showing a specialized subtype in  $\geq 90\%$  of the tumor are designated as a pure special



tumor type, such as mucinous cystadenocarcinoma or lobular, tubular, cribriform, mucinous, micropapillary, apocrine, or metaplastic carcinoma.

The phrase “mixed IBC-NST and special subtype carcinoma” can be used when the special subtype comprises 10% to 90% of the carcinoma. For mixed tumors, overall percentage of the special subtype, grade and biomarkers status of both IBC-NST and special type carcinoma components should be reported. Carcinomas in which the special subtype comprises < 10% should be classified as IBC-NST, with the optional comment of focal specialized subtype. Tumors lacking such specific features are designated IBC-NST, which accounts for the majority of IBC cases. Currently, estrogen receptor (ER) and human epidermal growth factor receptor type 2 (HER2) biomarker status are used for management purposes instead of histological subtype or pattern.

The traditionally used classifications of medullary carcinoma, atypical medullary carcinoma, and carcinoma with medullary features found in the 4th edition of the WHO Breast Tumor Classification were removed in the 5th edition. Carcinomas formerly classified as these subtypes are now categorized as “IBC-NST with medullary pattern,” representing one end of the spectrum of tumor-infiltrating lymphocyte (TIL)-rich IBC-NSTs, rather than a distinct morphological subtype. IBC-NST with medullary pattern belongs to triple negative breast carcinomas, characterized by high expression of immune-related genes.

Metaplastic carcinoma is a heterogeneous group of IBCs characterized by differentiation of the neoplastic epithelium toward squamous cells and/or mesenchymal-looking elements, including but not restricted to spindle, chondroid, and osseous cells. The type of metaplastic elements present may be recorded using

a descriptive classification system.

### Tumor focality

If multiple invasive carcinomas are present, tumor focality should be recorded. Multifocal tumors are associated with increased risk of lymph node involvement compared to similar unifocal disease [7-9], which reflects increased tumor load [10]. Counting the number of invasive foci is not essential but is recommended. When there is difficulty in determining whether two tumors are separate or not, microscopic examination of the tissue between the two masses should be performed. There are several occasions when multiple foci of invasion are present: extensive carcinoma in situ with multifocal invasion, invasive carcinoma with satellite foci, extensive lymphovascular invasion (LVI), multiple separate invasive carcinomas, invasive carcinomas after neoadjuvant chemotherapy, and transection of a single carcinoma [3].

Except for cases presenting multiple separate invasive carcinomas, most multifocal tumors have similar appearance and immunophenotype to the largest tumor. When multifocal tumors have similar histology, only the largest tumor is tested for ER, progesterone receptor (PR), and HER2. If multifocal tumors have different histological subtypes and grades, it is recommended to evaluate ER, PR, and HER2 status of each component, separately [3,11].

### Tumor size

The single greatest dimension of the largest invasive tumor is used to ascertain the pathologic tumor (pT) category, regardless of extent of accompanying in situ carcinoma [4] (Fig. 1A). Three-dimensional measurement of tumor size is essential. In cases in

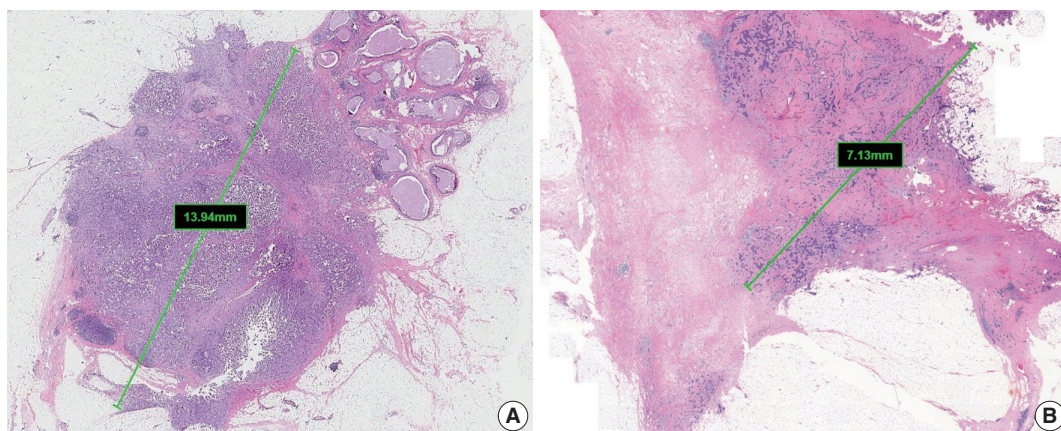


**Fig. 1.** Measurement of invasive tumor size. (A) Pathologic tumor (pT) category is based on the largest diameter of invasive carcinoma. Ductal carcinoma in situ, which is present on the upper right side of the invasive carcinoma, is not included in this measurement. (B) In post-treatment samples, the pT category (ypT) is based on the diameter of the largest contiguous focus (bar) of residual invasive carcinoma.

which it is difficult to determine the tumor size, information from imaging, gross findings, and microscopic evaluation should be used. For multifocal tumors, measurement of each tumor is recommended.

The post-treatment pT category (ypT) is based on the largest contiguous focus of residual invasive carcinoma. Treatment-associated fibrosis adjacent to residual tumor or between foci of residual invasive carcinoma is not included in the ypT category (Fig. 1B).

### Histological grade

Histological grading should be performed according to the Elston-Ellis modification of Bloom-Richardson grading [12]. Histological grading of IBCs is determined by three components: tubule formation, nuclear pleomorphism, and mitotic count (Supplementary Table S3). Tubule formation is assessed under low-power magnification. Scoring is performed according to the proportion of tumor cells forming tubules: more than 75% (score 1), 10%–75% (score 2), and less than 10% (score 3). Nuclear pleomorphism should be assessed in the area showing the highest degree of pleomorphism. A score of 1 is given to small (less than 1.5 times the size of benign epithelial cell nuclei) and uniform nuclei with finely dispersed chromatin. A score of 3 is given to large (more than two times the size of benign epithelial cell nuclei), vesicular, and pleomorphic nuclei with prominent nucleoli and irregular chromatin. A score of 2 is given to nuclei with characteristics that lie between those two categories. Mitotic count is the number of mitotic figures present in 10 high-power fields (HPFs). Counting should be performed in the hot spot (area with the most frequent mitotic figures), which is usually at the peripheral, leading edge of the tumor. Care should be taken not to count hyperchromatic and apoptotic nuclei. The

cutoff points for mitotic count scores differ according to the field diameter of the 40× objective lens. The 5th edition WHO Breast Tumor Classification system recommends the use of number of mitoses per mm<sup>2</sup> instead of number of mitoses per 10 HPFs for standardization [5].

These three scores are summed, and the total score of 3–9 is used for overall tumor grade: score 3–5 = grade 1, well differentiated; score 6–7 = grade 2, moderately differentiated; score 8–9 = grade 3, poorly differentiated (Fig. 2). The histological grade of IBC shows a strong correlation with prognosis [12,13].

### Ductal carcinoma in situ

Ductal carcinoma in situ (DCIS) is concomitantly present in as many as 80% of IBC cases and is associated with increased risk of local recurrence after breast-conserving surgery [5].

Extensive intraductal component (EIC)-positive carcinoma is present when (1) DCIS is a major component ( $\geq 25\%$ ) of the area of invasive carcinoma and also is present outside the area of invasive carcinoma (Fig. 3A) or (2) there is extensive DCIS associated with a small ( $\leq 10$  mm) invasive carcinoma (Fig. 3B) [3].

The histological features of DCIS associated with increased risk of recurrence are large lesion size, high nuclear grade, certain architectural patterns, central necrosis, and positive surgical margin [5]. It is essential to report the features of DCIS, including nuclear grade, presence of necrosis, and extent of DCIS, in cases of EIC-positive carcinoma [3].

Nuclear grade is determined according to pleomorphism, nuclear size, chromatin, nucleoli, mitoses, and orientation (Supplementary Table S4) and is predictive of clinical outcome (recurrence) [14]. Central (comedo) necrosis is easily detected at low magnification within the central portion of ducts affected by DCIS. Focal necrosis means necrosis in small foci or single-cell

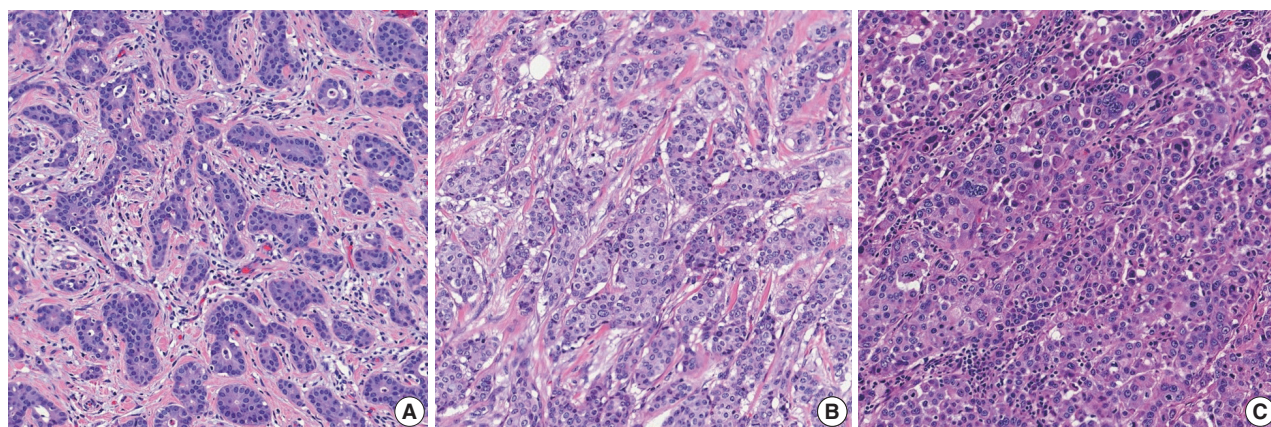


**Fig. 2.** Histological grades of invasive breast carcinoma of no special type: (A) grade 1, (B) grade 2, and (C) grade 3.



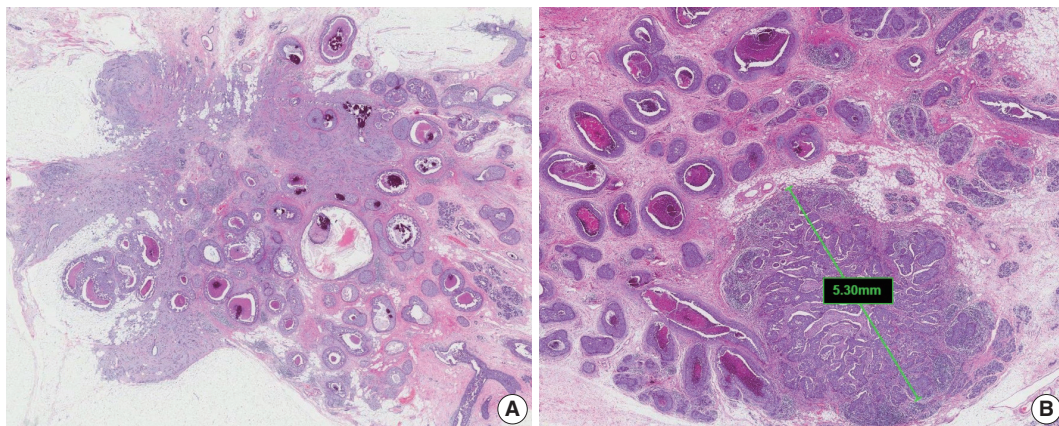


**Fig. 3.** Extensive intraductal component-positive invasive carcinoma. (A) Ductal carcinoma in situ (DCIS) constitutes  $\geq 25\%$  of the area of invasive carcinoma and also is present outside the area of invasive carcinoma. (B) A small invasive carcinoma is present in background of extensive DCIS.

necrosis and is indistinct at low magnification.

Reporting the architectural pattern of DCIS is not essential but is recommended. Comedo DCIS is characterized by high nuclear grade associated with central necrosis, often with calcification. Solid DCIS shows compact proliferation of tumor cells with low-to-intermediate nuclear grade that fills the entire duct. Small necrotic foci may be present. Cribriform DCIS is characterized by intraductal proliferation with a sieve-like or fenestrated pattern. The secondary lumens are round, rigid, and surrounded by low-to-intermediate grade nuclei or occasional high-grade nuclei. Micropapillary DCIS has papillary fronds that lack fibrovascular cores and that protrude into the ductal lumen in a regular distribution. Micropapillary DCIS tends to be extensive in distribution (multifocal and multicentric). Papillary DCIS contains arborizing papillae with thin fibrovascular cores. Although it may be seen only microscopically, papillary DCIS more commonly presents as a large mass [14]. Encapsulated papillary carcinoma without invasion and solid papillary carcinoma without invasion are unusual patterns of DCIS.

Reporting the extent of DCIS is essential in cases of EIC-positive carcinoma. However, a precise measurement of the extent of DCIS may be difficult or, at times, impossible. There are several methods for estimating the extent of DCIS. If DCIS is confined to a single tissue block, it is possible to estimate the extent of DCIS by direct measurement of the histological slides. If the entire specimen is blocked sequentially, the extent of DCIS can be calculated by multiplying the number of slices involved by average slice thickness. If the specimen is sampled, rather than sequentially blocked in its entirety, the extent of DCIS can be estimated by counting the number of blocks with DCIS [3,15].

### Tumor extension

Satellite tumor nodules in the skin are separate from the primary tumor and macroscopically identifiable. Skin and dermal satellite nodules identified only on microscopic examination and skin involvement without epidermal ulceration or skin edema (clinically peau d'orange) do not qualify as pT4b category (Fig. 4A, B). Such tumors should be categorized based on tumor size. Inflammatory carcinoma is categorized only when there are clinical symptoms of erythema and edema in more than one-third of the entire breast skin and not by the pathologic findings of tumor emboli in the dermal lymphatics.

The chest wall includes ribs, intercostal muscles, and serratus anterior muscle but not the pectoralis muscles. Therefore, involvement of the pectoralis muscles in the absence of invasion of these chest wall elements does not constitute chest wall invasion, and cancers with such involvement are categorized based on tumor size.

### Resection margin

Whenever possible, specimens should be oriented to identify specific margins for the pathologist. All identifiable margins should be evaluated for carcinoma involvement both grossly and microscopically [16].

Orientation may be conducted using sutures or clips placed on the specimen surface or by other means of communication between the surgeon and pathologist and should be documented in the pathology report. Margins can be identified in several ways, including using multiple colored inks, submitting the margins in specific cassettes, or submitting each margin as a separately excised specimen.

Margin status is listed as “positive” if there is ink on the cancer

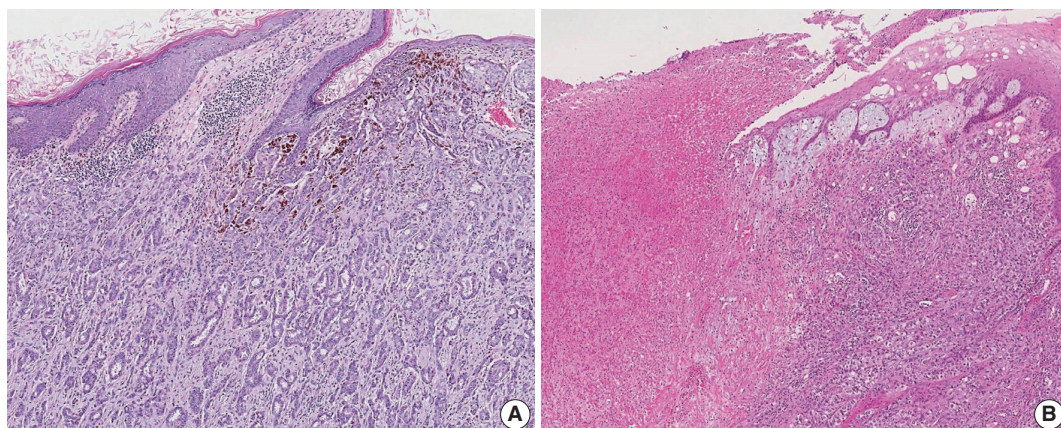


**Fig. 4.** Skin involvement in invasive breast carcinoma. (A) Tumor cells infiltrate into the upper dermis in the absence of ulceration. These cases should not be classified as pT4b category. (B) There is an ulceration of overlying epidermis accompanied by tumor extension, corresponding to the pT4b category.

cells during pathologic margin evaluation. If the specimen is oriented, the specific site(s) of involvement should be reported. The approximate extent of margin involvement can be reported as follows: unifocal, 1 focal area of carcinoma (< 4 mm) at the margin; multifocal, 2 or more carcinoma foci at the margin; extensive, carcinoma present at the margin over a broad front (> 5 mm).

In lobular carcinoma in situ (LCIS), assessment of resection margin is optional. However, for pleomorphic type LCIS, evaluation of resection margin is recommended.

### Regional lymph node metastasis

Most patients with invasive carcinoma will have lymph nodes sampled for pathologic regional lymph node (pN) categorization [4]. All lymph nodes must be examined histologically [4]. The nodes commonly examined include sentinel nodes, nonsentinel nodes, nodes from axillary dissections, and intramammary nodes. When the total number of sentinel and nonsentinel nodes removed is less than 6, the AJCC “sn” modifier is used.

Metastases are classified into three groups based on size: isolated tumor cells (ITCs), micrometastases, and macrometastases [4]. ITCs are defined as single cells, small clusters of cells no larger than 0.2 mm, or no more than 200 cells in a single cross section. The AJCC states that a cluster is a group of cells in contact with each other (confluent or contiguous). Cells that are not touching each other should be considered independent and measured independently. In cases of multiple clusters of tumor cells within a lymph node, only the largest should be considered when determining N category (Fig. 5A). The AJCC states that the size of the tumor should include both the tumor cells and the surrounding desmoplastic reaction. Some carcinomas, particularly lobular carcinomas, may metastasize as individual single cells

and not as clusters and present as a dispersed pattern of nodal metastases (Fig. 5B). In such cases, single cells are measured separately. If fewer than 200 tumor cells are present in a node cross section, then classification of ITCs is recommended (Fig. 5C). Nodes containing only ITCs are not included in the total number of positive nodes when determining N category, so cases with only ITCs are classified as node negative (pN0 (i+)). Micrometastases measure greater than 0.2 mm but not greater than 2 mm and/or comprise more than 200 cells in a single cross section. If only micrometastases are present on lymph node examination, the N category is pN1mi. If at least 1 macrometastasis is present, nodes with micrometastases are included in the total number of positive nodes. Any lesion where the largest cluster is greater than 2 mm represents a macrometastasis (Fig. 5D).

Extranodal extension is defined as the presence of full-thickness (i.e., into and through) lymph node capsular invasion, as seen with metastatic tumor invasion of extranodal fat with or without an associated desmoplastic stromal response (Fig. 5D). The area of extranodal extension is included when measuring the overall size of the lymph node metastasis. Extranodal extension is a marker of poor prognosis in breast cancer patients, and the status of extranodal extension should be reported [17]. Reporting of extranodal extension size based on a 2-mm cutoff is incorporated into the CAP reporting guidelines, but more evidence is needed for this practice to become widely accepted [3,17].

When cancerous nodules that are not associated with residual lymph node tissue are present in the axillary fat, the AJCC states that these nodules should be classified as positive lymph nodes [4]. However, if there is surrounding normal breast parenchyma or DCIS, then cancerous nodules in the axillary fat should be classified as invasive carcinoma and not as a nodal metastasis.



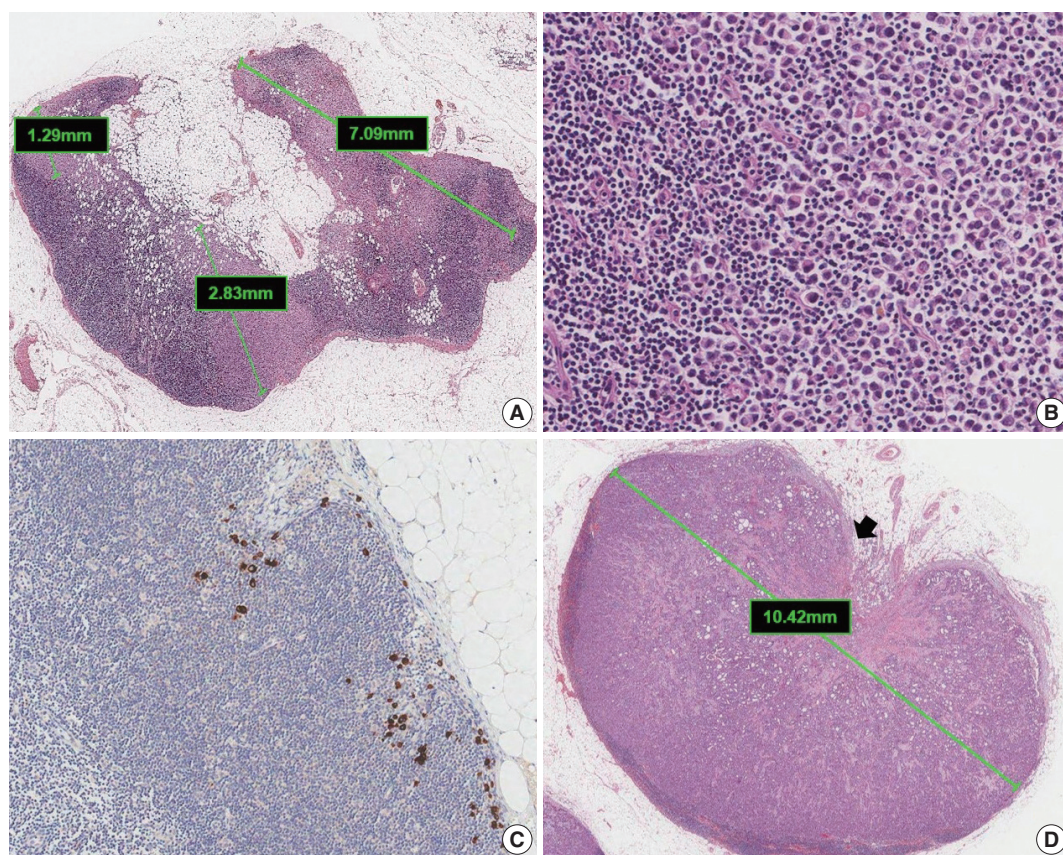


**Fig. 5.** Classification of lymph node metastases. (A) Multiple clusters of tumor cells. N category is based on the size of the largest contiguous cluster of tumor cells. (B) Dispersed pattern of metastasis. Some lobular carcinomas may metastasize as single cells and may not form cohesive clusters. If more than 200 tumor cells are present in a node cross section, then the category of micrometastasis is recommended. (C) Isolated tumor cells. A dispersed pattern of lobular carcinoma with fewer than 200 cells is detected by cytokeratin immunohistochemistry. (D) Macrometastasis with extranodal extension. This metastasis is classified as a macrometastasis based on the size of cluster (>2 mm). Extranodal extension, an area of invasion outside the lymph node capsule (arrow), is noted.

The post-treatment pN (ypN) classification system is the same as that for pre-treatment lymph nodes. Only the largest contiguous focus of residual tumor in the node evaluation is used for determining N category; any treatment-associated fibrosis is not included [3,4].

### Lymphovascular invasion

LVI is associated with local recurrence and reduced survival [18]. Strict criteria or immunohistochemistry (IHC) stains have been proposed to differentiate LVI from DCIS and retraction artifacts [3]. If a limited area is involved in LVI, a measurement in millimeters can be given. Alternatively, LVI can be quantified as focal or extensive, with ‘extensive’ defined as one or more foci in more than one block [19].

The presence of pure LVI without stromal invasion after neoadjuvant therapy may be called ypTX and should not be classified as pathologic complete response (pCR) [20].

### Pathologic stage classification [4]

Pathologic stage classification according to the AJCC 8th edition should be reported as a standard data element [4]. Classification of primary tumor (T), regional lymph nodes (N), and distant metastasis (M) by pathologic examination is denoted by the prefix “p” (pT, pN, and pM). The descriptor “m” is used when invasive cancer is observed in multiple foci, and the prefix “r” is used for recurrent cancer. If the patient has undergone neoadjuvant chemotherapy, hormonal therapy, immunotherapy, or radiation therapy before surgery, the prefix “y” is used. pM0 is not a valid category. When distant metastases cannot be confirmed by pathologic examination, staging can be performed by combining pT, pN, and the clinical evaluation of metastases (cM).

### pT category

Criteria for each pT category are summarized in Supplementary Table S5. For multiple invasive cancers, use the tumor with

the highest T category for classification and staging, and use the descriptor “m” or number of invasive cancers in parentheses (e.g., T2(m) or T2(3)). For simultaneous bilateral breast cancers, staging should be conducted separately because they are considered independent tumors in different organs.

#### *pN category*

Criteria for each pN category are summarized in Supplementary Table S6. If no lymph nodes were submitted for evaluation, record pNX. It is not the pathologist's obligation to record the pN status by integrating the previous pathologic results. pN1a, pN2a, and pN3a refer to metastases in 1 to 3, 4 to 9, and 10 or more axillary lymph nodes, respectively, with at least one macrometastasis. If the specimen contains internal mammary lymph nodes, infraclavicular lymph nodes, or supraclavicular lymph nodes with metastases, or if clinically metastatic internal mammary lymph node(s) are identified, refer to the AJCC staging manual for accurate lymph node categorization. A regional lymph node with direct extension of the primary tumor or a tumor nodule in a regional lymph node area should be considered as a positive node.

When nodal metastasis is confirmed by fine-needle aspiration cytology or core needle biopsy without further resection of nodes, use the “f” modifier (e.g., pN(f)).

#### *pM category*

The pM category is assigned only if metastasis larger than 0.2 mm (pM1) is histologically confirmed. When staging after neoadjuvant therapy, the classification should remain M1 regardless of responsiveness to therapy, if the case was confirmed to be M1 prior to therapy.

## CONDITIONAL DATA ELEMENTS

All conditional data elements for this report form are summarized in Table 2.

### Perineural invasion

Perineural invasion (PNI) is infrequently observed in IBC, occurring in approximately 1% of cases, perhaps in part because nerves of notable size are not numerous in mammary tissues [21].

PNI may occur more frequently in IBC-NST than in the other histological subtypes. It tends to occur in high-grade tumors, where it is frequently associated with LVI, but it has not been proven to have independent prognostic significance [21-24].

**Table 2.** Conditional data element

<b>Perineural invasion</b>			
<input type="checkbox"/> Not identified			
<input type="checkbox"/> Present			
<b>Tumor border</b>			
<input type="checkbox"/> Not applicable			
<input type="checkbox"/> Well-demarcated/Circumscribed			
<input type="checkbox"/> Ill-demarcated			
<input type="checkbox"/> Mixed			
<b>Microcalcification</b>			
<input type="checkbox"/> Not identified			
<input type="checkbox"/> Present in invasive carcinoma			
<input type="checkbox"/> Present in DCIS			
<input type="checkbox"/> Present in non-neoplastic tissue			
<b>Tumor-infiltrating lymphocytes (TILs)</b>			
_____ %			
<b>Treatment effect (RCB class)</b>			
<input type="checkbox"/> RCB class 0	<input type="checkbox"/> RCB class I	<input type="checkbox"/> RCB class II	<input type="checkbox"/> RCB class III
RCB index:			
<b>Additional pathologic findings</b>			
DCIS, ductal carcinoma in situ; RCB, Residual Cancer Burden.			

PNI can also be observed in some benign lesions, such as sclerosing adenosis, as well as in DCIS.

### Tumor border

The tumor margins of IBC can be grossly described as ill-demarcated, well-demarcated (circumscribed), or mixed [21].

Approximately one-third of tumors have grossly circumscribed margins. However, some carcinomas that appear to have circumscribed margins grossly exhibit an invasive growth pattern microscopically [21]. Grossly ill-demarcated tumors tend to be larger, and they are more likely to have axillary metastases than those with circumscribed margins [21].

### Microcalcification

DCIS/invasive carcinoma found in biopsies performed for microcalcifications will almost always be at the site of the microcalcifications or in close proximity [25,26]. The presence of targeted microcalcifications in the specimen can be confirmed by radiography.

The pathologist needs to confirm that the specimen has been sampled from the lesion responsible for the microcalcifications. Microcalcifications are commonly present in secretions and/or in necrotic materials [5]. The radiological and pathologic correlation of all microcalcifications, including information about the presence and site of microcalcifications (e.g., invasive carcinoma, DCIS, benign lesion, or mixed), should be indicated [5]. Information about the microcalcifications can be an important



consideration when correlating imaging findings with the pathologic diagnosis, when guiding further management of the disease, and when identifying recurrent carcinoma in the breast or metastatic diseases [21].

### Tumor-infiltrating lymphocytes

The prognostic and predictive value of TILs in breast cancer has been studied extensively [27,28]. TILs are lymphocytes present in the stroma of a tumor or inside tumor cell nests. Assessment of TIL level in hematoxylin and eosin (H&E) sections can be easily performed. The International Immuno-Oncology Biomarker Working Group on Breast Cancer published guidelines for evaluation of TIL level in H&E sections of invasive breast cancer in 2014, and they later extended this method to DCIS, metastatic tumor deposits, and specimens obtained after neoadjuvant chemotherapy [7,29,30]. In brief, TIL level is determined by measuring the percentage of the total stromal area, excluding tumor necrosis and crush artifacts, occupied by mononuclear inflammatory cells, including plasma cells, within the borders of the invasive carcinoma. TILs are usually evaluated in increments of 10% (e.g., < 10%, 10%–19%, 20%–29%) (Fig. 6). Since distribution of TILs is usually not even throughout the tumor tissue, assessment of the average number of TILs, without focusing on hot spots, is recommended. The International Immuno-Oncology Biomarker Working Group showed that proper training of pathologists could achieve more consistent results with regard to evaluation of TILs in ring studies and suggested potential pitfalls in assessment of TILs [31,32].

### Effect of treatment

Many classifications have been proposed to evaluate the

pathologic status of breast cancer after treatment, including those of Chevallier [33], Sataloff [34], the National Surgical Adjuvant Breast and Bowel Project (NSABP) B-18 [35], Miller-Payne [36], the Residual Cancer Burden (RCB) system [37], the Clinical-Pathologic Stage-Estrogen/Grade (CPS-EG) system [38], the Residual Disease in Breast and Nodes (RDBN) system [39], and the AJCC [4]. Among these classifications, the AJCC and the RCB calculator are the most widely used systems to measure residual disease [40].

The RCB index is calculated from the following five variables [37]: (1) primary tumor bed area ( $\text{mm}^2$ ), (2) overall cancer cellularity (%), (3) percentage of carcinoma in the tumor bed that is in situ disease (%), (4) number of positive lymph nodes, and (5) diameter of the largest lymph node metastasis (mm).

Primary tumor bed area is the two largest dimensions between invasive tumor cells, even if these are widely scattered and separated by treatment-induced fibrosis. Overall cancer cellularity is the overall percentage of the residual tumor bed area that is occupied by carcinoma (invasive and in situ). It is assessed in each slide, and the average is calculated using all fields that fall within the perimeter of the largest cross-sectional area of residual tumor bed, even those with very low cellularity or no disease [37]. The same method can be used for the in situ component to assess the percentage of cancer that is in situ disease [37]. Unlike the AJCC ypN category, the number of positive lymph nodes includes the number of lymph nodes with ITCs. The diameter of the largest lymph node metastasis used in the RCB system may be different from that used for AJCC staging because the former includes intervening treatment-related fibrosis [40,41].

A mathematical formula combines these variables into a con-

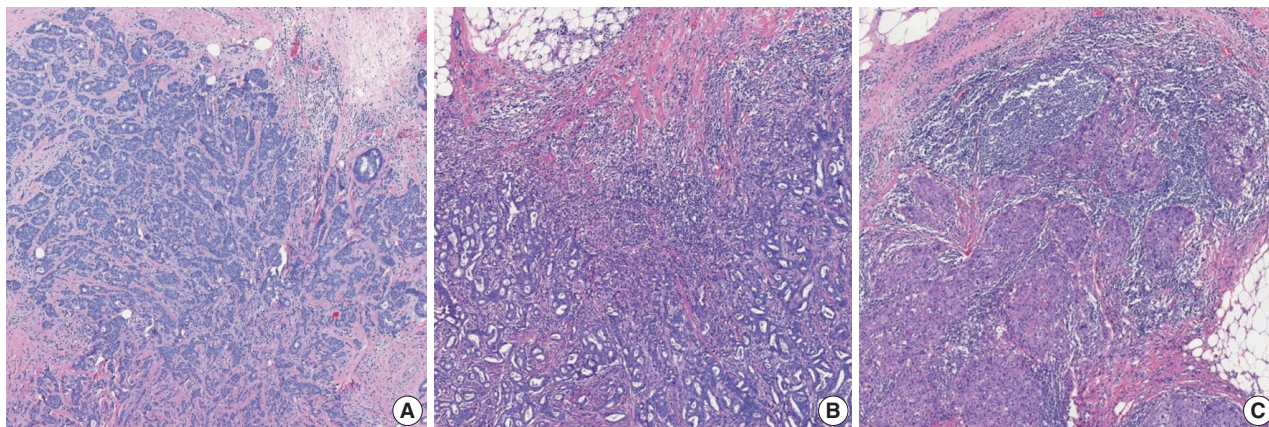


**Fig. 6.** Different levels of tumor-infiltrating lymphocyte (TIL) infiltration in invasive breast carcinoma: (A) TIL < 10%, (B) TIL 10%–50%, and (C) TIL > 50%.



tinuous index to define four RCB classes: RCB-0 for pCR and RCB 1 to 3, representing progressively greater extent of residual cancer [37]. A web-based calculator and detailed instructions for calculating RCB indices are publicly available (<http://www3.mdanderson.org/app/medcalc/index.cfm?pagename=jsconvert3>).

As the presence of positive lymph nodes after treatment represents a worse prognosis even when there is no residual invasive carcinoma in the breast [42,43], several classification systems and the CAP cancer protocol have recommended that effect of treatment be evaluated in both the breast and lymph nodes [3,4,34,37,39,44,45].

## BIOMARKERS

Determination of biomarker status, including ER, PR, and HER2 status, is essential for newly diagnosed IBC. ER, PR, and HER2 should be evaluated according to the current American Society of Clinical Oncology (ASCO)/CAP guidelines [46,47]. Currently, there are no established guidelines regarding re-evaluation of biomarkers in post-treatment specimens. However, it is recommended that ER, PR, and HER2 testing be repeated on post-treatment invasive carcinomas, such as when there was insufficient invasive tumor tissue or negative or equivocal results on pre-treatment core biopsy; when biopsies were performed and biomarkers assessed at other institutions; or when post-treatment tumors display heterogeneous morphology or no response to therapy.

All essential data elements for reporting biomarker status are summarized in Table 3. In addition, all data elements for biomarkers including all recommended issues as well as essential data elements can be found in Supplementary Table S7.

### ER and PR status

ER or PR positivity is defined when more than 1% of tumor cells demonstrate nuclear positivity [46] (Fig. 7A, B). The proportion of positive cells can be reported as a specific percentage or as a discrete range. The intensity is defined as the degree of nuclear positivity (weak, moderate, strong) and is recommended for reporting.

Alternatively, the Allred scoring system can be used to evaluate ER and PR status semi-quantitatively. The Allred score combines the percentage of stained nuclei (0, < 1%, 1%–10%, 11%–33%, 34%–66%, and > 67%) and the average intensity of the immunoreactivity (0, 1, 2, and 3) for a final score out of 8. Scores between 0 and 2 are classified as a negative result, while scores 3 and above are considered positive. Very rarely, carcinomas

**Table 3.** Biomarker report form

<b>Estrogen receptor</b>	
<input type="checkbox"/> Positive (≥ 1% of tumor cells with nuclear positivity)	
<input type="checkbox"/> Negative (< 1%)	
<b>Progesterone receptor</b>	
<input type="checkbox"/> Positive (≥ 1% of tumor cells with nuclear positivity)	
<input type="checkbox"/> Negative (< 1%)	
<b>HER2 status by immunohistochemistry</b>	
<input type="checkbox"/> Negative (0)	
<input type="checkbox"/> Negative (1+)	
<input type="checkbox"/> Equivocal (2+)	
<input type="checkbox"/> Positive (3+)	
<b>HER2 status by in situ hybridization</b>	
<input type="checkbox"/> ISH negative	
<input type="checkbox"/> ISH positive	
No. of counted cells:	
HER2/CEP17 ratio:	
Average HER2 copy number per cell:	
Average CEP17 copy number per cell:	
<b>Ki-67 index</b>	
Ki-67 index:	%

HER2, human epidermal growth factor receptor type 2; ISH, in situ hybridization; CEP17, centromere on chromosome 17.

with < 1% positive cells and intensity scores of 2 or 3 are classified as positive, as the total score would be 3 or 4. However, responses to hormonal therapy in these tumors have not been specifically proven [48].

Recently, it has been recommended that invasive carcinomas with 1%–10% positive ER staining be reported as ER low positive [46] (Fig. 7C). There are data that suggest that invasive cancers with these results are heterogeneous in both behavior and biology and often have gene expression profiles similar to those of ER-negative cancers [46].

The status of controls should be reported in cases with ER/PR negative or ER low positive tumors [46]. On-slide controls are ideal and, wherever possible, routine evaluation of internal normal epithelial elements or inclusion of normal breast sections (or other appropriate control) on each tested slide is recommended.

Inadequate samples and technical issues, such as prolonged cold ischemia time, insufficient sample amount, severe processing artifacts, inappropriate external/internal controls, and unavailable information on pre-analytical variables associated with fixation, may cause difficulties in interpretation of results, including production of false-negative results. These cases are uninterpretable, and repeat staining of another block or specimen is recommended [46].



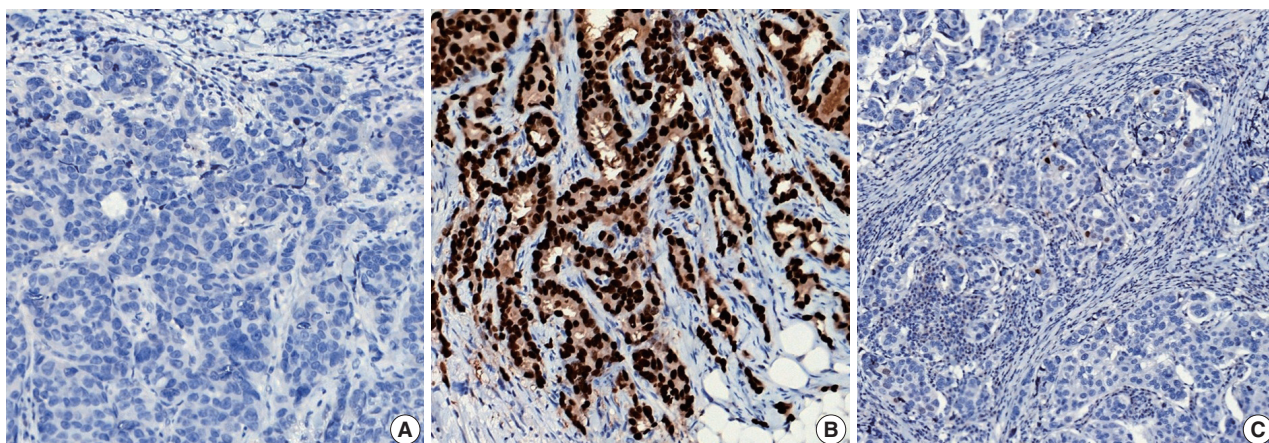


**Fig. 7.** Representative examples of estrogen receptor (ER) expression assessed by immunohistochemistry in invasive breast carcinoma: (A) ER negative, (B) ER positive, and (C) ER low positive.

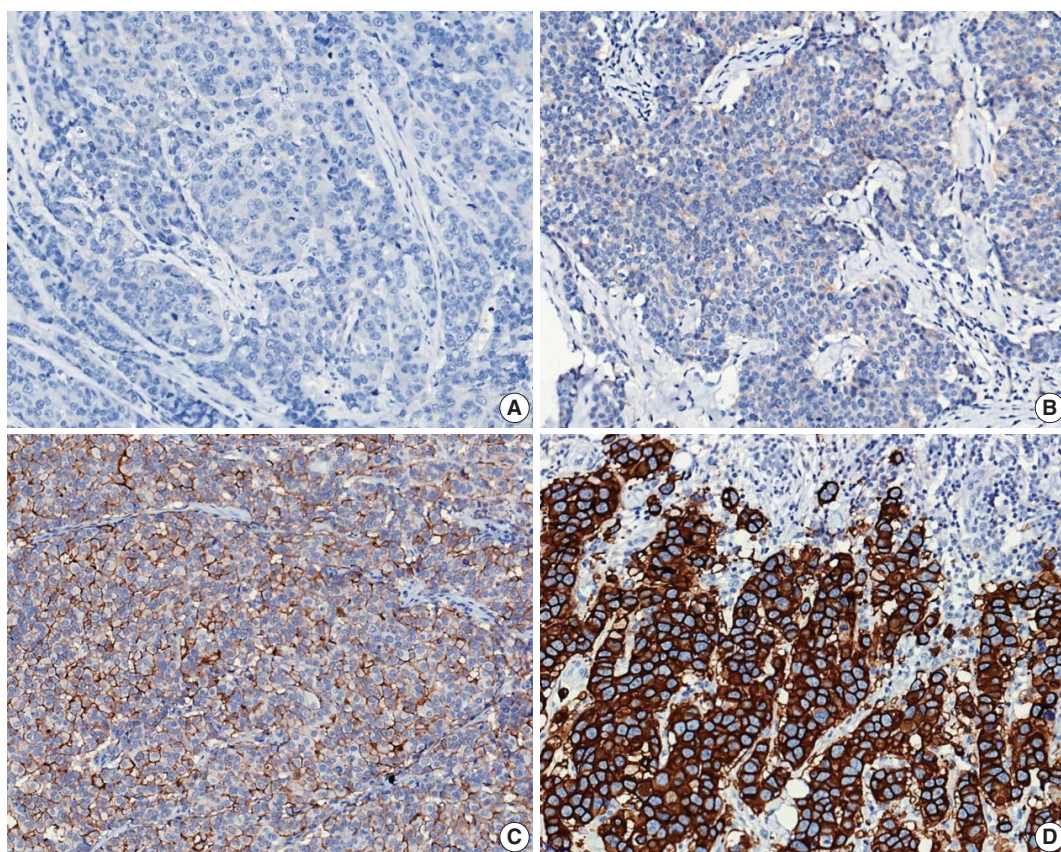


**Fig. 8.** Representative examples of human epidermal growth factor receptor 2 (HER2) immunohistochemistry (IHC) scores in invasive breast carcinoma: (A) HER2 IHC score 0, (B) HER2 IHC score 1+, (C) HER2 IHC score 2+, and (D) HER2 IHC score 3+.

### HER2 status

IHC and in situ hybridization (ISH) are regarded as standard methods to assess HER2 status in breast cancer. The ASCO/CAP have jointly released guidelines and recommendations on HER2 testing in breast cancer since 2007, and, recently, have

updated these guidelines to provide clear instructions for HER2 testing and accurate determination of HER2 status in breast cancer [49].

Currently, HER2 status determined by IHC and ISH should be interpreted based on the 2018 updated ASCO/CAP guide-



lines [47]. HER2 IHC status should be assessed using a semi-quantitative scoring system (Fig. 8A–D). For HER2 IHC equivocal (2+) cases, HER2 status should be confirmed by ISH.

Interpretation of HER2 ISH is performed by counting at least 20 cells in the invasive tumor area. Scanning of entire slides or use of IHC slides prior to counting is mandatory to define the areas of potential HER2 amplification [50]. Please refer to a previous article for interpretation of HER2 heterogeneity [49].

For a diagnostic approach using HER2 ISH, concomitant IHC review for dual-probe ISH groups 2 to 4 is required in the updated guidelines [47]. In laboratories using single-probe ISH assays, concomitant IHC review is included as part of the interpretation of all ISH assay results [47]. By this approach, the HER2 ISH status is designated as positive or negative, with no equivocal category. Determining HER2 ISH status using dual-probe ISH is summarized in Supplementary Table S8. In reporting the results of HER2 ISH, final HER2 ISH status (negative or positive), number of counted cells, *HER2*/centromere on chromosome 17 (CEP17) ratio, average *HER2* copy number per cell, average CEP17 copy number per cell, and designation of ISH group (optional) should be included.

### Ki-67 index

The Ki-67 index is defined by the percentage of tumor cells with positive Ki-67 nuclear staining out of all tumor cells counted in a given field. A high Ki-67 index is regarded as a prognostic marker associated with high risk of recurrence and as a predictive marker for treatment response in breast cancer [51–54]. However, there remain controversies in its use as a standard prognostic or predictive biomarker owing to high inter-observer variability and lack of a standardized measurement method. Currently, assessment of Ki-67 can be performed applying recommendations from the International Ki-67 in Breast Cancer Working Group [55] in clinical practice. Briefly, at least three high-power (40× objective) fields should be selected to represent the spectrum of staining on initial overview of the whole section. If there are clear hot spots, data from these should be included in the overall average score. Scoring should involve the counting of at least 500 malignant invasive cells (and preferably at least 1,000 cells). Currently, computational imaging analysis methods are widely used for Ki-67 quantification, but their superiority over the direct counting method is unclear. When morphological analysis is used, the number of tumor cells counted and the number of tumor cells with positive Ki-67 nuclear staining should be included in the report form.

## CONCLUSION

In accordance with recent advances in collective understanding of breast cancer biology and in treatment of breast cancer patients, a committee of the Breast Pathology Study Group of the Korean Society of Pathologists presents in this publication a ‘Standardized Pathology Report for Breast Cancer.’ This report form is composed of ‘standard data elements,’ ‘conditional data elements,’ and a biomarker report form to guide diagnosis, prognosis, and treatment of breast cancer patients. It is our hope that this report will lead to standardization of the pathologic diagnosis of breast cancer and to improvement in communication between clinicians and pathologists, as well as between pathologists.

### Supplementary Information

The Data Supplement is available with this article at <https://doi.org/10.4132/jptm.2020.11.20>.

### Ethics Statement

Not applicable.

### ORCID

Soo Youn Cho	<a href="https://orcid.org/0000-0001-9714-7575">https://orcid.org/0000-0001-9714-7575</a>
So Yeon Park	<a href="https://orcid.org/0000-0002-0299-7268">https://orcid.org/0000-0002-0299-7268</a>
Young Kyung Bae	<a href="https://orcid.org/0000-0002-6689-9413">https://orcid.org/0000-0002-6689-9413</a>
Jee Yeon Kim	<a href="https://orcid.org/0000-0002-0503-984X">https://orcid.org/0000-0002-0503-984X</a>
Eun Kyung Kim	<a href="https://orcid.org/0000-0001-6701-6988">https://orcid.org/0000-0001-6701-6988</a>
Woo Gyeong Kim	<a href="https://orcid.org/0000-0003-1694-6602">https://orcid.org/0000-0003-1694-6602</a>
Youngmee Kwon	<a href="https://orcid.org/0000-0002-1370-2496">https://orcid.org/0000-0002-1370-2496</a>
Ahwon Lee	<a href="https://orcid.org/0000-0002-2523-9531">https://orcid.org/0000-0002-2523-9531</a>
Hee Jin Lee	<a href="https://orcid.org/0000-0002-4963-6603">https://orcid.org/0000-0002-4963-6603</a>
Ji Shin Lee	<a href="https://orcid.org/0000-0003-4634-2228">https://orcid.org/0000-0003-4634-2228</a>
Jee Young Park	<a href="https://orcid.org/0000-0002-1857-813X">https://orcid.org/0000-0002-1857-813X</a>
Gyungyub Gong	<a href="https://orcid.org/0000-0001-5743-0712">https://orcid.org/0000-0001-5743-0712</a>
Hye Kyoung Yoon	<a href="https://orcid.org/0000-0003-0714-8537">https://orcid.org/0000-0003-0714-8537</a>

### Author Contributions

Conceptualization: HKY. Project administration: SYP, YKB. Supervision: HKY. Writing—original draft: SYC, SYP, YKB, JYK, EKK, WGK, YK, AL, HJL, JSL, JYP. Writing—review & editing: SYC, SYP, YKB, GG, HKY. Approval of final manuscript: all authors.

### Conflicts of Interest

SYP, the editor-in-chief and YKB and GG, contributing editors of the *Journal of Pathology and Translational Medicine*, were not involved in the editorial evaluation or decision to publish this article. All remaining authors have declared no conflicts of interest.

### Funding Statement

No funding to declare.

### References

1. Kang SY, Kim YS, Kim Z, et al. Breast cancer statistics in Korea in 2017: data from a breast cancer registry. *J Breast Cancer* 2020; 23: 115–28.



2. Li X, Oprea-Ilie GM, Krishnamurti U. New developments in breast cancer and their impact on daily practice in pathology. *Arch Pathol Lab Med* 2017; 141: 490-8.
3. Fitzgibbons PL, Connolly JL, Bose S, et al. Protocol for the examination of resection specimens from patients with invasive carcinoma of the breast [Internet]. Northfield: College of American Pathologists, c2020 [cited 2020 Sep 10]. Available from: <https://documents.cap.org/protocols/cp-breast-invasive-resection-20-4400.pdf>.
4. Hortobagyi GN, Connolly JL, D'Orsi CJ, et al. Breast. In: Amin MB, Edge S, Greene F, et al., eds. *AJCC cancer staging manual*. 8th ed. New York: Springer; 2017; 589-636.
5. WHO Classification of Tumours Editorial Board. *WHO classification of tumours: breast tumours*. 5th ed. Lyon: International Agency for Research on Cancer, 2019.
6. Lester SC, Bose S, Chen YY, et al. Protocol for the examination of specimens from patients with invasive carcinoma of the breast. *Arch Pathol Lab Med* 2009; 133: 1515-38.
7. Salgado R, Aftimos P, Sotiriou C, Desmedt C. Evolving paradigms in multifocal breast cancer. *Semin Cancer Biol* 2015; 31: 111-8.
8. Andea AA, Wallis T, Newman LA, Bouwman D, Dey J, Visscher DW. Pathologic analysis of tumor size and lymph node status in multifocal/multicentric breast carcinoma. *Cancer* 2002; 94: 1383-90.
9. Weissenbacher TM, Zschage M, Janni W, et al. Multicentric and multifocal versus unifocal breast cancer: is the tumor-node-metastasis classification justified? *Breast Cancer Res Treat* 2010; 122: 27-34.
10. Coombs NJ, Boyages J. Multifocal and multicentric breast cancer: does each focus matter? *J Clin Oncol* 2005; 23: 7497-502.
11. Choi Y, Kim EJ, Seol H, et al. The hormone receptor, human epidermal growth factor receptor 2, and molecular subtype status of individual tumor foci in multifocal/multicentric invasive ductal carcinoma of breast. *Hum Pathol* 2012; 43: 48-55.
12. Elston CW, Ellis IO. Pathological prognostic factors in breast cancer. I. The value of histological grade in breast cancer: experience from a large study with long-term follow-up. *Histopathology* 1991; 19: 403-10.
13. Rakha EA, El-Sayed ME, Lee AH, et al. Prognostic significance of Nottingham histologic grade in invasive breast carcinoma. *J Clin Oncol* 2008; 26: 3153-8.
14. Jaffer S, Bleiweiss JJ. Histologic classification of ductal carcinoma in situ. *Microsc Res Tech* 2002; 59: 92-101.
15. Grin A, Horne G, Ennis M, O'Malley FP. Measuring extent of ductal carcinoma in situ in breast excision specimens: a comparison of 4 methods. *Arch Pathol Lab Med* 2009; 133: 31-7.
16. Morrow M, Van Zee KJ, Solin LJ, et al. Society of Surgical Oncology-American Society for Radiation Oncology-American Society of Clinical Oncology consensus guideline on margins for breast-conserving surgery with whole-breast irradiation in ductal carcinoma in situ. *Pract Radiat Oncol* 2016; 6: 287-95.
17. Choi AH, Blount S, Perez MN, et al. Size of extranodal extension on sentinel lymph node dissection in the American College of Surgeons Oncology Group Z0011 trial era. *JAMA Surg* 2015; 150: 1141-8.
18. Mohammed RA, Martin SG, Mahmmoud AM, et al. Objective assessment of lymphatic and blood vascular invasion in lymph node-negative breast carcinoma: findings from a large case series with long-term follow-up. *J Pathol* 2011; 223: 358-65.
19. Provenzano E, Bossuyt V, Viale G, et al. Standardization of pathologic evaluation and reporting of postneoadjuvant specimens in clinical trials of breast cancer: recommendations from an international working group. *Mod Pathol* 2015; 28: 1185-201.
20. Baker GM, King TA, Schnitt SJ. Evaluation of breast and axillary lymph node specimens in breast cancer patients treated with neoadjuvant systemic therapy. *Adv Anat Pathol* 2019; 26: 221-34.
21. Hoda SA, Brogi E, Koerner FC, Rosen PP. *Rosen's breast pathology*. Philadelphia: Wolters Kluwer, 2014.
22. Duraker N, Caynak ZC, Turkoz K. Perineural invasion has no prognostic value in patients with invasive breast carcinoma. *Breast* 2006; 15: 629-34.
23. McCready DR, Chapman JA, Hanna WM, et al. Factors affecting distant disease-free survival for primary invasive breast cancer: use of a log-normal survival model. *Ann Surg Oncol* 2000; 7: 416-26.
24. McCready DR, Chapman JA, Hanna WM, et al. Factors associated with local breast cancer recurrence after lumpectomy alone: postmenopausal patients. *Ann Surg Oncol* 2000; 7: 562-7.
25. Owings DV, Hann L, Schnitt SJ. How thoroughly should needle localization breast biopsies be sampled for microscopic examination? A prospective mammographic/pathologic correlative study. *Am J Surg Pathol* 1990; 14: 578-83.
26. Silverstein MJ, Lagios MD, Recht A, et al. Image-detected breast cancer: state of the art diagnosis and treatment. *J Am Coll Surg* 2005; 201: 586-97.
27. Aaltomaa S, Lipponen P, Eskelinen M, et al. Lymphocyte infiltrates as a prognostic variable in female breast cancer. *Eur J Cancer* 1992; 28a: 859-64.
28. Wein L, Savas P, Luen SJ, Virassamy B, Salgado R, Loi S. Clinical validity and utility of tumor-infiltrating lymphocytes in routine clinical practice for breast cancer patients: current and future directions. *Front Oncol* 2017; 7: 156.
29. Hendry S, Salgado R, Gevaert T, et al. Assessing tumor-infiltrating lymphocytes in solid tumors: a practical review for pathologists and proposal for a standardized method from the International Immunology Biomarkers Working Group: part 2: TILs in melanoma, gastrointestinal tract carcinomas, non-small cell lung carcinoma and mesothelioma, endometrial and ovarian carcinomas, squamous cell carcinoma of the head and neck, genitourinary carcinomas, and primary brain tumors. *Adv Anat Pathol* 2017; 24: 311-35.
30. Dieci MV, Radošević-Robin N, Fineberg S, et al. Update on tumor-infiltrating lymphocytes (TILs) in breast cancer, including recommendations to assess TILs in residual disease after neoadjuvant therapy and in carcinoma in situ: a report of the International Immunology Biomarker Working Group on Breast Cancer. *Semin Cancer Biol* 2018; 52: 16-25.
31. Denkert C, Wienert S, Poterie A, et al. Standardized evaluation of tumor-infiltrating lymphocytes in breast cancer: results of the ring studies of the international immunology biomarker working group. *Mod Pathol* 2016; 29: 1155-64.
32. Kos Z, Roblin E, Kim RS, et al. Pitfalls in assessing stromal tumor-infiltrating lymphocytes (sTILs) in breast cancer. *NPJ Breast Cancer* 2020; 6: 17.
33. Chevallier B, Roche H, Olivier JB, Chollet P, Hurteloup P. Inflammatory breast cancer. Pilot study of intensive induction chemotherapy (FEC-HD) results in a high histologic response rate. *Am J Clin Oncol* 1993; 16: 223-8.
34. Sataloff DM, Mason BA, Prestipino AJ, Seinige UL, Lieber CP, Baloch Z. Pathologic response to induction chemotherapy in locally advanced carcinoma of the breast: a determinant of outcome. *J Am Coll Surg* 1995; 180: 297-306.

35. Fisher ER, Wang J, Bryant J, Fisher B, Mamounas E, Wolmark N. Pathobiology of preoperative chemotherapy: findings from the National Surgical Adjuvant Breast and Bowel (NSABP) protocol B-18. *Cancer* 2002; 95: 681-95.
36. Ogston KN, Miller ID, Payne S, et al. A new histological grading system to assess response of breast cancers to primary chemotherapy: prognostic significance and survival. *Breast* 2003; 12: 320-7.
37. Symmans WF, Peintinger F, Hatzis C, et al. Measurement of residual breast cancer burden to predict survival after neoadjuvant chemotherapy. *J Clin Oncol* 2007; 25: 4414-22.
38. Mittendorf EA, Jeruss JS, Tucker SL, et al. Validation of a novel staging system for disease-specific survival in patients with breast cancer treated with neoadjuvant chemotherapy. *J Clin Oncol* 2011; 29: 1956-62.
39. Chollet P, Abrial C, Durando X, et al. A new prognostic classification after primary chemotherapy for breast cancer: residual disease in breast and nodes (RDBN). *Cancer J* 2008; 14: 128-32.
40. Mrkonjic M, Berman HK, Done SJ, Youngson B, Mulligan AM. Breast specimen handling and reporting in the post-neoadjuvant setting: challenges and advances. *J Clin Pathol* 2019; 72: 120-32.
41. Bossuyt V. Processing and reporting of breast specimens in the neoadjuvant setting. *Surg Pathol Clin* 2018; 11: 213-30.
42. Hennessy BT, Hortobagyi GN, Rouzier R, et al. Outcome after pathologic complete eradication of cytologically proven breast cancer axillary node metastases following primary chemotherapy. *J Clin Oncol* 2005; 23: 9304-11.
43. von Minckwitz G, Untch M, Blohmer JU, et al. Definition and impact of pathologic complete response on prognosis after neoadjuvant chemotherapy in various intrinsic breast cancer subtypes. *J Clin Oncol* 2012; 30: 1796-804.
44. Pinder SE, Provenzano E, Earl H, Ellis IO. Laboratory handling and histology reporting of breast specimens from patients who have received neoadjuvant chemotherapy. *Histopathology* 2007; 50: 409-17.
45. Smith IC, Heys SD, Hutcheon AW, et al. Neoadjuvant chemotherapy in breast cancer: significantly enhanced response with docetaxel. *J Clin Oncol* 2002; 20: 1456-66.
46. Allison KH, Hammond ME, Dowsett M, et al. Estrogen and progesterone receptor testing in breast cancer: ASCO/CAP guideline update. *J Clin Oncol* 2020; 38: 1346-66.
47. Wolff AC, Hammond MEH, Allison KH, et al. Human epidermal growth factor receptor 2 testing in breast cancer: American Society of Clinical Oncology/College of American Pathologists clinical practice guideline focused update. *J Clin Oncol* 2018; 36: 2105-22.
48. Harvey JM, Clark GM, Osborne CK, Allred DC. Estrogen receptor status by immunohistochemistry is superior to the ligand-binding assay for predicting response to adjuvant endocrine therapy in breast cancer. *J Clin Oncol* 1999; 17: 1474-81.
49. Ahn S, Woo JW, Lee K, Park SY. HER2 status in breast cancer: changes in guidelines and complicating factors for interpretation. *J Pathol Transl Med* 2020; 54: 34-44.
50. Wolff AC, Hammond ME, Hicks DG, et al. Recommendations for human epidermal growth factor receptor 2 testing in breast cancer: American Society of Clinical Oncology/College of American Pathologists clinical practice guideline update. *J Clin Oncol* 2013; 31: 3997-4013.
51. Luporsi E, Andre F, Spyrtos F, et al. Ki-67: level of evidence and methodological considerations for its role in the clinical management of breast cancer: analytical and critical review. *Breast Cancer Res Treat* 2012; 132: 895-915.
52. Yerushalmi R, Woods R, Ravdin PM, Hayes MM, Gelmon KA. Ki67 in breast cancer: prognostic and predictive potential. *Lancet Oncol* 2010; 11: 174-83.
53. Viale G, Giobbie-Hurder A, Regan MM, et al. Prognostic and predictive value of centrally reviewed Ki-67 labeling index in postmenopausal women with endocrine-responsive breast cancer: results from Breast International Group Trial 1-98 comparing adjuvant tamoxifen with letrozole. *J Clin Oncol* 2008; 26: 5569-75.
54. Penault-Llorca F, André F, Sagan C, et al. Ki67 expression and docetaxel efficacy in patients with estrogen receptor-positive breast cancer. *J Clin Oncol* 2009; 27: 2809-15.
55. Dowsett M, Nielsen TO, A'Hern R, et al. Assessment of Ki67 in breast cancer: recommendations from the International Ki67 in Breast Cancer working group. *J Natl Cancer Inst* 2011; 103: 1656-64.

# Imaging features of breast cancer molecular subtypes: state of the art

Nariya Cho<sup>1,2,3</sup>

<sup>1</sup>Department of Radiology, Seoul National University Hospital, Seoul;

<sup>2</sup>Department of Radiology, Seoul National University College of Medicine, Seoul;

<sup>3</sup>Institute of Radiation Medicine, Seoul National University Medical Research Center, Seoul, Korea

Characterization of breast cancer molecular subtypes has been the standard of care for breast cancer management. We aimed to provide a review of imaging features of breast cancer molecular subtypes for the field of precision medicine. We also provide an update on the recent progress in precision medicine for breast cancer, implications for imaging, and recent observations in longitudinal functional imaging with radiomics.

**Key Words:** Breast neoplasms; Magnetic resonance imaging; Gene expression profiles

**Received:** August 9, 2020 **Revised:** September 3, 2020 **Accepted:** September 6, 2020

**Corresponding Author:** Nariya Cho, MD, PhD, Department of Radiology, Seoul National University Hospital, 101 Daehak-ro, Jongno-gu, Seoul 03080, Korea  
Tel: +82-2-2072-1862, Fax: +82-2-743-6385, E-mail: river7774@gmail.com

Gene expression profiling has revealed that there are four major breast cancer subtypes: luminal A, luminal B, human epidermal growth factor receptor 2 (HER2)-enriched, and basal-like tumors [1-3]. Each subtype has varied prognoses, risk of progression, response to treatment, and survival outcomes. In general, basal-like tumors have the worst prognosis, while luminal A tumors have the best prognosis. However, as full genomic analysis is costly and time consuming in clinical practice, the St. Gallen International Expert Consensus panel has suggested surrogate subtypes based on semiquantitative immunohistochemistry (IHC) scoring of estrogen receptor (ER), progesterone receptor (PR), and in situ hybridization tests for HER2 overexpression as follows: luminal A (ER and/or PR positive, HER2 negative), luminal B (ER and/or PR positive and HER2 positive or Ki67  $\geq 14\%$ ), HER2-enriched (HER2 amplified, ER and PR negative), and triple-negative breast cancer (TNBC; ER, PR, and HER2 negative) [4-6] (Table 1). Type determination by percutaneous image-guided biopsy is the first step in managing systemic therapy strategy for breast cancer, because traditional prognostic factors including tumor size, histologic grade, and lymph node status do not fully reflect the heterogeneity of breast cancer, and treatment guidelines are no longer based solely on anatomic stage. The biological diversity of tumors requires the continual refinement of treatment algorithms, which are more and more person-

alized in the recent St. Gallen Consensus Guidelines [6]. The escalating strategy includes longer duration of anti-estrogen therapy, ovarian function suppression, dual blockade with anti-HER2 therapy, and residual tumor treatment following neoadjuvant chemotherapy [6]. The de-escalating strategy includes omission of adjuvant chemotherapy, shortening of radiation therapy, and avoidance of axillary dissection [6]. However, percutaneous biopsy sampling does not represent the topographic heterogeneity of a whole tumor. Moreover, as breast cancer continuously evolves following systemic therapy, spatio-longitudinal monitoring of a whole tumor using imaging modalities during systemic therapy is crucial.

The earliest imaging studies have reported that the triple-negative subtype has non-calcified and circumscribed margins, the luminal subtype mass is irregular with spiculated margins, and the HER2-positive subtype mass has pleomorphic calcifications [7]. While repeated measurements of voxel-based signal intensity of whole tumor is feasible, with breast magnetic resonance imaging (MRI) there are several studies that link imaging phenotypes using radiomics analysis with breast cancer molecular subtypes. In this article, we aim to help readers to stay up-to-date and play a role as key members of a multidisciplinary team for breast cancer treatment.



## RADIOMICS IN BREAST CANCER

Radiomics is a technique to extract and select the quantitative features of radiologic images, to create a high-dimensional data set, and to draw hypotheses, which will lead to better clinical decisions [8]. In breast radiomics analysis, determination of benign or malignant lesion, correlation with prognostic factors, prediction of the response to systemic chemotherapy or lymph node metastasis have been studied. Radiomics features are mathematically defined and classified into morphology, histogram, texture, or transformed features [8]. Morphology features are compactness, roundness, or convexity. Histogram features are median, entropy, uniformity, skewness, or kurtosis, in which spatial information is not included. Conversely, texture features include the spatial information. Gray-level co-occurrence matrix (GLCM)-based features are the most commonly used method for textural analysis [8]. The relationship between voxels and their neighborhoods are characterized in GLCM analysis. Entropy, contrast, and homogeneity, which reflect the uniformity or heterogeneity of the voxel signal intensities, are the main parameters of GLCM models. Transform-based features such as Laplacian of Gaussian and wavelet are commonly used; these transform the original image, creating a new image from which the features

can be quantified.

Application of radiomics in distinguishing molecular subtypes is one of the most intensely studied areas (Table 2) [9–20]. Leithner et al. [9] reported accuracies of 81%–89% in distinguishing luminal A from luminal B, luminal B from triple-negative, luminal B from all others, and HER2-enriched from all others. In their study, the region of interest of a tumor was drawn, and gray-level normalization was performed to minimize the effect of contrast variations. Then, first-order histogram, GLCM, and transform-based features were calculated. Feature selection to reduce the dimensionality of texture features, to select the minimal numbers of features explaining the phenomenon, were performed. K-nearest neighbor classification with leave-one-out cross validation was performed for classification [9]. More recent studies using radiomic analysis reported an area under the receiver operating characteristic curve (AUC) of 0.844 in the prediction of disease-free survival of TNBC [10] and an AUC of 0.890 in the differentiation of HER2-positive tumors vs. -negative tumors [11]. The radiomics approach is based on the premise that microstructural variations between molecular subtypes would cause various gray-level textures on contrast enhanced MRI. The radiomics approach has the potential to provide prognostic information of spatio-longitudinal

**Table 1.** Treatment-oriented classification of subgroups of breast cancer from St. Gallen consensus guidelines

Clinical grouping	Notes	Type of therapy
Triple-negative	Negative ER, PR, and HER2	Cytotoxic chemotherapy including anthracycline and taxane Consideration of capecitabine for residual tumor after neoadjuvant chemotherapy
ER negative and HER2 positive	American Society of Clinical Oncology (ASCO)/College of American Pathologists (CAP) guideline 2018 <sup>a</sup>	Stage 1: paclitaxel+trastuzumab as adjuvant therapy Stage 2 or 3: Neoadjuvant anthracycline, alkylator-, and taxane-based chemotherapy + trastuzumab- and pertuzumab-based treatment (dual anti-HER2 therapy) Trastuzumab emtansine therapy for residual tumor after neoadjuvant chemotherapy in adjuvant setting
ER positive and HER2 positive	ASCO/CAP guidelines 2018 <sup>a</sup>	As above + endocrine therapy appropriate to menopausal status
ER positive and HER2 negative	ER and/or PR-positive $\geq 1\%$ <sup>b</sup>	Endocrine therapy alone according to menopausal status
Luminal A-like (high receptor, low proliferation, low grade)	Multi-parameter molecular marker 'good' if available <sup>c</sup> High ER/PR and clearly low Ki-67 or grade	Endocrine therapy + adjuvant chemotherapy
Intermediate	Multi-parameter molecular marker 'intermediate' if available Uncertainty persists about degree of risk and responsiveness to endocrine and cytotoxic therapies	
Luminal B-like (low receptor, high proliferation, high grade)	Multi-parameter molecular marker 'bad' if available. Lower ER/PR with clearly high Ki-67, high histological grade 3	Endocrine therapy + adjuvant chemotherapy

Modified from Coates AS et al. *Ann Oncol* 2015;26:1533–46 [4] and Burstein HJ et al. *Ann Oncol* 2019;30:1542–57 [6], according to the Creative Commons license.

ER, estrogen receptor; PR, progesterone receptor; HER2, human epidermal growth factor receptor 2; TNBC, triple-negative breast cancer.

<sup>a</sup>An immunohistochemistry of c-erbB-2 staining 3+ score was defined as HER2-positive, while a 0 or 1+ score was negative. For tumors with 2+ score, *HER2* gene copies to the centromeric region of chromosome 17 ratios  $< 2.0$  by fluorescence in situ hybridization must be interpreted as negative due to the lack of evidence for any benefit from HER2 targeted therapy; <sup>b</sup>If ER values fall between 1% and 9%, the term equivocal should not be used, suggesting response to endocrine therapy even in low ER (1%–9%). Low HR expression is associated with higher Ki-67, higher grade, and loss PR positivity, as well as higher recurrence score and higher chemo-sensitivity. Chemotherapy should be given following guidelines for TNBC. Endocrine therapy should be recommended despite the likely extremely small benefit; <sup>c</sup>No role for gene testing in clinical pathologic low risk cases (pT1a, pT1b, G1, ER high, pN0).

**Table 2.** Publications regarding radiomics features of breast cancer according to molecular subtype

Study	No.	Imaging Parameters	Outcomes	Results
Leithner et al. (2019) [9]	143	First order histogram, co-occurrence matrix	Luminal A, luminal B, TNBC, HER2-enriched	Accuracy: luminal B vs. luminal A, 84.2%; luminal B vs. TNBC, 83.9%; luminal B vs. all others, 89%; HER2-enriched vs. all others, 81.3%
Kim et al. (2020) [10]	228	Radiomics score from 5 MRI features	Disease free survival outcome of TNBC	Combined clinicopathological and radiomics feature model showed highest AUC (0.844) in prediction of DFS
Song et al. (2020) [11]	92	GLCM features	HER2-positive vs. -negative tumors determined by FISH test	Among 3 machine learning methods, LRA, QDA, and SVM, AUC of SVM was the best (0.890)
Mazurowski et al. (2014) [12]	48	Semiautomatically extracted MRI features	TCGA database contains full genomic sequencing	Higher ratio of lesion enhancement rate to background parenchymal enhancement was more likely to be luminal B subtype
Grimm et al. (2015) [13]	275	56 Features (morphologic, texture, and dynamic features)	luminal A, luminal B, HER2, basal	Luminal A and luminal B molecular subtype were associated with semiautomatically extracted imaging features
Bae et al. (2015) [14]	280	Tumor roundness score	ER, PR, Ki-67	ER score and Ki-67 index were independent factors determining tumor roundness. TNBC showed the highest mean roundness scores compared with the other subtypes
Sutton et al. (2015) [15]	95	Morphology, histogram features, GLCM features	Oncotype DX recurrence score of Luminal A tumor	An increased kurtosis was found to be a statistically significant factor correlating with Oncotype DX recurrence score
Vaughn et al. (2016) [16]	221	Texture features	Hormone receptor-positive and -negative cancers demonstrated significantly different entropy features	Textural differences on contrast-enhanced MR images might reflect underlying lesion subtypes
Li et al. (2016) [17]	91	Texture features	Luminal A, luminal B, HER2-enriched, and basal-like subtype	Enhancement texture (entropy) and molecular subtypes were related. AUC of ER+ vs. ER-: 0.89, PR+ vs. PR-: 0.69, HER2+ vs. HER2-: 0.65, TNBC vs. others: 0.67
Agner et al. (2014) [18]	76	Morphology, kinetic intensity, histogram features, GLCM features	TNBC, HER2, ER-positive tumors	AUC of texture features (more heterogeneity) for TNBC vs. other subtypes: 0.73 to 0.74
Chamming's et al. (2018) [19]	85	Fine, medium, and coarse texture for mean, standard deviation, mean proportion of positive pixels, entropy, skewness, and kurtosis	pCR of TNBC	kurtosis appears to be associated with pCR to neoadjuvant chemotherapy in non-TNBC and may be a promising biomarker for the identification of TNBC
Braman et al. (2017) [20]	117	Intratumoral and peritumoral texture features	Prediction of pCR	Combined intratumoral and peritumoral radiomics for prediction of pCR yielded AUC 0.83 for HR+ HER2-, Non-pCR was characterized by elevated peritumoral heterogeneity during initial phase. For TNBC/HER+ tumors were best characterized by a peritumoral speckled enhancement.

TNBC, triple-negative breast cancer; HER2, human epidermal growth factor receptor 2; MRI, magnetic resonance imaging; AUC, area under the receiver operating characteristic curve; DFS, disease-free survival; GLCM, gray-level co-occurrence matrix; FISH, fluorescence in situ hybridization; LRA, logistic regression analysis; QDA, quadratic discriminant analysis; SVM, support vector machine; TCGA, The Cancer Genome Atlas; ER, estrogen receptor; PR, progesterone receptor; pCR, pathological complete response.

biology changes of the peritumoral parenchyma as well as of the tumor itself. Moreover, deep learning methods have increasingly been applied in recent radiomics studies [8,11]. The deep learning approach, which is data driven and capable of learning relevant features from the data themselves, has shown superior performance in various tasks in radiology [8,11]. In the near future, radiomics parameters based on a deep learning algorithm would be useful surrogate markers for precision medicine in breast cancer treatment.

## LUMINAL SUBTYPE

About 70% of breast cancers are ER positive and show a more favorable prognosis than ER-negative cancers. Within ER-positive/HER2-negative breast cancer, 90%–95% are luminal A or B subtypes [3]. The luminal B subtype shows higher proliferation gene expression [2] and worse recurrence-free survival outcomes compared with the luminal A subtype, although the luminal B subtype shows higher pathological complete response

(pCR) rate following neoadjuvant chemotherapy [3]. Thus, differentiation between luminal A and B tumors is important for deciding the duration of endocrine therapy or to predict resistance to endocrine therapy [3]. There is a 30 to 44% discordance rate between the gene expression profiling and surrogate IHC classifications [3,21]. Within ER-positive/HER2-negative breast cancers, 5%–10% of tumors are non-luminal subtypes (HER2 enriched and basal-like tumors) by gene expression profiling [3]. Non-luminal (ER positive/HER2 negative) breast cancers show worse outcomes compared with the luminal A subtype when they were treated with 5 years of adjuvant tamoxifen-only [22]. One study reported that 80% of tumors showing low expression ER positive (1%–9%) were non-luminal subtypes [23].

For patients with ER-positive tumors, prognostic signatures including 70-gene MammaPrint microarray assay (Agendia, Amsterdam, The Netherlands), the 50-gene PAM50 assay (Prosigna, Nanostring Technologies, Seattle, WA, USA), and the 21-gene Oncotype DX assay (Genomic Health, Redwood City, CA, USA) are commercially available [24]. These signatures al-

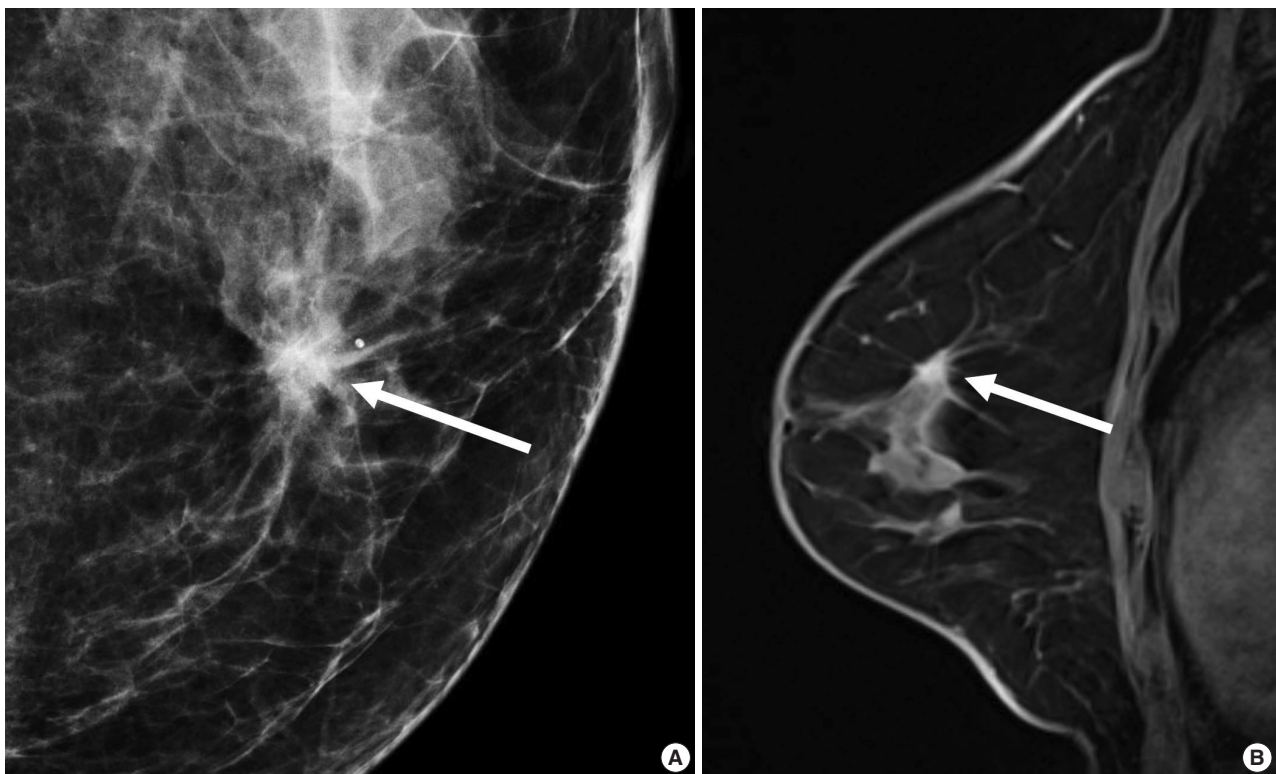


**Fig. 1.** A 56-year-old woman with a luminal A-like breast cancer. (A) Mammography shows a spiculated mass with calcifications (arrow). (B) Enhanced T1-weighted magnetic resonance imaging shows an irregular, spiculated mass (arrow). Histopathology revealed a 1.5-cm invasive ductal carcinoma with low histologic grade. American Joint Committee on Cancer (AJCC) anatomic stage was T1N0M0. Immunohistochemistry analysis revealed that estrogen receptor 90% positive, progesterone receptor 1% positive, human epidermal growth factor receptor 2–negative, and Ki-67, 1% positive. Multigene assay recurrence score was 10 and low risk. The 9-year distant recurrence risk was estimated as 3%. She did not receive adjuvant chemotherapy, but received aromatase inhibitor.



low us to distinguish prognosis of patients according to the proliferation-associated genes expression levels [24]. However, the signatures do not apply to patients with ER-negative tumors, because more than 95% of them already have high expression of proliferation-associated genes [24,25]. The oncotype DX assay analyzes a panel of 21 genes to decide a recurrence score (RS) representing the possibility of recurrent cancer within 10 years. Adjuvant chemotherapy provides greater benefits for patients with high-RS tumors and does very little for patients with low-RS tumors (Fig. 1) [26].

In morphologic analyses for mammography, ER-positive tumor tends to show a not-circumscribed margin (Fig. 1), which is in contrast to ER-negative tumors [12,13,27]. Tumor roundness score, quantifying the relative similarity to a perfect circle, has been shown to have an inverse correlation with the ER expression (%) and a positive correlation with the Ki-67 index [14]. By ultrasonography, parallel orientation (odds ratio [OR], 5.53;  $p = .02$ ) and tumor roundness (OR, 1.70 per 10 increase in the roundness value;  $p = .01$ ) were independent features associated

with high RS on Oncotype DX [28]. The high-risk group was also associated with the presence of calcifications, similar to a previous study in which a mass with pleomorphic microcalcifications might be associated with an intermediate to high RS in ER-positive, HER2-negative early breast cancer at mammography [29].

A previous report on MRI results demonstrated that patients with luminal B subtype tended to have multifocal or multicentric cancer 2.8 times more often than patients with luminal A subtype [30]. Sutton et al. [15] reported that an increased kurtosis was associated with high RS on Oncotype DX for ER-positive/HER2-negative tumors (Fig. 2). Kurtosis is a second order parameter quantifying the amount of histogram deviating from a Gaussian shape. High kurtosis might reflect the amount of heterogeneity in a complex way, and these tumors are believed to be more biologically aggressive [19]. This result is in line with a study reporting that both ER-positive and ER-negative tumors showed statistically different entropy levels [16]. The entropy reflecting spatial distribution pattern of grayness of voxel is also believed to be an important biomarker at textural analysis of medical image.

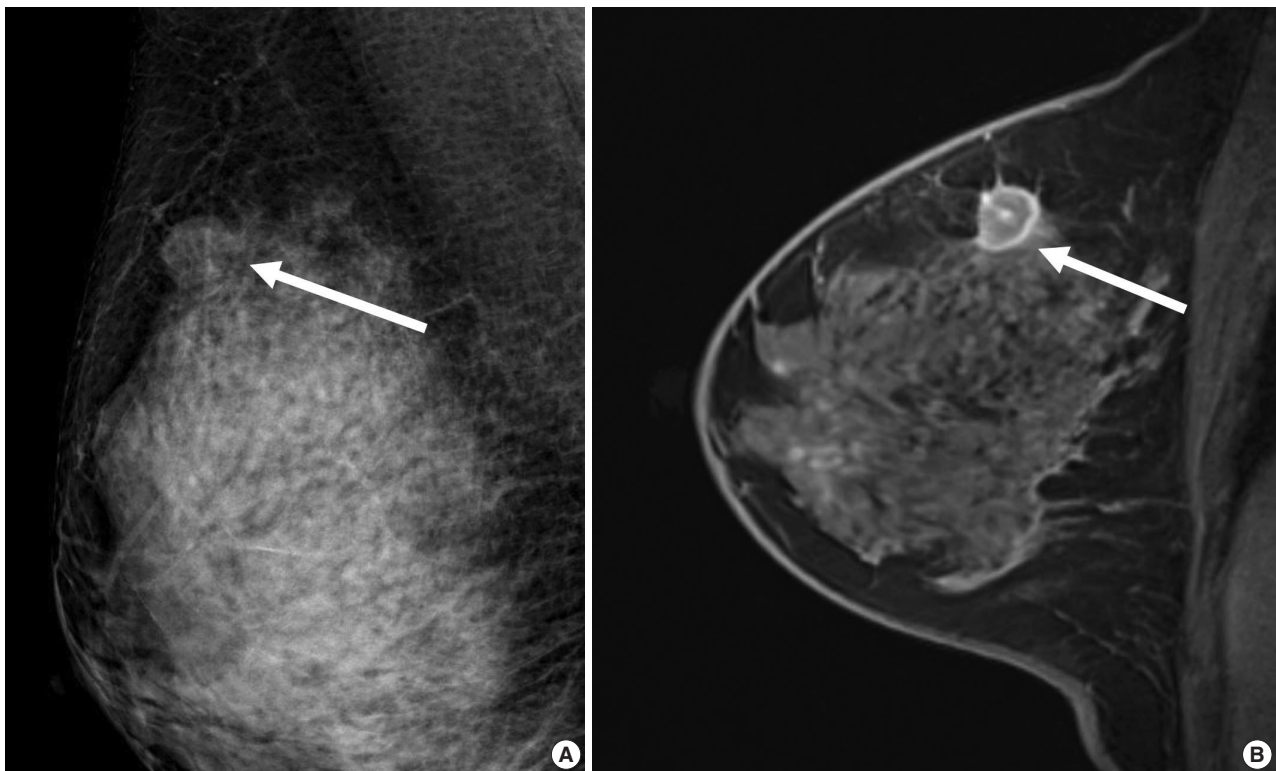


**Fig. 2.** A 44-year-old woman with a luminal A-like breast cancer. (A) Mammography shows an oval non-calcified mass (arrow). (B) Enhanced T1-weighted magnetic resonance imaging shows an irregular mass with internal rim-enhancement (arrow). Histopathology revealed a 1.7-cm invasive ductal carcinoma with intermediate histologic grade. American Joint Committee on Cancer (AJCC) anatomic stage was T1N0M0. Immunohistochemistry analysis revealed that estrogen receptor 90% positive, progesterone receptor 5% positive, human epidermal growth factor receptor 2 negative, and Ki-67, 4% positive. Multigene assay recurrence score was 23. The 10-year distant recurrence risk was estimated as 12% and high risk. She received adjuvant chemotherapy and tamoxifen.

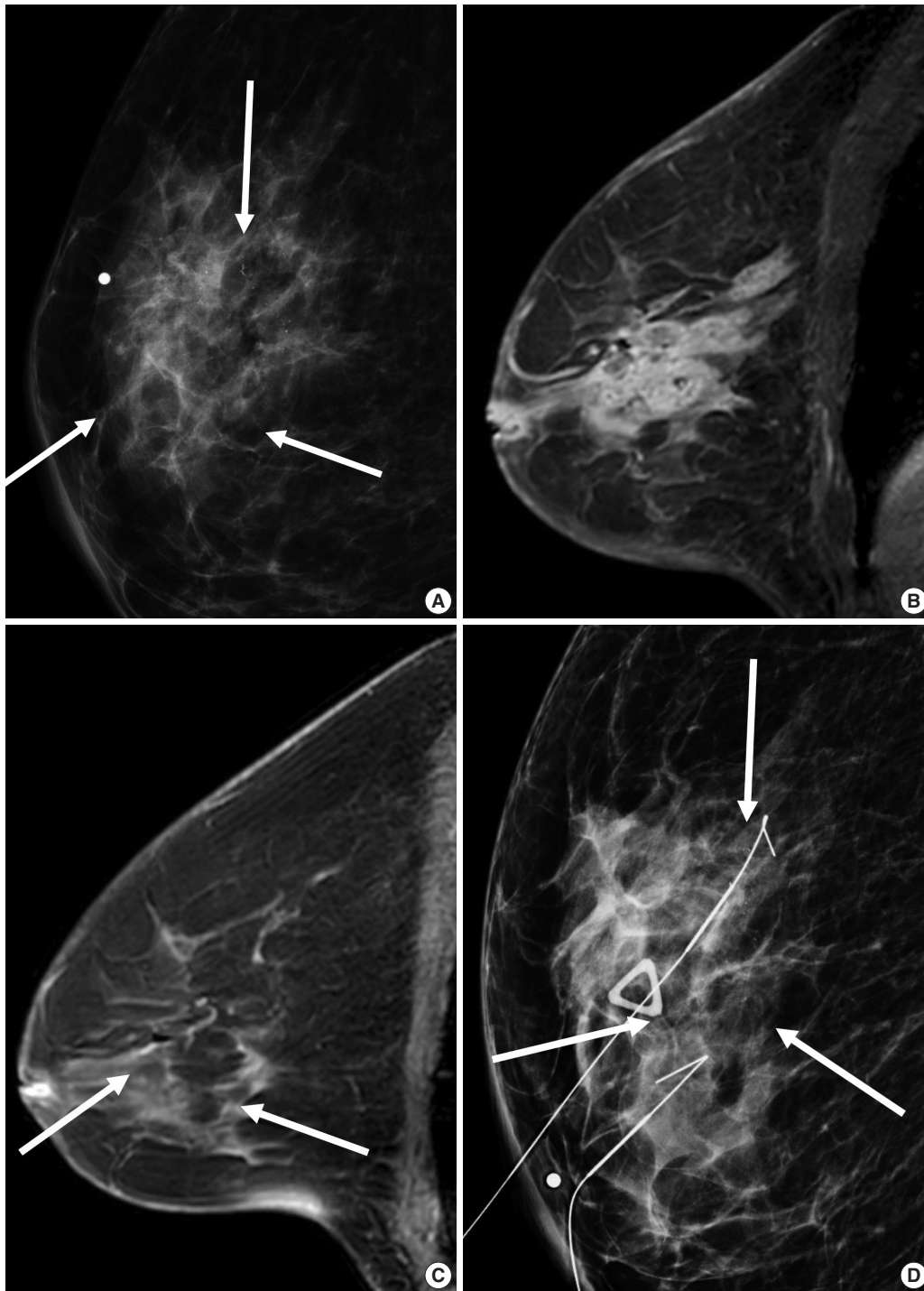


**Fig. 3.** A 67-year-old woman with a human epidermal growth factor receptor 2 (HER2)-positive breast cancer. (A) Mammography shows ill-defined asymmetry with pleomorphic microcalcifications (arrows). (B) Enhanced T1-weighted magnetic resonance imaging (MRI) shows an 8.2-cm ill-defined, diffuse irregular mass with internal heterogeneous enhancement. Needle biopsy revealed an invasive ductal carcinoma with high histologic grade. Immunohistochemistry analysis revealed that estrogen receptor and progesterone receptor negative, and HER2 positive. (C) Following combined docetaxel, carboplatin and dual HER2 blockade, there is no residual mass and but subtle enhancements in the breast on MRI (arrows). (D) Mammography shows two hookwires around the residual calcifications (arrows). Surgical histopathology revealed pathological complete response in the breast and axilla.

## HUMAN EPIDERMAL GROWTH FACTOR RECEPTOR 2-ENRICHED SUBTYPE

HER2 overexpression is found in approximately 20% of invasive breast cancers. It is associated with worse prognosis but good response to HER2-targeted therapies [31] and is reported to increase cell proliferation, survival, mobility, and invasiveness, as well as neo-angiogenesis at the cellular level [32]. The Cancer Genome Atlas (TCGA) and clinical trials have suggested that HER2-positive tumors are a heterogeneous group of cancers [3]. Compared with ER-positive/HER2-positive tumors, patients with ER-negative/HER2-positive tumors show a higher risk of death within 5 years of diagnosis; the first recurrence in brain was higher and in bone was lower, and the response rate to neoadjuvant chemotherapy was higher [33,34]. HER2-targeted agents combined with chemotherapy are recommended for ER-negative/HER2-positive tumors, and HER2-targeted agents with endocrine therapy are recommended for ER-positive/HER2-positive tumors [4]. A higher pCR rate was observed in patients with ER-negative/HER2-positive tumors than in patients with ER-positive/HER2-positive tumors [35]. The pCR rate was over 70% using the dual HER2 blockade, either with trastuzumab with lapatinib or trastuzumab with pertuzumab in combination with chemotherapy [6].

HER2 overexpression was also associated with the presence of calcifications, branching or fine linear shape calcifications, high

level of suspicion on mammography, and a washout or fast early enhancement kinetic curve pattern on MRI (Fig. 3) [36]. MRI showed that patients with the HER2 subtype tended to have 4.1 times more multifocal or multicentric cancers than patients with the luminal A subtype [30]. Fine pleomorphic/fine linear or linear branching calcification morphology on mammography (OR, 7.23), PR negativity (OR, 6.76), and a high TILs (tumor-infiltrating lymphocytes) level (OR, 5.92) were independent factors associated with pCR in patients receiving neoadjuvant chemotherapy with dual HER2 blockade (Fig. 3) [37]. Low tumor peak enhancement at MRI indicating less aggressiveness was significantly associated with high TILs (OR, 1.01;  $p = .020$ ) [38]. These results are consistent with previous studies showing that TILs observed in breast cancers were associated with higher rate of pCR or improved overall survival outcomes [5,6]. Moreover, increasing TILs during systemic therapy was reported to be correlated with pCR [39], which suggests that MRI could provide valuable information regarding response during treatment.

## BASAL-LIKE SUBTYPES

TNBC comprises 10%–20% of all breast cancers. The term of TNBC and basal-like tumors are interchangeably used because 86% of TNBC are the basal-like subtype [3]. However, each of the intrinsic subtypes exist within a TNBC [40], and TNBC is a very heterogeneous group of tumors based on ge-

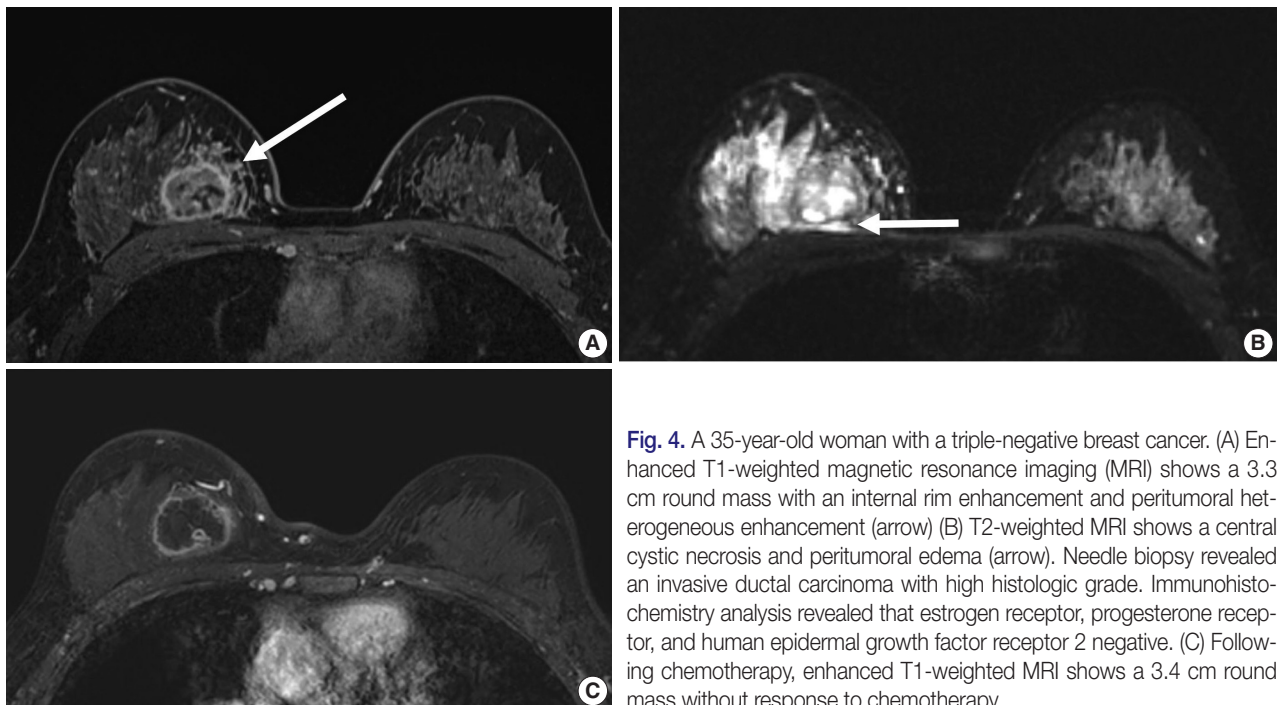


**Fig. 4.** A 35-year-old woman with a triple-negative breast cancer. (A) Enhanced T1-weighted magnetic resonance imaging (MRI) shows a 3.3 cm round mass with an internal rim enhancement and peritumoral heterogeneous enhancement (arrow) (B) T2-weighted MRI shows a central cystic necrosis and peritumoral edema (arrow). Needle biopsy revealed an invasive ductal carcinoma with high histologic grade. Immunohistochemistry analysis revealed that estrogen receptor, progesterone receptor, and human epidermal growth factor receptor 2 negative. (C) Following chemotherapy, enhanced T1-weighted MRI shows a 3.4 cm round mass without response to chemotherapy.



netic profiling [41]. Rates of pCR after receiving anthracycline/taxane regimen are 25%–35% and patients with pCR show a better outcome in patients with TNBC [25]. Recent St. Gallen Consensus Conference Guidelines recommended that TILs should be routinely characterized for TNBC in view of their prognostic value [6]. Tumor programmed death-ligand 1 and immune-cell programmed death-1 expression are considered as markers to predict benefit from immunotherapy for advanced TNBC [6]. Also, in TNBC with residual disease following neoadjuvant chemotherapy, post-neoadjuvant treatment with capecitabine showed survival benefits [42].

Unifocal, circumscribed margin, round shape, and no associated calcifications are signatures of TNBC [43]. Circumscribed margin and round shape are more commonly found in high-grade tumors and spiculation is more frequently found in low-grade tumors [44]. TNBC has been shown to have a higher tumor roundness score compared with the other subtypes, reflecting a more biologically aggressive tumor type. Absence of calcifications is also considered representative of rapid malignant transformation of TNBC with bypassing of the in-situ stage [43]. TNBC shows a round mass with rim enhancement on MRI and frequently has internal high signal intensity on T2-weighted MRI [45–47] (Fig. 4). Recent studies using radiomics analysis have reported that TNBC masses tend to be larger, have a more heterogeneous enhancement texture, are more irregularly shaped, and have a rapid enhancement rate compared with other subtypes [17,18]. Notably, the heterogeneous enhancement texture, quantified at the first post-contrast enhanced MRI, has emerged as a discriminatory indicator for tumor subtype, regardless of tumor size [17,18]. Waugh et al. [16] also reported that TNBC and HER2 subtypes showed increased entropy values compared with luminal A and luminal B subtypes.

In the neoadjuvant chemotherapy setting, intratumoral necrosis was associated with non-response to chemotherapy [48] and peritumoral edema was associated with worse recurrence-free-survival outcome of TNBC (Fig. 4) [49]. With textural analysis, increased kurtosis of non-TNBC on T2 weighted image was independently associated with pCR; however, the association between increased kurtosis and pCR was not found in TNBC [19]. In another study predicting pCR by using radiomics, Braman et al. reported that combined intratumoral and peritumoral radiomic features yielded a maximum AUC of 0.83 for the ER-positive/HER2-negative group and 0.93 for TNBC or HER2-positive group [20]. In Braman et al's study [20], elevated peritumoral heterogeneity was associated with non-pCR in ER-positive/HER2-negative tumors, and peritumoral speckled en-

hancement pattern was associated with non-pCR in TNBC or HER2-positive tumors (Fig. 4A) [20]. These results are in line with peritumoral lymphatics or vascular invasion, and peritumoral immune response as predictors of survival. In addition, TILs, known as a favorable prognostic factor in TNBC, could be quantified by textural analysis [20]. Thus, peritumoral radiomics features on MRI could be valuable predictors of pCR in TNBC and HER2-positive tumors.

## CONCLUSION

Breast cancer consists of heterogeneous subtypes and evolves continuously after systemic therapy. Earlier studies linking imaging features and molecular subtypes have reported presence of calcifications, margin or shape features, and enhancement features on dynamic contrast enhanced MRI according to each subtype. Recent studies using radiomics parameters, which are indiscernible by the human eye, have shown high accuracy in distinguishing molecular subtypes, prediction of responses to chemotherapy, and prediction of survival outcomes. Imaging biomarkers could be helpful in realizing better precision medicine due to the feasibility of repeated measurements for whole tumors and the applicability of deep-learning based algorithms.

### Ethics Statement

Not applicable.

### ORCID

Nariya Cho <https://orcid.org/0000-0003-4290-2777>

### Conflicts of Interest

The authors declare that they have no potential conflicts of interest.

### Funding Statement

No funding to declare.

### References

1. Cancer Genome Atlas Network. Comprehensive molecular portraits of human breast tumours. *Nature* 2012; 490: 61–70.
2. Sorlie T, Perou CM, Tibshirani R, et al. Gene expression patterns of breast carcinomas distinguish tumor subclasses with clinical implications. *Proc Natl Acad Sci U S A* 2001; 98: 10869–74.
3. Prat A, Pineda E, Adamo B, et al. Clinical implications of the intrinsic molecular subtypes of breast cancer. *Breast* 2015; 24 Suppl 2: S26–35.
4. Coates AS, Winer EP, Goldhirsch A, et al. Tailoring therapies--improving the management of early breast cancer: St Gallen International Expert Consensus on the Primary Therapy of Early Breast Cancer 2015. *Ann Oncol* 2015; 26: 1533–46.
5. Curigliano G, Burstein HJ, Winer EP, et al. De-escalating and escalating treatments for early-stage breast cancer: the St. Gallen Inter-

- national Expert Consensus Conference on the Primary Therapy of Early Breast Cancer 2017. *Ann Oncol* 2017; 28: 1700-12.
6. Burstein HJ, Curigliano G, Loibl S, et al. Estimating the benefits of therapy for early-stage breast cancer: the St. Gallen International Consensus Guidelines for the primary therapy of early breast cancer 2019. *Ann Oncol* 2019; 30: 1541-57.
  7. Cho N. Molecular subtypes and imaging phenotypes of breast cancer. *Ultrasonography* 2016; 35: 281-8.
  8. Lee SH, Park H, Ko ES. Radiomics in breast imaging from techniques to clinical applications: a review. *Korean J Radiol* 2020; 21: 779-92.
  9. Leithner D, Horvat JV, Marino MA, et al. Radiomic signatures with contrast-enhanced magnetic resonance imaging for the assessment of breast cancer receptor status and molecular subtypes: initial results. *Breast Cancer Res* 2019; 21: 106.
  10. Kim S, Kim MJ, Kim EK, Yoon JH, Park VY. MRI radiomic features: association with disease-free survival in patients with triple-negative breast cancer. *Sci Rep* 2020; 10: 3750.
  11. Song L, Lu H, Yin J. Preliminary study on discriminating HER2 2+ amplification status of breast cancers based on texture features semi-automatically derived from pre-, post-contrast, and subtraction images of DCE-MRI. *PLoS One* 2020; 15: e0234800.
  12. Mazurowski MA, Zhang J, Grimm LJ, Yoon SC, Silber JI. Radiogenomic analysis of breast cancer: luminal B molecular subtype is associated with enhancement dynamics at MR imaging. *Radiology* 2014; 273: 365-72.
  13. Grimm LJ, Zhang J, Mazurowski MA. Computational approach to radiogenomics of breast cancer: Luminal A and luminal B molecular subtypes are associated with imaging features on routine breast MRI extracted using computer vision algorithms. *J Magn Reson Imaging* 2015; 42: 902-7.
  14. Bae MS, Seo M, Kim KG, Park IA, Moon WK. Quantitative MRI morphology of invasive breast cancer: correlation with immunohistochemical biomarkers and subtypes. *Acta Radiol* 2015; 56: 269-75.
  15. Sutton EJ, Oh JH, Dashevsky BZ, et al. Breast cancer subtype inter-tumor heterogeneity: MRI-based features predict results of a genomic assay. *J Magn Reson Imaging* 2015; 42: 1398-406.
  16. Waugh SA, Purdie CA, Jordan LB, et al. Magnetic resonance imaging texture analysis classification of primary breast cancer. *Eur Radiol* 2016; 26: 322-30.
  17. Li H, Zhu Y, Burnside ES, et al. Quantitative MRI radiomics in the prediction of molecular classifications of breast cancer subtypes in the TCGA/TCIA data set. *NPJ Breast Cancer* 2016; 2: 16012.
  18. Agner SC, Rosen MA, Englander S, et al. Computerized image analysis for identifying triple-negative breast cancers and differentiating them from other molecular subtypes of breast cancer on dynamic contrast-enhanced MR images: a feasibility study. *Radiology* 2014; 272: 91-9.
  19. Chamming's F, Ueno Y, Ferre R, et al. Features from computerized texture analysis of breast cancers at pretreatment MR imaging are associated with response to neoadjuvant chemotherapy. *Radiology* 2018; 286: 412-20.
  20. Braman NM, Etesami M, Prasanna P, et al. Intratumoral and peritumoral radiomics for the pretreatment prediction of pathological complete response to neoadjuvant chemotherapy based on breast DCE-MRI. *Breast Cancer Res* 2017; 19: 57.
  21. Chia SK, Bramwell VH, Tu D, et al. A 50-gene intrinsic subtype classifier for prognosis and prediction of benefit from adjuvant tamoxifen. *Clin Cancer Res* 2012; 18: 4465-72.
  22. Prat A, Parker JS, Fan C, et al. Concordance among gene expression-based predictors for ER-positive breast cancer treated with adjuvant tamoxifen. *Ann Oncol* 2012; 23: 2866-73.
  23. Iwamoto T, Booser D, Valero V, et al. Estrogen receptor (ER) mRNA and ER-related gene expression in breast cancers that are 1% to 10% ER-positive by immunohistochemistry. *J Clin Oncol* 2012; 30: 729-34.
  24. Ng CK, Schultheis AM, Bidard FC, Weigelt B, Reis-Filho JS. Breast cancer genomics from microarrays to massively parallel sequencing: paradigms and new insights. *J Natl Cancer Inst* 2015; 107:djv015.
  25. Liedtke C, Mazouni C, Hess KR, et al. Response to neoadjuvant therapy and long-term survival in patients with triple-negative breast cancer. *J Clin Oncol* 2008; 26: 1275-81.
  26. Paik S, Tang G, Shak S, et al. Gene expression and benefit of chemotherapy in women with node-negative, estrogen receptor-positive breast cancer. *J Clin Oncol* 2006; 24: 3726-34.
  27. Shin HJ, Kim HH, Huh MO, et al. Correlation between mammographic and sonographic findings and prognostic factors in patients with node-negative invasive breast cancer. *Br J Radiol* 2011; 84: 19-30.
  28. Chae EY, Moon WK, Kim HH, et al. Association between ultrasound features and the 21-gene recurrence score assays in patients with oestrogen receptor-positive, HER2-negative, invasive breast cancer. *PLoS One* 2016; 11: e0158461.
  29. Yepes MM, Romilly AP, Collado-Mesa F, et al. Can mammographic and sonographic imaging features predict the Oncotype DX recurrence score in T1 and T2, hormone receptor positive, HER2 negative and axillary lymph node negative breast cancers? *Breast Cancer Res Treat* 2014; 148: 117-23.
  30. Grimm LJ, Johnson KS, Marcom PK, Baker JA, Soo MS. Can breast cancer molecular subtype help to select patients for preoperative MR imaging? *Radiology* 2015; 274: 352-8.
  31. Arteaga CL, Sliwkowski MX, Osborne CK, Perez EA, Puglisi F, Gianni L. Treatment of HER2-positive breast cancer: current status and future perspectives. *Nat Rev Clin Oncol* 2011; 9: 16-32.
  32. Zhou BP, Hung MC. Dysregulation of cellular signaling by HER2/neu in breast cancer. *Semin Oncol* 2003; 30: 38-48.
  33. Perez EA, Romond EH, Suman VJ, et al. Four-year follow-up of trastuzumab plus adjuvant chemotherapy for operable human epidermal growth factor receptor 2-positive breast cancer: joint analysis of data from NCCTG N9831 and NSABP B-31. *J Clin Oncol* 2011; 29: 3366-73.
  34. Vaz-Luis I, Ottesen RA, Hughes ME, et al. Impact of hormone receptor status on patterns of recurrence and clinical outcomes among patients with human epidermal growth factor-2-positive breast cancer in the National Comprehensive Cancer Network: a prospective cohort study. *Breast Cancer Res* 2012; 14: R129.
  35. Gianni L, Eiermann W, Semiglazov V, et al. Neoadjuvant and adjuvant trastuzumab in patients with HER2-positive locally advanced breast cancer (NOAH): follow-up of a randomised controlled superiority trial with a parallel HER2-negative cohort. *Lancet Oncol* 2014; 15: 640-7.
  36. Elias SG, Adams A, Wisner DJ, et al. Imaging features of HER2 overexpression in breast cancer: a systematic review and meta-analysis. *Cancer Epidemiol Biomarkers Prev* 2014; 23: 1464-83.
  37. Yoon GY, Chae EY, Cha JH, et al. Imaging and clinicopathologic features associated with pathologic complete response in HER2-positive breast cancer receiving neoadjuvant chemotherapy with

- dual HER2 blockade. *Clin Breast Cancer* 2020; 20: 25-32.
38. Choi WJ, Kim Y, Cha JH, et al. Correlation between magnetic resonance imaging and the level of tumor-infiltrating lymphocytes in patients with estrogen receptor-negative HER2-positive breast cancer. *Acta Radiol* 2020; 61: 3-10.
  39. Nuciforo P, Pascual T, Cortes J, et al. A predictive model of pathologic response based on tumor cellularity and tumor-infiltrating lymphocytes (CeTIL) in HER2-positive breast cancer treated with chemo-free dual HER2 blockade. *Ann Oncol* 2018; 29: 170-7.
  40. Prat A, Adamo B, Cheang MC, Anders CK, Carey LA, Perou CM. Molecular characterization of basal-like and non-basal-like triple-negative breast cancer. *Oncologist* 2013; 18: 123-33.
  41. Lehmann BD, Bauer JA, Chen X, et al. Identification of human triple-negative breast cancer subtypes and preclinical models for selection of targeted therapies. *J Clin Invest* 2011; 121: 2750-67.
  42. Masuda N, Lee SJ, Ohtani S, et al. Adjuvant capecitabine for breast cancer after preoperative chemotherapy. *N Engl J Med* 2017; 376: 2147-59.
  43. Dogan BE, Turnbull LW. Imaging of triple-negative breast cancer. *Ann Oncol* 2012; 23 Suppl 6: vi23-9.
  44. Lamb PM, Perry NM, Vinnicombe SJ, Wells CA. Correlation between ultrasound characteristics, mammographic findings and histological grade in patients with invasive ductal carcinoma of the breast. *Clin Radiol* 2000; 55: 40-4.
  45. Uematsu T, Kasami M, Yuen S. Triple-negative breast cancer: correlation between MR imaging and pathologic findings. *Radiology* 2009; 250: 638-47.
  46. Youk JH, Son EJ, Chung J, Kim JA, Kim EK. Triple-negative invasive breast cancer on dynamic contrast-enhanced and diffusion-weighted MR imaging: comparison with other breast cancer subtypes. *Eur Radiol* 2012; 22: 1724-34.
  47. Kim GR, Ku YJ, Cho SG, Kim SJ, Min BS. Associations between gene expression profiles of invasive breast cancer and Breast Imaging Reporting and Data System MRI lexicon. *Ann Surg Treat Res* 2017; 93: 18-26.
  48. Kawashima H, Inokuchi M, Furukawa H, Kitamura S. Triple-negative breast cancer: are the imaging findings different between responders and nonresponders to neoadjuvant chemotherapy? *Acad Radiol* 2011; 18: 963-9.
  49. Bae MS, Shin SU, Ryu HS, et al. Pretreatment MR imaging features of triple-negative breast cancer: association with response to neoadjuvant chemotherapy and recurrence-free survival. *Radiology* 2016; 281: 392-400.



## DNA-protein biomarkers for immunotherapy in the era of precision oncology

Binnari Kim<sup>1,2</sup>, So Young Kang<sup>1</sup>, Kyoung-Mee Kim<sup>1,3</sup>

<sup>1</sup>Department of Pathology and Translational Genomics, Samsung Medical Center, Sungkyunkwan University School of Medicine, Seoul;

<sup>2</sup>Department of Pathology, Ulsan University Hospital, Ulsan;

<sup>3</sup>Center of Clinical Genomics, Samsung Medical Center, Seoul, Korea

The use of biomarkers to guide patient and therapy selection has gained much attention to increase the scope and complexity of targeted therapy options and immunotherapy. Clinical trials provide a basis for discovery of biomarkers, which can then aid in development of new drugs. To that end, samples from cancer patients, including DNA, RNA, protein, and the metabolome isolated from cancer tissues and blood or urine, are analyzed in various ways to identify relevant biomarkers. In conjunction with nucleotide-based, high-throughput, next-generation sequencing techniques, therapy-guided biomarker assays relying on protein-based immunohistochemistry play a pivotal role in cancer care. In this review, we discuss the current knowledge regarding DNA and protein biomarkers for cancer immunotherapy.

**Key Words:** Biomarker; Clinical trial; Next-generation sequencing; Immunohistochemistry

**Received:** June 12, 2020 **Revised:** September 7, 2020 **Accepted:** September 23, 2020

**Corresponding Author:** Kyoung-Mee Kim, MD, Department of Pathology and Translational Genomics, Samsung Medical Center, Sungkyunkwan University School of Medicine, 81 Irwon-ro, Gangnam-gu, Seoul 06351, Korea  
Tel: +82-2-3410-2807, Fax: +82-2-3410-6396, E-mail: kkmkys@skku.edu

Translational research is a two-way process in which new findings from basic research are applied in clinical trials and development of new drugs or treatments. Samples of DNA, RNA, proteins, the metabolome, etc. collected from cancer tissues and blood or urine are analyzed in clinical trials to search for valuable and relevant biomarkers that are crucial for drug development. Next-generation sequencing (NGS) has helped us understand and characterize many cancers, identify new cancer subtypes, develop biomarkers, and discover new treatment targets. NGS also has allowed us to learn about the mutational landscape of several cancers and to develop technologies and drugs targeting “driver” molecular abnormalities. Thus, the oncological community considers NGS as a tool to improve the effectiveness of cancer treatment. Comprehensive, integrated molecular analyses identify molecular relationships across a diverse set of human cancers, suggesting future directions to explore clinical actionability in cancer treatments [1]. Early successes in targeting and identifying individual oncogenic drivers and increased feasibility of tumor genome sequencing have made possible genome-driven oncology

care [2]. We are now using NGS to capture genetic algorithms and register them for clinical trials.

Immunotherapy, especially use of immune checkpoint inhibitors (ICI), has led to dramatic changes in the treatment of several types of cancer in recent years [3]. Given that a small number of patients experience a long-lasting response, development of biomarkers to predict responsiveness to immunotherapy has become important. The most widely investigated biomarkers for immunotherapy are programmed death-ligand 1 (PD-L1), microsatellite instability/defective mismatch repair (MSI/dMMR), and tumor mutational burden (TMB). Although MSI/dMMR has been used for immunotherapy regardless of tumor type, PD-L1 is being used in specific cancer types [3]. In this article, we concisely review the applications of NGS and immunohistochemistry (IHC)-based protein biomarkers, especially PD-L1, in precision oncology and clinical trials.

## TUMOR MUTATIONAL BURDEN

### Clinical significance and cutoff points

Although not yet approved for clinical use, TMB has been shown to predict the response to several forms of immunotherapy across multiple cancer types. Specifically, cancer patients with a high neoantigen load or high TMB are more likely to have a good clinical response to ICI [4].

While not all mutations result in immunogenic neoantigens and determining which mutations are likely to induce immunogenic neoantigens remains a challenge, TMB represents a quantifiable measure of the number of mutations in a tumor that can be used for treatment selection [5]. TMB has been traditionally determined using whole-exome sequencing (WES); however, the high cost and long work time limit its widespread use in clinical settings. Therefore, current precision oncology platforms generally use NGS of targeted gene panels [6]. A recent study analyzing clinical data from 7,033 ICI- and non-ICI-treated advanced-stage cancer patients and genomic data from cancers sequenced with targeted NGS showed that higher somatic TMB (highest 20% in each histology subtype) was associated with better overall survival in all patients [7]. However, the TMB cutoff points associated with improved survival varied markedly between cancer types, suggesting that a universal definition of high TMB may not be possible. Similar findings in patients with gastric cancer were observed when the following cutoff points were applied: 11% for the higher mutation group in 330 non-ICI-treated patients [8] and 14.31 mt/mg in 63 ICI-treated patients [6].

Despite efforts to standardize TMB from multiple genomic profiling cancer panels [4], the cutoff value for TMB remains

inconsistent. TMB is generally defined as the number of non-synonymous somatic mutations per megabase of genome examined, and a detailed description of TMB definitions in recently published papers using targeted sequencing is summarized in Table 1 [6-18].

### Factors affecting tumor mutation burden

Measurement of mutation load using WES can be difficult due to its high cost and extensive analysis and data management requirements. To be applicable in a clinical setting, the following requirements need to be met: the test must be suitable for clinical samples even with a limited amount of DNA; and the test results should be delivered within a limited time, be accurate, help clinical decision-making, and must be affordable. Thus, targeted sequencing with comprehensive gene panels is desirable because of the lower sequencing costs, lower DNA input amounts, and shorter turnaround time [19]. However, the following factors affect TMB calculation: (1) Contents of tumor cell and coverage of sequencing, as targeted cancer panels enable deeper sequencing compared with WES. (2) Presence of sequence artifacts that can be caused by formalin fixation as formalin can cause various crosslinks and is a well-known source of sequencing artifacts due to fragmentation of DNA, denaturation, and deamination of cytosine bases. Specifically, using formalin-fixed paraffin-embedded tissues for NGS causes an increase in DNA sequence artifacts (C:G > T:A) [20].

Pre-analytical factors also affect TMB measurement [19]. Among the most important factors are the size and number of genes included within the targeted cancer panel. The most widely used panels are the MSK-IMPACT panel, which in its latest ver-

**Table 1.** Tumor mutation burden measured by targeted sequencing in various cancer types

Cancer type	No. of patients	Methods	Name of panel	No. of genes	Cutoff (mt/Mb)	Cutoff (percentile)	ICI responses	Study
Pan-cancer	1,638	Targeted sequencing	FoundationOne	~315	20	90	Yes	Goodman et al. [9]
Pan-cancer	2,189	Targeted sequencing	Custom Panel	592	17	92.3	Yes	Vanderwalde et al. [10]
Pan-cancer	1,662	Targeted sequencing	MSK-IMPACT v3	468	8.8	80	Yes	Samstein et al. [7]
SCLC	134	Targeted sequencing	DFCI OncoPanel	447	9.68	50	Yes	Ricciuti et al. [11]
Colorectal	6,004	Targeted sequencing	Comprehensive Genomic Profiling (CGP)	315	11.7	NA	No	Fabrizio et al. [12]
NSCLC	1,649	Targeted sequencing	FoundationOne	324	10	50	Yes	Hellmann et al. [13]
NSCLC	98	Targeted sequencing	FoundationOne	324	10	50	Yes	Ready et al. [14]
Urothelial	316	Targeted sequencing	FoundationOne	315	16	75	Yes	Rosenberg et al. [15]
Urothelial	931	Targeted sequencing	FoundationOne	NA	9.65	50	Yes	Powles et al. [16]
Gastric	330	Targeted sequencing	CancerScan	404	10.5	89	No	Cho et al. [8]
Gastric	581	Targeted sequencing	Custom Panel	592	17	93.1	No	Weinberg et al. [17]
Gastric	80	Targeted sequencing	Oncomine Comprehensive Assay v3	161	10	41	Yes	Mishima et al. [18]
Gastric	63	Targeted sequencing	Oncomine Tumor Mutation Load Assay	409	10.6	80	Yes	Kim et al. [6]

ICI, immune checkpoint inhibitors; SCLC, small cell lung cancer; NA, not available; NSCLC, non-small cell lung cancer.

sion targets 468 genes (1.22 Mb of the genome), and the Foundation Medicine Panel, which targets 315 genes (1.2 Mb). Recently, two commercially available panels have been developed: the OncoPrint Tumor Mutation Load Assay (Life Technologies; 409 genes, 1.7 Mb) and the TruSight Oncology 500 (Illumina; 523 genes, 1.94 Mb). As the size of panels decreases, the zone of uncertainty associated with TMB measurement rapidly increases. Moreover, uncertainty rapidly increases when the size of the panels is less than 1 Mb. Therefore, a minimum panel size of 300 genes or 1 Mb has been suggested for TMB determination [5,21]. The final factor is the bioinformatic pipeline. For tumor-only sequencing in a clinical setting, germline false-positive variants can be filtered out using large, publicly available germline variant data sets. Use of germline databases is a critical step in measurement of TMB. These germline databases need to provide a sufficiently broad representation of all populations and patients with ethnic backgrounds whose underrepresentation would result in elevated rates of germline false-positive mutations [19]. The factors influencing TMB measurements and cutoff values are summarized in Table 2.

MICROSATELLITE INSTABILITY

Clinical significance

Microsatellite instability-high (MSI-H) is characterized by accumulation of mutations, such as insertion or deletion of a small number of nucleotides, in microsatellites (repeated sequences of 1–9 nucleotides) [22]. The MSI phenotype has been extensively studied in colorectal cancer and is caused by deficiency in the DNA mismatch repair (MMR) system [23–25]. MSI has recently been shown to occur in 6%–20% of colorectal cancer, 9%–20% of gastric cancer, and 17%–31% of endometrial cancer patients, with an incidence < 5% in other cancer types [26]. In addition, MSI correlates positively with survival outcome and predicts the response to ICI therapy [27]. For MSI, different

microsatellites and microsatellite panels have been proposed, including the Bethesda/NCI panel, which is the gold standard microsatellite panel for MSI detection. Continuous development of NGS has resulted in the emergence of new computational algorithms allowing detection of MSI and changes in the standard of MSI detection in cancer [27].

Diagnosis of MSI with NGS

To diagnose MSI, conventional IHC or polymerase chain reaction (PCR) methods are widely used. For an IHC test to determine MSI status, antibodies for the four MMR proteins (MLH1, PMS2, MSH2, and MSH6) are used, and additional analysis for *MLH1* methylation or *BRAF* V600E mutation might be necessary depending on the expression of the MMR proteins [28]. MLH1, PMS2, MSH2, and MSH6 form heterodimers by pairing two proteins (MSH2/MSH6 and MLH1/PMS2), so that one defective protein shows loss of expression in one or two proteins [29]. The IHC results are interpreted as intact antibody when unequivocal nuclear staining in viable tumor cells appears in the presence of an internal positive control. Using PCR-amplified microsatellite loci with fluorescently labeled primers, the labeled PCR products can be analyzed by capillary electrophoresis to separate the amplicons by size. If there is allelic size variation in two or more microsatellite markers, it is considered MSI-H; otherwise, it is categorized microsatellite-stable (MSS) [8].

Since the development of NGS, a larger number of microsatellites can be analyzed for MSI detection. Ideally, MSI in cancer can be detected with a limit of detection at 1% in an MSS background and will further improve MSI detection in cancer.

After the first study [30] describing an MSI detection approach using WES and whole-genome sequencing data on colorectal and endometrial cancers from The Cancer Genome Atlas (TCGA), several NGS-based computational methods have been developed. These methods were based on length differences of selected microsatellites obtained from the read count of all alleles. Using Kolmogorov-Smirnov statistics for TCGA MSI analyses, several MSI detection programs were developed, including MSIsensor [31], mSINGs [30], and MANTIS [32], which present higher overall specificity and sensitivity compared with prior methods [27]. To detect MSI in cancer, two critical parameters should be taken into consideration. First, given that microsatellite marker changes markedly differ between cancer types, selection of microsatellite markers should be carefully conducted to ensure high sensitivity and specificity for MSI detection. Second, the analytical method should be highly resolute to allow discrimination of MSI and mutant allele genotype recog-

**Table 2.** Factors influencing measurement and cutoff values of tumor mutation burden by next-generation sequencing

Factor
Type of tumor (organ)
Indications including types of drug
Pre-analytic factors (input DNA amount, tumor cell percentages, quality and quantity of DNA)
Method (type of panel sequencing including size and number of genes, read depth and coverage)
Bioinformatics (limit of detection, threshold for allele frequency and definition of mutation, filter settings for germline variants and deamination artifacts)



dition and should present the lowest possible limit of detection for employment in samples with low mutant allele frequency [27].

RNA sequencing data have demonstrated that MSIseq is the only method to detect MSI based on the proportion of insertions and deletions in mono- to hexa-nucleotide repeat microsatellites among all insertions and deletions found in RNA transcripts [33]. Since MSI has been discovered in many cancer types by NGS and is a major predictive biomarker to understand the responses to ICI therapy in solid tumors, it is critical to develop and use new sensitive tools for MSI diagnosis in clinical applications.

## PROTEIN BIOMARKERS BY IMMUNOHISTOCHEMISTRY

### IHC as an important biomarker assay

IHC studies the localization of proteins or antigens in tissue sections through antigen-antibody interactions using labeled antibodies as specific reagents. This method is widely used in diagnosis and biomarker discovery because of its easy accessibility, relatively lower cost compared with other methods, and high effectivity if the target (biomarker) is a protein. IHC plays a pivotal role in cancer care, providing information about the expression status of a protein target. However, over the past decade, IHC use as a platform for biomarkers has been challenged by development of more sensitive quantitative molecular assays, which provide reference standards but lack morphological context. For IHC to be considered a “top-tier” biomarker assay, it must provide quantitative data, digitization of images, and automatic image analysis [34]. Unlike manual interpretation of IHC, which is subjective, time consuming, and presents inherent inter-observer and intra-observer variability, digital image analysis offers rapid and uniform interpretation [35]. Recently, a study on tumor classification and mutation prediction in non-small cell lung cancer using hematoxylin and eosin imaging and deep learning

found that digital image analysis offered a significant benefit of providing important prognostic information based on initial diagnosis [36]. Automatic quantification of biomarkers such as tumor-infiltrating lymphocytes (TIL) and PD-L1 is one of the most studied topics in imageomics, digital image analysis.

### Factors affecting IHC results

The use of biomarkers to guide therapy selection is gaining unprecedented support as a targeted therapy option to increase scope and complexity [37]. To be applicable for therapy in a clinical setting, several conditions must be met: adequate sampling, fast fixation with proper fixatives and proper fixation time, development of assays with positive and negative controls, accurate interpretation, and quality control and assurance. Standardized, commercially available IHC assays are preferred over in house assays to ensure reliability and reproducibility [38]. During interpretation, the test should be rejected when following factors are present: (1) preanalytical parameters, especially fixation, are not in accordance with validated procedures, (2) analytical parameters are not as expected due to artifacts, (3) unsatisfactory results in the controls, or (4) lack or very low percentage (< 10%) of tumor cells in the stained section. Consistent quality control and assurance will help ensure reliable and consistent results. All laboratories should comply with the best practice guidelines to improve the accuracy and reliability of the test. The advantages, shortcomings, and methods regarding IHC are described in Table 3.

### PD-L1 as a biomarker

PD-L1 is a well-known and broadly used biomarkers for immunotherapy. Until now, it has been standard to perform IHC to evaluate PD-L1 expression. It is important for pathologists to pay attention to the reproducibility and accuracy in evaluating PD-L1 expression. Although the criteria differ depending on tumor type, both the tumor proportion score (TPS) and combined positive score (CPS) are widely used. For TPS, the repre-

**Table 3.** Advantages, shortcomings, and methods as options for immunohistochemistry

Advantages	Shortcomings	Solutions for shortcomings
Simple	Issues with reproducibility and false positive/negative results	Strict interpretation criteria, validation, quality control, and accuracy
Inexpensive	Suffer from inter-observer variation or subjective interpretation	Digital microscopy and precision image analysis technologies
Processed slides can be stored for years and reassessed	Fixation can affect results	Standardization of analytical and pre-analytical variables
Cell morphology can be viewed in parallel	Staining quality affects results	Assay optimization with best-in-class primary antibody selection
	Usually only 1–2 proteins can be analyzed per a section	Multiplex immunohistochemistry

sentative cancer type is lung cancer ([https://www.agilent.com/cs/library/usermanuals/public/29158\\_pd-l1-ihc-22C3-pharmdx-nsclc-interpretation-manual.pdf](https://www.agilent.com/cs/library/usermanuals/public/29158_pd-l1-ihc-22C3-pharmdx-nsclc-interpretation-manual.pdf)). TPS is the percentage of viable tumor cells showing partial or complete membrane staining relative to all viable tumor cells (Fig. 1). For CPS, the representative tumors are urothelial carcinoma ([https://www.agilent.com/cs/library/usermanuals/public/29276\\_22C3-pharmdx-uc-interpretation-manual\\_us.pdf](https://www.agilent.com/cs/library/usermanuals/public/29276_22C3-pharmdx-uc-interpretation-manual_us.pdf)) and gastric cancer ([https://www.agilent.com/cs/library/usermanuals/public/29219\\_pd-l1-ihc-22C3-pharmdx-gastric-interpretation-manual\\_us.pdf](https://www.agilent.com/cs/library/usermanuals/public/29219_pd-l1-ihc-22C3-pharmdx-gastric-interpretation-manual_us.pdf)).

CPS is identified as the number of PD-L1–stained cells including tumor cells, lymphocytes, and macrophages divided by the total number of viable tumor cells, multiplied by 100. In gastric cancer, PD-L1–stained tumor cells and tumor-associated mononuclear inflammatory cells in gastric cancer exhibit distinct staining patterns (Fig. 2).

PD-L1 is a cell surface protein encoded by the *CD274* gene. Tumor cells up-regulate the expression of PD-L1 after exposure

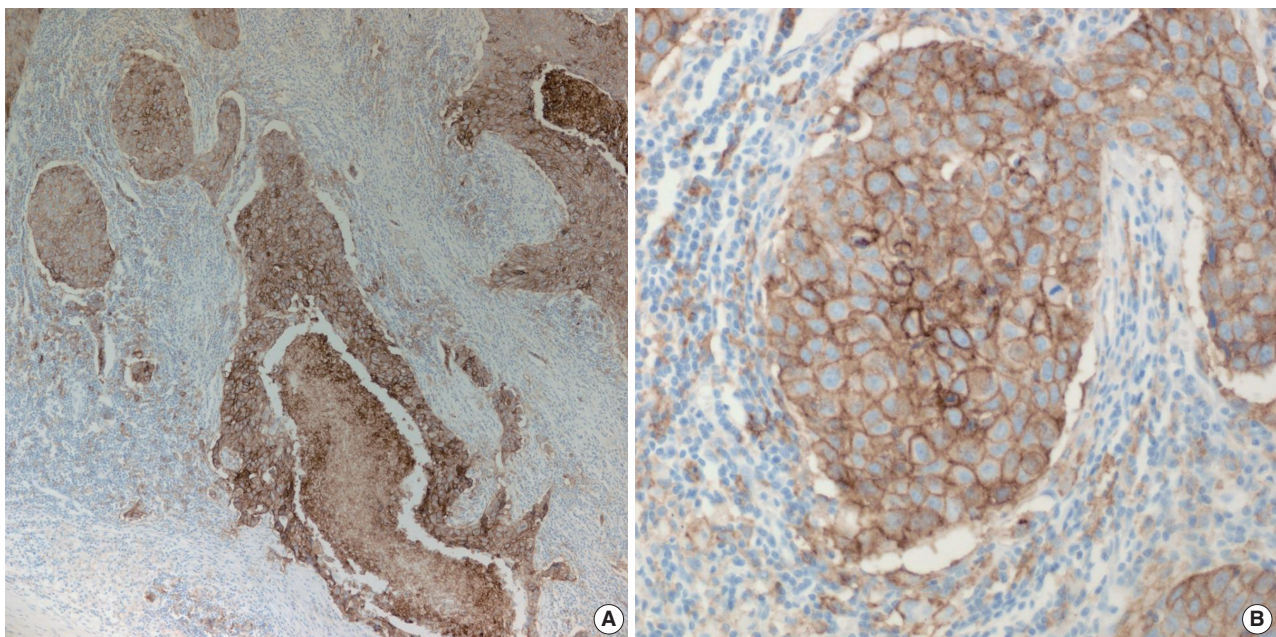


**Fig. 1.** High programmed death-ligand 1 ( $\geq 50\%$ ) staining in partial or complete cell membrane ( $\geq 1+$ ) in  $\geq 50\%$  of viable tumor cells in non-small cell lung cancers. (A) Lower magnification. (B) Higher magnification.

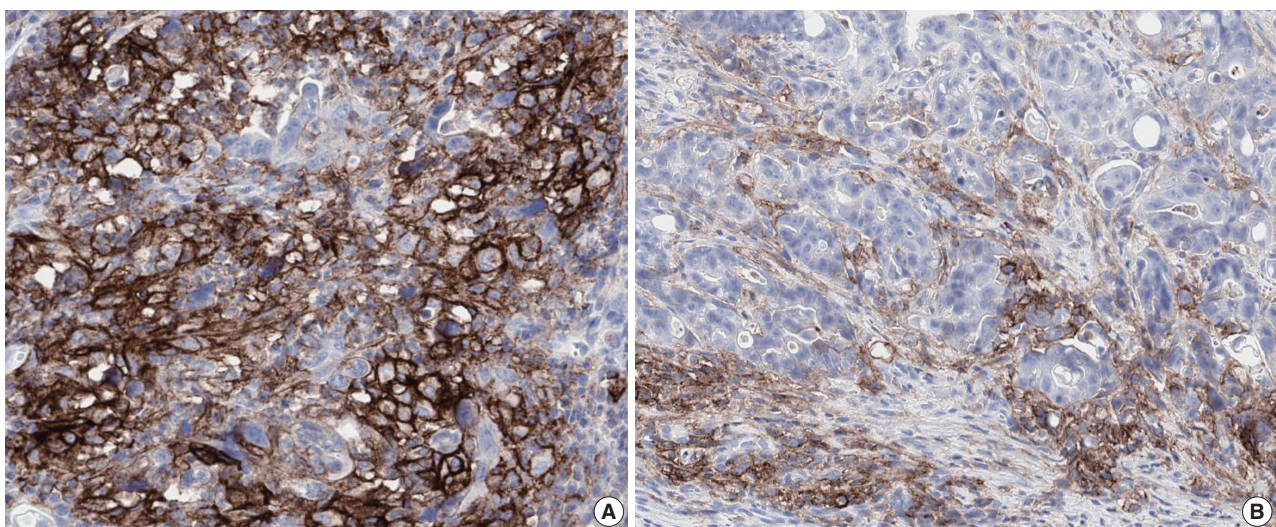


**Fig. 2.** Programmed death-ligand 1 staining of tumor cells and tumor-associated mononuclear inflammatory cells in gastric cancer, exhibiting two distinct staining patterns: lattice (A) and interface (B).



to interferon- $\gamma$  and other cytokines [39]. Moreover, some immune cells in the tumor microenvironment (TME) such as antigen presenting cells, dendritic cells, macrophages, and T cells also show increased PD-L1 expression [40]. Evaluation using IHC has demonstrated that pre-treatment positive PD-L1 expression on tumor or immune cells may be used as a biomarker to predict favorable prognosis of ICI therapy in various cancer types [41]. Recently, there was an attempt to classify tumors into four types of TME based on PD-L1 expression status and TIL [42,43]: type I (PD-L1<sup>+</sup>/TIL<sup>+</sup>, adaptive immune resistance; 38%), type II (PD-L1<sup>+</sup>/TIL<sup>-</sup>, immune ignorance; 41%), type III (PD-L1<sup>+</sup>/TIL<sup>-</sup>, intrinsic induction of PD-L1; 1%), and type IV (PD-L1<sup>-</sup>/TIL<sup>+</sup>, tolerance; 20%) [44]. Patients with TME subtype I are the most likely to respond to programmed death-1/PD-L1 blockade, and the proportion of this TME type in various kinds of cancer can differ depending on genetic alterations, oncogene drivers of the cancer, and tissue type [42]. Since TME is heterogeneous between tumor types and between patients [45], in silico insights on TME are critical for successful immunotherapy [22]. Recently, it was shown that PD-L1 mRNA expression examined by RNA-seq [46] or Nanostring [47] correlates well with PD-L1 protein expression by IHC. Development of additional platforms will allow prediction of cancer progression and increase the length and quality of life of cancer patients.

In conclusion, despite the many obstacles, gene-targeted clinical trials may be very successful, and combined biomarkers will allow us to select optimal individual treatment strategies.

### Ethics Statement

Not applicable.

### ORCID

Binnari Kim <https://orcid.org/0000-0001-7707-0857>  
 So Young Kang <https://orcid.org/0000-0003-2142-2803>  
 Kyoung-Mee Kim <https://orcid.org/0000-0002-1162-9205>

### Author Contributions

Writing—original draft: BK, SYK. Writing—review & editing: KMK. Approval of final manuscript: all authors.

### Conflicts of Interest

The authors declare that they have no potential conflicts of interest.

### Funding Statement

This work was supported by the Basic Science Research Program through the National Research Foundation of Korea (NRF) funded by the Ministry of Science and ICT (NRF-2017R1E1A1A01075005 and NRF-2017R1A2B4012436) and by a grant from the Korea Health Technology R&D Project through the Korea Health Industry Development Institute (KHIDI) funded by the Ministry of Health & Welfare, Republic of Korea (HR20C0025).

### References

- Hoadley KA, Yau C, Hinoue T, et al. Cell-of-origin patterns dominate the molecular classification of 10,000 tumors from 33 types of cancer. *Cell* 2018; 173: 291-304.
- Hyman DM, Taylor BS, Baselga J. Implementing genome-driven oncology. *Cell* 2017; 168: 584-99.
- Duffy MJ, Crown J. Biomarkers for predicting response to immunotherapy with immune checkpoint inhibitors in cancer patients. *Clin Chem* 2019; 65: 1228-38.
- Stenzinger A, Allen JD, Maas J, et al. Tumor mutational burden standardization initiatives: Recommendations for consistent tumor mutational burden assessment in clinical samples to guide immunotherapy treatment decisions. *Genes Chromosomes Cancer* 2019; 58: 578-88.
- Chalmers ZR, Connelly CF, Fabrizio D, et al. Analysis of 100,000 human cancer genomes reveals the landscape of tumor mutational burden. *Genome Med* 2017; 9: 34.
- Kim J, Kim B, Kang SY, et al. Tumor mutational burden determined by panel sequencing predicts survival after immunotherapy in patients with advanced gastric cancer. *Front Oncol* 2020; 10: 314.
- Samstein RM, Lee CH, Shoushtari AN, et al. Tumor mutational load predicts survival after immunotherapy across multiple cancer types. *Nat Genet* 2019; 51: 202-6.
- Cho J, Ahn S, Son DS, et al. Bridging genomics and phenomics of gastric carcinoma. *Int J Cancer* 2019; 145: 2407-17.
- Goodman AM, Kato S, Bazhenova L, et al. Tumor mutational burden as an independent predictor of response to immunotherapy in diverse cancers. *Mol Cancer Ther* 2017; 16: 2598-608.
- Vanderwalde A, Spetzler D, Xiao N, Gatalica Z, Marshall J. Microsatellite instability status determined by next-generation sequencing and compared with PD-L1 and tumor mutational burden in 11,348 patients. *Cancer Med* 2018; 7: 746-56.
- Ricciuti B, Kravets S, Dahlberg SE, et al. Use of targeted next generation sequencing to characterize tumor mutational burden and efficacy of immune checkpoint inhibition in small cell lung cancer. *J Immunother Cancer* 2019; 7: 87.
- Fabrizio DA, George TJ Jr, Dunne RF, et al. Beyond microsatellite testing: assessment of tumor mutational burden identifies subsets of colorectal cancer who may respond to immune checkpoint inhibition. *J Gastrointest Oncol* 2018; 9: 610-7.
- Hellmann MD, Ciuleanu TE, Pluzanski A, et al. Nivolumab plus ipilimumab in lung cancer with a high tumor mutational burden. *N Engl J Med* 2018; 378: 2093-104.
- Ready N, Hellmann MD, Awad MM, et al. First-line nivolumab plus ipilimumab in advanced non-small-cell lung cancer (CheckMate 568): outcomes by programmed death ligand 1 and tumor mutational burden as biomarkers. *J Clin Oncol* 2019; 37: 992-1000.
- Rosenberg JE, Hoffman-Censits J, Powles T, et al. Atezolizumab in patients with locally advanced and metastatic urothelial carcinoma who have progressed following treatment with platinum-based chemotherapy: a single-arm, multicentre, phase 2 trial. *Lancet* 2016; 387: 1909-20.
- Powles T, Duran I, van der Heijden MS, et al. Atezolizumab versus chemotherapy in patients with platinum-treated locally advanced or metastatic urothelial carcinoma (IMvigor211): a multicentre, open-label, phase 3 randomised controlled trial. *Lancet* 2018; 391: 748-57.
- Weinberg BA, Xiu J, Hwang JJ, Shields AF, Salem ME, Marshall JL.



- Immuno-oncology biomarkers for gastric and gastroesophageal junction adenocarcinoma: why PD-L1 testing may not be enough. *Oncologist* 2018; 23: 1171-7.
18. Mishima S, Kawazoe A, Nakamura Y, et al. Clinicopathological and molecular features of responders to nivolumab for patients with advanced gastric cancer. *J Immunother Cancer* 2019; 7: 24.
  19. Melendez B, Van Campenhout C, Rorive S, Remmelink M, Salmon I, D'Haene N. Methods of measurement for tumor mutational burden in tumor tissue. *Transl Lung Cancer Res* 2018; 7: 661-7.
  20. Kim S, Park C, Ji Y, et al. Deamination effects in formalin-fixed, paraffin-embedded tissue samples in the era of precision medicine. *J Mol Diagn* 2017; 19: 137-46.
  21. Garofalo A, Sholl L, Reardon B, et al. The impact of tumor profiling approaches and genomic data strategies for cancer precision medicine. *Genome Med* 2016; 8: 79.
  22. Cho J, Chang YH, Heo YJ, et al. Four distinct immune microenvironment subtypes in gastric adenocarcinoma with special reference to microsatellite instability. *ESMO Open* 2018; 3: e000326.
  23. Ionov Y, Peinado MA, Malkhosyan S, Shibata D, Perucho M. Ubiquitous somatic mutations in simple repeated sequences reveal a new mechanism for colonic carcinogenesis. *Nature* 1993; 363: 558-61.
  24. Peltomäki P, Løthe RA, Aaltonen LA, et al. Microsatellite instability is associated with tumors that characterize the hereditary non-polyposis colorectal carcinoma syndrome. *Cancer Res* 1993; 53: 5853-5.
  25. Thibodeau SN, Bren G, Schaid D. Microsatellite instability in cancer of the proximal colon. *Science* 1993; 260: 816-9.
  26. Zhao P, Li L, Jiang X, Li Q. Mismatch repair deficiency/microsatellite instability-high as a predictor for anti-PD-1/PD-L1 immunotherapy efficacy. *J Hematol Oncol* 2019; 12: 54.
  27. Baudrin LG, Deleuze JF, How-Kit A. Molecular and computational methods for the detection of microsatellite instability in cancer. *Front Oncol* 2018; 8: 621.
  28. Chen W, Swanson BJ, Frankel WL. Molecular genetics of microsatellite-unstable colorectal cancer for pathologists. *Diagn Pathol* 2017; 12: 24.
  29. Richman S. Deficient mismatch repair: read all about it (review). *Int J Oncol* 2015; 47: 1189-202.
  30. Salipante SJ, Scroggins SM, Hampel HL, Turner EH, Pritchard CC. Microsatellite instability detection by next generation sequencing. *Clin Chem* 2014; 60: 1192-9.
  31. Niu B, Ye K, Zhang Q, et al. MSIsensor: microsatellite instability detection using paired tumor-normal sequence data. *Bioinformatics* 2014; 30: 1015-6.
  32. Kautto EA, Bonneville R, Miya J, et al. Performance evaluation for rapid detection of pan-cancer microsatellite instability with MAN-TIS. *Oncotarget* 2017; 8: 7452-63.
  33. Lu Y, Soong TD, Elemento O. A novel approach for characterizing microsatellite instability in cancer cells. *PLoS One* 2013; 8: e63056.
  34. Dunstan RW, Wharton KA Jr, Quigley C, Lowe A. The use of immunohistochemistry for biomarker assessment: can it compete with other technologies? *Toxicol Pathol* 2011; 39: 988-1002.
  35. Jain KK. *The handbook of biomarkers*. New York: Springer, 2010.
  36. Coudray N, Ocampo PS, Sakellaropoulos T, et al. Classification and mutation prediction from non-small cell lung cancer histopathology images using deep learning. *Nat Med* 2018; 24: 1559-67.
  37. Khoury JD, Wang WL, Prieto VG, et al. Validation of immunohistochemical assays for integral biomarkers in the NCI-MATCH EAY131 clinical trial. *Clin Cancer Res* 2018; 24: 521-31.
  38. Kim KM, Bilous M, Chu KM, et al. Human epidermal growth factor receptor 2 testing in gastric cancer: recommendations of an Asia-Pacific task force. *Asia Pac J Clin Oncol* 2014; 10: 297-307.
  39. Garcia-Diaz A, Shin DS, Moreno BH, et al. Interferon receptor signaling pathways regulating PD-L1 and PD-L2 expression. *Cell Rep* 2017; 19: 1189-201.
  40. Zou W, Wolchok JD, Chen L. PD-L1 (B7-H1) and PD-1 pathway blockade for cancer therapy: Mechanisms, response biomarkers, and combinations. *Sci Transl Med* 2016; 8: 328rv4.
  41. Yang Q, Xu Z, Zheng L, Zhang L, You Q, Sun J. Multimodal detection of PD-L1: reasonable biomarkers for immune checkpoint inhibitor. *Am J Cancer Res* 2018; 8: 1689-96.
  42. Teng MW, Ngiew SF, Ribas A, Smyth MJ. Classifying cancers based on T-cell infiltration and PD-L1. *Cancer Res* 2015; 75: 2139-45.
  43. Taube JM, Anders RA, Young GD, et al. Colocalization of inflammatory response with B7-h1 expression in human melanocytic lesions supports an adaptive resistance mechanism of immune escape. *Sci Transl Med* 2012; 4: 127ra37.
  44. Lee J, Kim KM. Biomarkers for gastric cancer: molecular classification revisited. *Precis Future Med* 2017; 1: 59-68.
  45. Fridman WH, Pages F, Sautès-Fridman C, Galon J. The immune contexture in human tumours: impact on clinical outcome. *Nat Rev Cancer* 2012; 12: 298-306.
  46. Conroy JM, Pabla S, Nesline MK, et al. Next generation sequencing of PD-L1 for predicting response to immune checkpoint inhibitors. *J Immunother Cancer* 2019; 7: 18.
  47. Park C, Cho J, Lee J, et al. Host immune response index in gastric cancer identified by comprehensive analyses of tumor immunity. *Oncimmunology* 2017; 6: e1356150.

# Automated immunohistochemical assessment ability to evaluate estrogen and progesterone receptor status compared with quantitative reverse transcription-polymerase chain reaction in breast carcinoma patients

Taesung Jeon, Aeree Kim, Chungyeul Kim

Department of Pathology, Korea University Guro Hospital, Korea University College of Medicine, Seoul, Korea

**Background:** This study aimed to investigate the capability of an automated immunohistochemical (IHC) evaluation of hormonal receptor status in breast cancer patients compared to a well-validated quantitative reverse transcription–polymerase chain reaction (RT-qPCR) method. **Methods:** This study included 93 invasive breast carcinoma cases that had both standard IHC assay and Oncotype Dx assay results. The same paraffin blocks on which Oncotype Dx assay had been performed were selected. Estrogen receptor (ER) and progesterone receptor (PR) receptor status were evaluated through IHC stains using SP1 monoclonal antibody for ER, and 1E2 monoclonal antibody for PR. All ER and PR immunostained slides were scanned, and invasive tumor areas were marked. Using the Quant-Center image analyzer provided by 3DHISTECH, IHC staining of hormone receptors was measured and converted to histochemical scores (H scores). Pearson correlation coefficients were calculated between Oncotype Dx hormone receptor scores and H scores, and between Oncotype Dx scores and Allred scores. **Results:** H scores measured by an automated imaging system showed high concordance with RT-qPCR scores. ER concordance was 98.9% (92/93), and PR concordance was 91.4% (85/93). The correlation magnitude between automated H scores and RT-qPCR scores was high and comparable to those of Allred scores (for ER, 0.51 vs. 0.37 [ $p = .121$ ], for PR, 0.70 vs. 0.72 [ $p = .39$ ]). **Conclusions:** Automated H scores showed a high concordance with quantitative mRNA expression levels measured by RT-qPCR.

**Key Words:** Breast neoplasm; Hormone; RNA, messenger; Analysis

Received: June 23, 2020 Revised: August 25, 2020 Accepted: August 29, 2020

Corresponding Author: Chungyeul Kim, MD, PhD, Department of Pathology, Korea University Guro Hospital, Korea University College of Medicine, 148 Gurodong-ro, Guro-gu, Seoul 08308, Korea

Tel: +82-2-2626-1472, Fax: +82-2-2626-1486, E-mail: [idea1@hanmail.net](mailto:idea1@hanmail.net)

Multimodality therapy has resulted in improved survival rates for breast cancer patients. Hormonal receptor status is especially important when considering therapeutic options and categorizing prognostically significant molecular subgroups. Routinely conducted immunohistochemistry plays a role in determining whether a patient needs anti-hormone therapy or not by measuring the expression of protein levels. To measure hormonal receptor status, a few scoring systems have been used, including the Allred score, histochemical scores (H scores), and quick score. The Allred and quick scores are semi-quantitative scores based on the sum of the percentage (PS) and intensity scores (IS). The Allred scoring system is a well-known, successfully clinically-validated scoring system [1]. An Allred score above 2, which corresponds to a

weak staining intensity of greater than 1% of tumor cells, is the best cutoff for both disease-free survival and overall survival [2].

It is well established that multigene panels can accurately predict disease recurrence. Among them, Oncotype Dx has been widely used to determine high-risk groups for chemotherapy treatment since it was introduced [3]. The Oncotype Dx Recurrence Score (RS) is derived from quantitative measurement of mRNA expression that includes estrogen receptor (ER) and progesterone receptor (PR) and uses the quantitative reverse transcription–polymerase chain reaction (RT-qPCR) method. RS can predict anti-hormone therapy sensitivity in patients with ER-positive, node-negative breast cancer [4]. Previous studies have shown a high correlation between immunohistochemi-

cal scores and Oncotype Dx receptor scores [5-11]. Low levels of ER and PR are associated with high RS.

ER status is used as a dichotomous rather than a continuous variable when assessing patient suitability for anti-hormone therapy, and the degree of ER positivity has no impact on recommendations for the use of anti-hormonal therapy [12,13]. In a study conducted by Qureshi and Pervez [13], most tumors were either unequivocally ER-positive or ER-negative while weakly ER-positive tumors were rare [13]. Badve et al. [6] also stated that ER and PR by central immunohistochemical (IHC) were bimodal. However, some authors stated that ER expression is not bimodal in breast cancer [14].

The degree of nuclear expression measured by semi-quantitative scoring systems is dichotomous and skewed to a high score. In contrast, RT-qPCR methods can provide linear quantitative mRNA expression values that enable more precise decisions for clinicians and patients. However, not all patients can afford the high cost of these methods. If quantitative IHC scores show a good correlation with RT-qPCR results, they would accurately predict hormone receptor status and response to anti-hormone therapy.

The H score (histochemical score) is calculated by the sum of the proportion of tumor cells multiplied by the staining reactivity [1]. The score ranges from 0 to 300. A score of < 50 is considered negative and scores of 50–100, 101–200, and 201–300 are considered weakly positive (1+), moderately positive (2+), and strongly positive (3+), respectively [15].

We obtained the H score using a computer-aided image analysis program to secure faster and reproducible results. Computational approaches can play a role in better quantitative characterization of diseases and quantitative histomorphometry [16]. Current American Society of Clinical Oncology/College of American Pathologists (ASCO/CAP) recommendations encourage the use of quantitative image analysis techniques to improve the consistency of clinical interpretation [17]. ER and PR status assessment by image analysis presented an excellent agreement with visual histoscores and were predictive of recurrence-free survival and cancer-specific survival [18].

In our study, we compared the hormone scores of Oncotype Dx and the results of immunohistochemical expression scores—Allred score and computer-aided H score—and tested their agreements.

## MATERIALS AND METHODS

### Patient selection and data collection

Among those who had undergone surgery due to invasive breast carcinoma from 2014 to 2019 at Korea University Guro Hospital, 98-patient cases who had Oncotypes Dx test (Oncotype DX, Genomic Health, CA, USA) results were included. Five cases that were missing paraffin blocks were excluded. Eighty of the remaining 93 cases for which immunohistochemistry had been performed in the biopsy sample alone, were stained again in the paraffin block where Oncotype Dx was implemented.

Information such as patient age at diagnosis, tumor size, tumor grade, Ki-67 labeling index, and mitotic count was collected from pathologic review. ER score, PR score, and RS score data were collected from the Oncotype Dx report. To improve comparability, we stained the same paraffin block where the Oncotype Dx assay had been implemented. We also analyzed the whole invasive tumor area of the same section by obtaining the Allred score and computer-aided H score.

The clinical and pathologic characteristics of the final 93 cases are summarized in Table 1.

**Table 1.** Patient characteristics

Characteristic	Value
Age at diagnosis (yr)	53.47 (30–79)
Tumor size (cm)	1.29 (0.5–2.9)
Ki-67 labeling index (%)	12.93 (0.5–74.7)
Histologic type	
Invasive NST	81 (87.1)
Invasive lobular	8 (8.6)
Pleomorphic lobular	2 (2.2)
Mucinous	2 (2.2)
Histologic grade	
1	55 (59.1)
2	37 (39.8)
3	1 (1.1)
Tubule formation	
1	19 (20.4)
2	37 (39.8)
3	37 (39.8)
Nuclear grade	
1	17 (18.3)
2	71 (76.3)
3	5 (5.4)
Mitosis	
1	82 (88.2)
2	10 (10.8)
3	1 (1.1)

Values are presented as mean (range) or number (%).  
NST, no special type.



### Immunohistochemical stain

The same paraffin blocks on which the Oncotype Dx assay was performed were selected. ER and PR receptor status were evaluated through immunohistochemical stains using the SP1 monoclonal antibody for ER, and the 1E2 monoclonal antibody for PR (Ventana Medical Systems, Tucson, AZ, USA). Formalin-fixed paraffin-embedded tissue samples were sliced with a microtome at 4 µm and placed on slides. The slides containing tissue sections were deparaffinized at 75°C, and cell conditioning was done with EDTA solution at 100°C for 4 minutes. Primary antibodies were applied for 20 minutes. A Ventana Benchmark Ultra instrument automatically stained the slides.

### Allred score

The stained slides were reviewed and Allred scores for ER and PR were given by two skilled pathologists. Allred score was derived from the sum of PS (range, 0 to 5) and IS (range, 0 to 3).

### Slide scanning and calculating IHC scores by image analysis

All ER and PR immunostained slides were scanned, and whole invasive tumor areas were marked by a pathologist. Using a QuantCenter image analyzer provided by 3DHISTECH (Budapest, Hungary), the results of the immunohistochemical staining of hormone receptors were measured and converted to H scores. The image analyzing system also provided automatically calculated Allred score results.

We set “score intensity” cutoff values in the QuantCenter program at 200, 160, and 100 to define negative, weakly positive, moderately positive, and strong positive staining intensity that corresponded to the reactivity of staining (0, 1, 2, 3, respectively) (255–200, 0; 200–160, 1; 160–100, 2; 100–0, 3).

### Statistics

Pearson correlation coefficients were calculated between Oncotype Dx hormone receptor scores and H scores, and between Oncotype Dx scores and Allred scores. The RS score was also compared with IHC scores. Further, the automatically calculated Allred scores were compared with RT-qPCR scores and RS scores as well. Fisher's z transformation was used to compare each correlation coefficient. Statistical analyses were performed with GraphPad Prism ver. 8.3 software (GraphPad Software Inc., San Diego, CA, USA).

The patients were subcategorized into a high score group ( $\geq 200$ ), an intermediate score group ( $\geq 100$  and  $< 200$ ), and a low score group ( $< 100$ ) to identify which subgroup was more correlated with the RT-qPCR score. The high score group ( $\geq 200$ )

was subcategorized into  $< 250$  and  $\geq 250$  groups.

## RESULTS

Immunohistochemical and RT-qPCR score results for ER and PR are summarized in Table 2. ER and PR concordance rate between the H score and the RT-qPCR assay was 98.9% (92/93) and 91.4% (85/93), respectively. The correlation coefficient between ER H score and ER RT-qPCR score was 0.51, and that between ER Allred score and ER RT-qPCR score was 0.37 (Table 3). The correlation coefficient between PR H score and PR RT-qPCR score was 0.70, and that between the PR Allred score and PR RT-qPCR score was 0.72. The correlation coefficients were higher for PR compared to ER (0.70 vs. 0.51 [ $p = .021$ ] and 0.72 vs. 0.37 [ $p < .01$ ]). The correlation coefficients for automatically calculated Allred scores were similar to those for the manual Allred score (Table 3). Fig. 1 demonstrates the correlation status between scores. Among all three measuring methods, the RT-qPCR score was closest to the normal distribution (Fig. 2). In general, the PR IHC stain showed a more heterogeneous staining intensity compared to ER IHC (Fig. 3). When we examined the cases of Allred score 8, computer-aided H score results showed a significant portion of moderately positive (intensity 2) nuclei as well as strong positive nuclei (intensity 3) (Fig. 4).

**Table 2.** Hormone receptor status

	Mean (range)
ER H score	250.6 (128.86–296.23)
PR H score	196.51 (1.37–293.17)
ER Allred score	7.88 (4–8)
PR Allred score	6.73 (0–8)
ER RT-qPCR score	9.86 (4.3–12.5)
PR RT-qPCR score	7.44 (3.2–10)
RS score	15.16 (0–68)

ER, estrogen receptor; H, histochemical; PR, progesterone receptor; RT-qPCR, quantitative reverse transcription–polymerase chain reaction; RS, recurrence score.

**Table 3.** The correlation coefficient (R) between IHC scores and RT-qPCR scores

Correlation coefficient (R)	H score	Allred score	Automated allred score
ER			
RT-qPCR score	0.51	0.37	0.35
RS	0.28	0.42	0.30
PR			
RT-qPCR score	0.70	0.72	0.72
RS	0.43	0.50	0.50

IHC, immunohistochemical; RT-qPCR, quantitative reverse transcription–polymerase chain reaction; H, histochemical; ER, estrogen receptor; RS, recurrence score; PR, progesterone receptor.

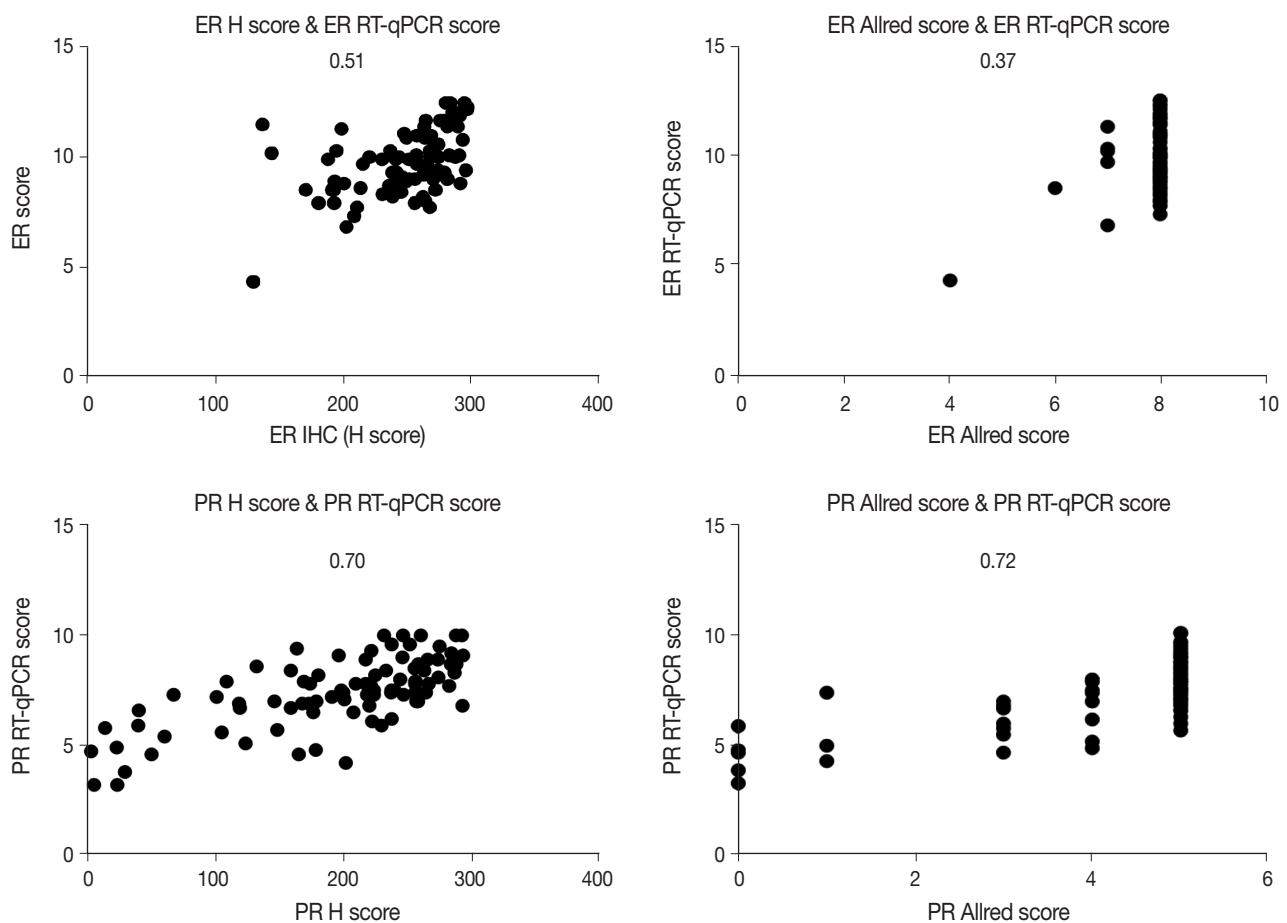


**Fig. 1.** Correlation between IHC scores and RT-qPCR scores. The number in each graph indicates correlation coefficient (R). ER, estrogen receptor; PR, progesterone receptor; H, histochemical; RT-qPCR, quantitative reverse transcription-polymerase chain reaction; IHC, immunohistochemical. (Continued on the next page)

We inspected correlation magnitudes for each subgroup categorized by H score values. The intermediate H score group (range, 100 to 200) and low H score group (< 100) demonstrated the lowest correlation (Table 4). As the high H score group (range, 200 to 300) comprised a significant portion of all subjects, this group was further subcategorized into a 200–250 group and a 250–300 group. Compared to the 250–300 group, the 200–250 group showed a higher correlation with both ER and PR, although not statistically significant (0.59 vs. 0.52 for ER; 0.44 vs. 0.29 for PR) ( $p = .35$  and  $p = .27$ ) (Table 4).

There were eight discordant cases for PR, while there was one discordant case for ER (Table 5). For ER, one case had IHC-positive and polymerase chain reaction (PCR)-negative results (ER score, 4.3; H score, 128.86). For PR, six cases had negative results across all measuring systems (mean PR score, 4.06; mean H, score 20.8). Five cases were only PCR-negative (mean PR score, 4.82; mean H score, 144.95). Two cases were only H score-negative

(mean PR score, 6.25; mean H score, 38.49). One case was IHC-negative and PCR-positive (PR score, 5.8; H score, 12.24). Our results were consistent with previous studies in that more IHC-positive and RT-qPCR-negative cases were observed compared to the opposite [5,7,9,10]. In concordance with earlier studies, no PR-positive, ER-negative case was found.

We reviewed the discordant cases between IHC scores and RT-qPCR scores. Regarding the IHC-positive and RT-qPCR-negative cases (one for ER and five for PR), the immunostained slides showed positivity for both the Allred score and H score (Table 5). One PR IHC-negative, RT-qPCR-positive case demonstrated a strong PR-positive ductal carcinoma in situ component within the area of hormone-negative invasive carcinoma (Fig. 5A). Under secondary review, the automatically recognized staining intensities and subsequently calculated H scores seemed accurate (Fig. 5B).

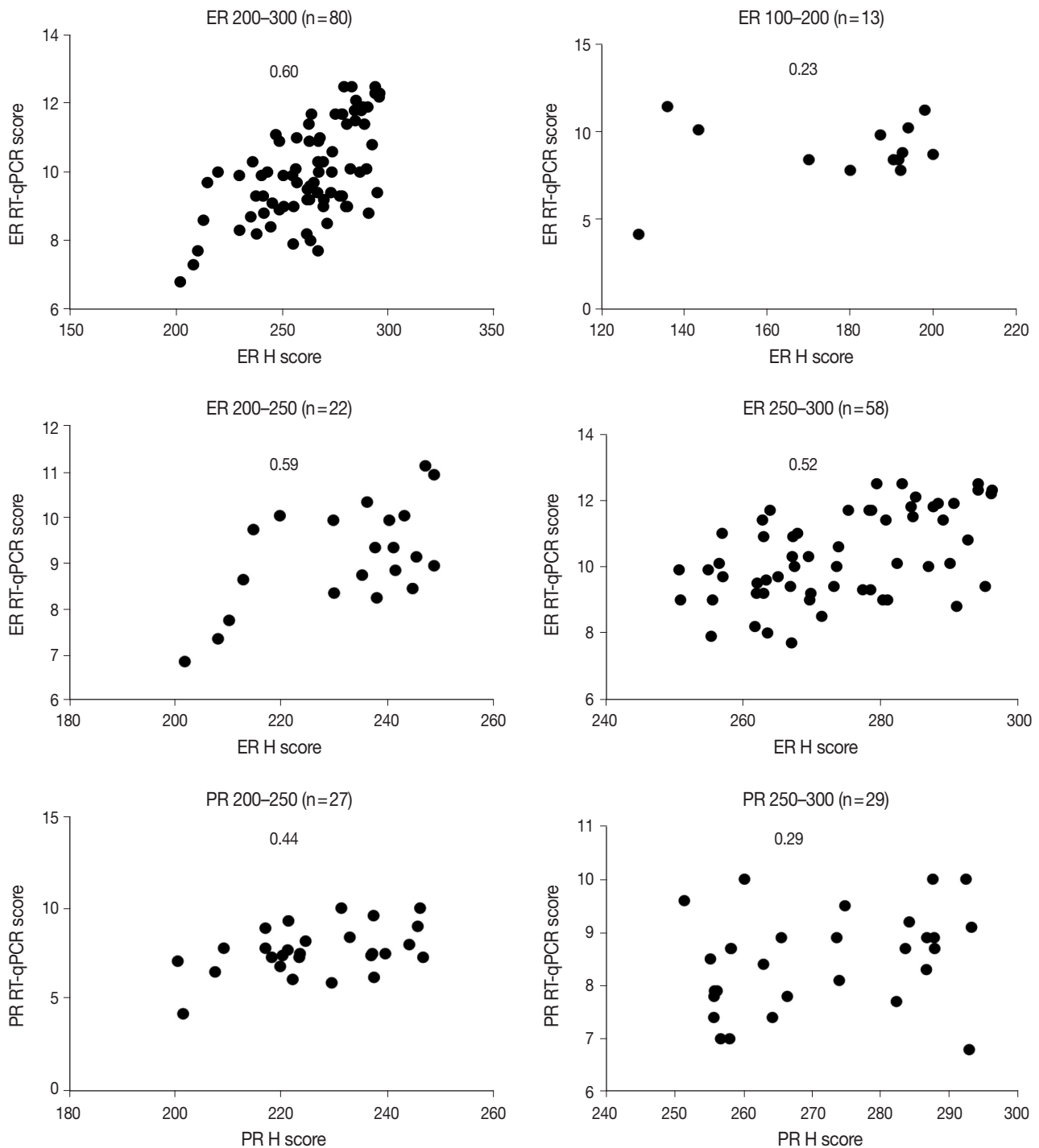


Fig. 1. (Continued from the previous page).

## DISCUSSION

RT-qPCR methods enable quantitative and consistent measurement of clinically significant gene expression levels. In contrast, currently used manual immunohistochemical assessment systems may demonstrate a lack of reproducibility. Scoring sys-

tems that use image analyzers are expected to overcome this weakness. In this study, we found high correlations between automatically calculated immunohistochemical scores and RT-qPCR hormone expression levels.

Immunohistochemical evaluation of hormonal receptor expression status captured the tendency to oversaturation—skewed



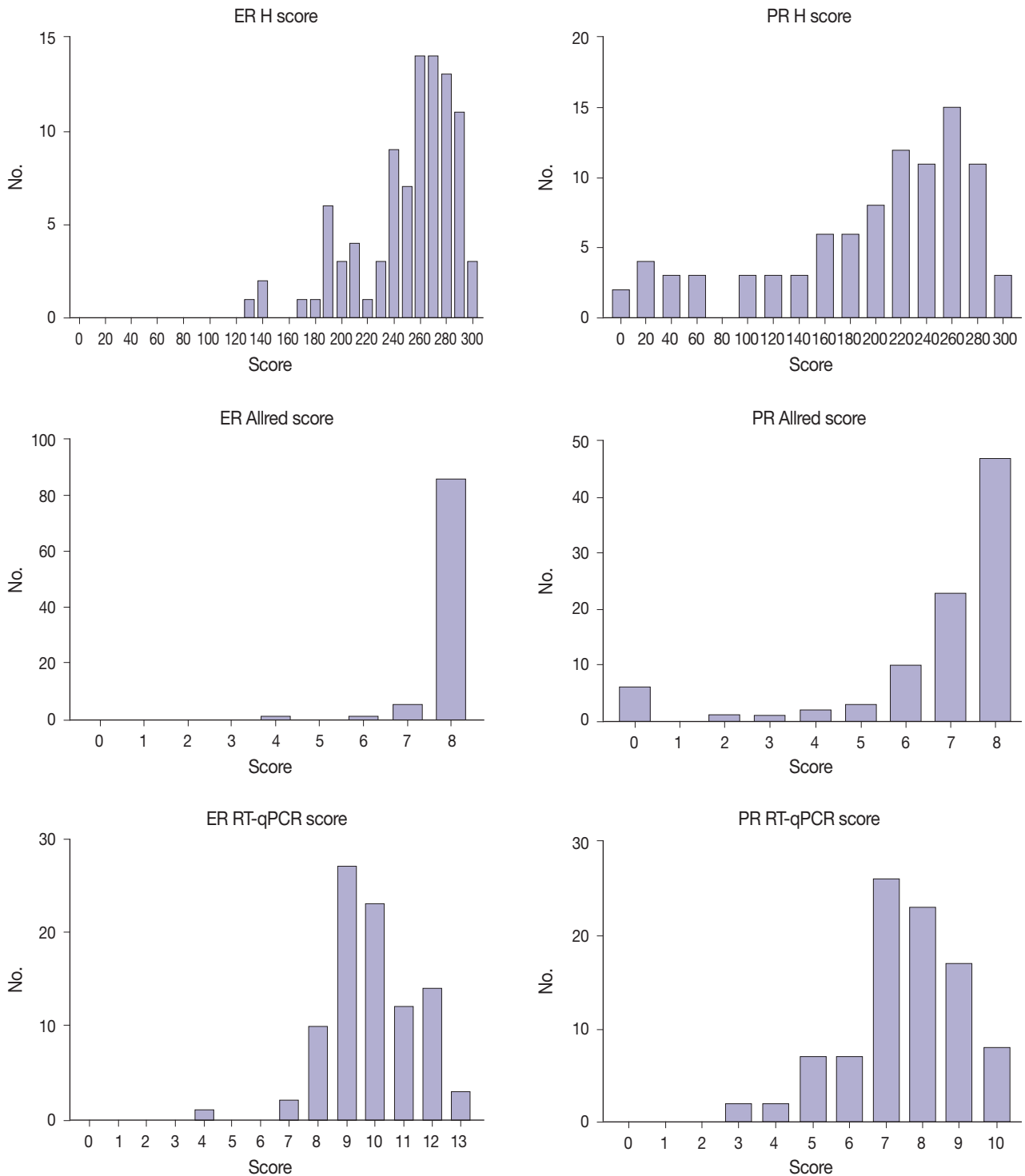


**Fig. 2.** Distribution of H scores, Allred scores, and RT-qPCR scores. ER, estrogen receptor; PR, progesterone receptor; H, histochemical; RT-qPCR, quantitative reverse transcription-polymerase chain reaction; IHC, immunohistochemical.

to the high expression side—, especially in the ER and a high score groups. Among all three measuring methods, the RT-qPCR score was closest to the normal distribution. Despite that the number of discordant cases for PR was higher, the correlation was higher

for PR than for ER. This is because the distribution was more right-shifted in ER, resulting in a non-linear correlation with the RT-qPCR score. As the IHC score was somewhat shifted to the right, it would lose linearity as it approached a high score.

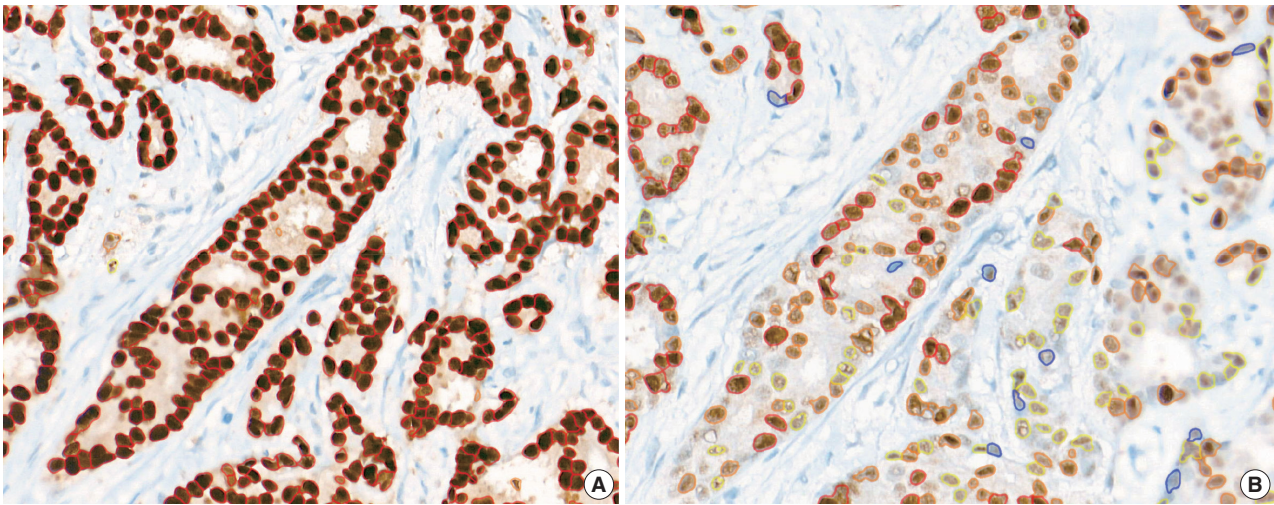


**Fig. 3.** PR-IHC stain showed more heterogeneous staining tendency (B) than ER-IHC stain (A) in the same tumor section. ER, estrogen receptor; PR, progesterone receptor; IHC, immunohistochemical.

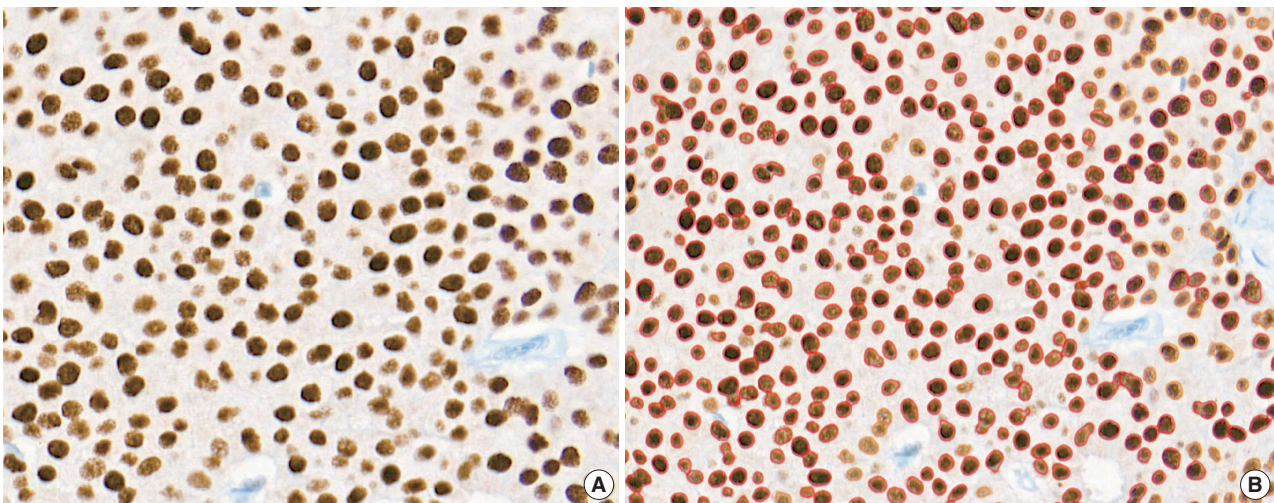


**Fig. 4.** (A) ER-stained slide with Allred score 8. (B) However, a significant portion of moderate nuclear staining (2+) was present as well as strong nuclear staining (3+) by image analysis. ER, estrogen receptor.

Measurements obtained with the Allred scoring system were even more right-shifted than H scores for both ER and PR [10]. More than 90% of cases had an ER Allred score of 8, and more than 50% of cases had a PR Allred score of 8. No single case had an ER Allred score less than 4. Compared to the Allred score, the H score system demonstrated a linear quantitative measurement for receptor status.

The correlation magnitude between H scores and RT-qPCR scores was not significantly different than that between Allred scores and RT-qPCR scores. ER H score showed a higher correlation coefficient compared to the Allred score in this study 0.51 vs. 0.37 ( $p = .121$ ). In contrast, the PR Allred score showed a

higher correlation coefficient than the H score 0.70 vs. 0.72 ( $p = .39$ ). Additionally, we compared the correlation magnitude when the image analysis system calculated both the H scores and Allred scores. After excluding confounding factors, the results showed a similar tendency to the manual Allred score. Compared to the H score, the Allred score was more correlated with the RS score in both ER (0.42 vs. 0.28) ( $p = .14$ ) and PR (0.50 vs. 0.43) ( $p = .27$ ). When we looked into the cases of Allred score 8, computer-aided H score results showed a significant portion of moderately positive (intensity 2) nuclei as well as strong positive nuclei (intensity 3). Sometimes, moderately positive nuclei were observed more often than strong positive nuclei. The computer-



recognized variation in staining intensity may have resulted in a lower correlation than the Allred score due to its complexity [19].

We reviewed the discordant cases between IHC scores and RT-qPCR scores. Regarding the IHC-positive and RT-qPCR-negative cases (one for ER and five for PR), the immunostained slides showed positivity for both the Allred score and H score.

**Table 4.** The correlation coefficient (R) in each subgroup

Subgroup	ER		PR	
	No.	R	No.	R
≥ 200	80	0.60	55	0.47
200–250	22	0.59	27	0.44
250–300	58	0.52	30	0.29
100–200	13	0.23	25	0.22
< 100	0	N/A	13	0.69

ER, estrogen receptor; PR, progesterone receptor; N/A, not available.

**Table 5.** Discordant cases

Discordant results	No. of cases	Results	Mean RT-qPCR score	Mean H score
ER	1	IHC (+), PCR (–)	4.3	128.86
PR	5	Allred (+), H (+), PCR (–)	4.82	144.95
	2	Allred (+), H (–), PCR (+)	6.25	38.49
	1	Allred (–), H (–), PCR (+)	5.8	12.24

ER RT-qPCR score was considered positive when  $\geq 6.5$ , PR RT-qPCR score  $\geq 5.5$ ; H score was considered positive when  $\geq 50$ , and negative when  $< 50$ .

RT-qPCR, quantitative reverse transcription-polymerase chain reaction; H score, histochemical score; ER, estrogen receptor; IHC, immunohistochemical; PCR, polymerase chain reaction; PR, progesterone receptor.

From this result, we speculated that the RT-qPCR method may have lower sensitivity compared to IHC methods in certain situations. One PR IHC-negative, RT-qPCR-positive case demonstrated a strong PR-positive ductal carcinoma in situ component within the area of hormone-negative invasive carcinoma. This intraductal component may have caused false-positive RT-qPCR results. While immunohistochemical methods detect and count only invasive tumor areas, the RT-qPCR method may incorporate intraductal components and non-tumor areas as well.

Two cases had a negative PR H score and positive Allred score and RT-qPCR score. They both had positive Allred scores under secondary review. The automatically recognized staining intensities and subsequently calculated H scores seemed accurate. These two cases had a mean H score of 38.49. We set the “score intensity” cutoff points in the image analyzing system to define nuclear staining intensities, and the cutoff points could be finely adjusted to obtain more precise results. The H score cutoff value itself (which was set at 50 in this study) can be adjusted to reduce false-negative H score results.

In our study, PR had more intermediate H score cases than ER (13/93 [13.97%] vs. 25/93 [26.88%]). As mentioned above, the intermediate group showed the lowest correlation. The intermediate group may have had more intratumoral heterogeneity and stromal influence. Intratumoral heterogeneity of PR and contaminated non-tumor areas could have caused lower RT-qPCR sensitivity compared to IHC.

Although only weak staining of more than 1% of tumor cells is a well-known cutoff value for predicting anti-hormone therapy

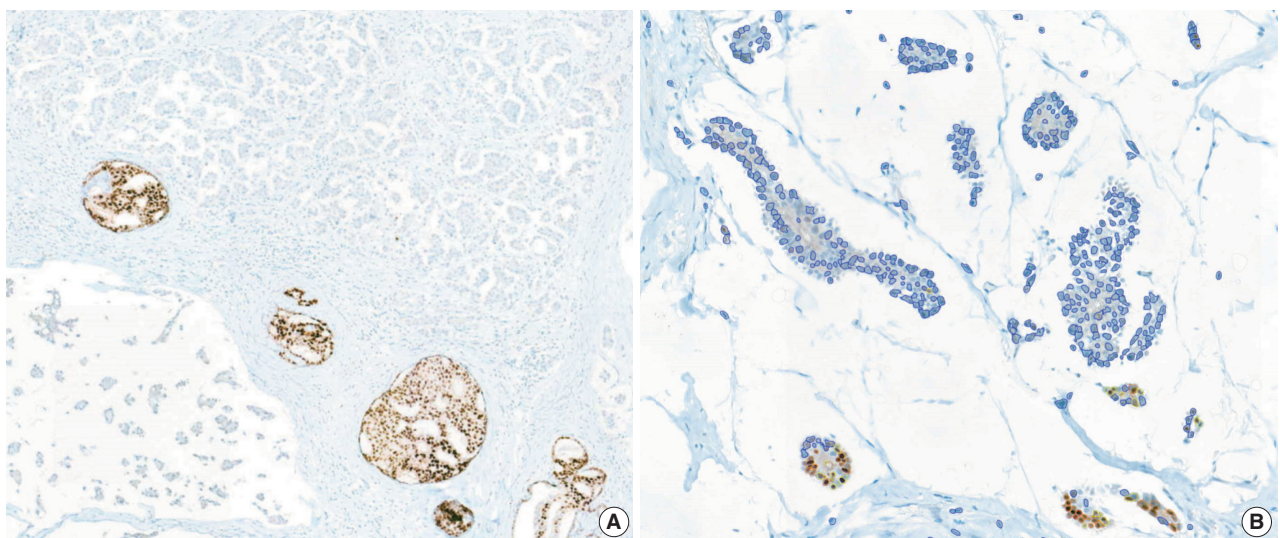


**Fig. 5.** (A) Strong PR-positive intraductal component within PR-negative invasive cancer area. (B) During a secondary review for the case which had false-negative H score, nuclear staining intensity and H score recognized by an image analyzer seemed accurate. PR, progesterone receptor; H, histochemical.



response, the value is quite left-shifted on a percentile scale. Allred score has been assessed visually, and an inherent problem could occur because the 1% cutoff value can be arbitrary by visual assessment [20]. The therapeutic benefit of anti-hormone therapy in low ER and PR receptor groups (positivity ranges from 1% to 10%) has not yet been established. True low ER and PR groups are rare, according to some the previous reports [13,21]. More recently, some portions of this low hormonal receptor group had characteristics more like basal-like and triple-negative groups than hormone receptor-positive groups [19,22]. No low ER tumor was found in our study, while one low PR tumor case was present. The low PR (Allred score 3 [1 + 2]) case had a positive H score value (201.22), negative RT-qPCR score (4.2), and positive ER result (Allred score, 8; H score, 278.64). More careful assessment is required for these low ER and PR groups. Various methods including the RT-qPCR method and computer-aided quantification will be helpful.

In conclusion, the correlation magnitude between automated H scores and RT-qPCR scores was high and comparable to those of Allred scores. Automated H scores may become more predictive when further large-scale studies with refined methods are conducted.

The antibodies used in this study (SP1 for ER and 1E2 for PR) are well known for being more sensitive than other ER and PR antibodies, thus can reduce false-negative results [23,24]. These widely used antibodies have shown a good correlation with patient outcomes [23,24]. With the use of these antibodies, the distribution of IHC scores could be more skewed to high scores.

The Oncotype Dx test targets ER-positive, node-negative breast cancer patients only. Thus, this study was conducted only with ER-positive and high score patients, which could have led to an incomplete interpretation of the results. Further study designs that include all hormonal receptor statuses, especially low ER, PR groups (1%–10% positive cells), would be informative.

### Ethics Statement

The Institutional Review Board (IRB) of Korea University Guro Hospital (IRB No. 2019GR0410) approved this study. The requirement for informed consent was waived by the IRB. Investigations were conducted as per the rules of the Declaration of Helsinki of 1975, revised in 2013.

### ORCID

Taesung Jeon <https://orcid.org/0000-0002-9852-0084>  
Aeree Kim <https://orcid.org/0000-0001-9645-2156>  
Chungyeul Kim <https://orcid.org/0000-0002-9636-5228>

### Author Contributions

Conceptualization: CK. Data curation: TJ. Formal analysis: TJ. Funding ac-

quisition: CK, AK. Investigation: TJ. Methodology: TJ, CK. Project administration: CK. Resources: TJ, CK, AK. Supervision: CK, AK. Validation: TJ, CK. Visualization: TJ. Writing—original draft: TJ. Writing—review & editing: TJ, CK, AK. Approval of final manuscript: all authors.

### Conflicts of Interest

AK, a contributing editor of the *Journal of Pathology and Translational Medicine*, was not involved in the editorial evaluation or decision to publish this article. All remaining authors have declared no conflicts of interest.

### Funding Statement

No funding to declare.

### Acknowledgments

The biospecimens and data used for this study were provided by the Biobank of Korea University Guro Hospital, a member of the Korea Biobank Network. This research was supported by a grant (HI14C3396) by the Korea Health Technology R&D Project through the Korea Health Industry Development Institute (KHIDI) funded by the Ministry of Health & Welfare (MOHW), Republic of Korea.

### References

1. Umemura S, Kurosumi M, Moriya T, et al. Immunohistochemical evaluation for hormone receptors in breast cancer: a practically useful evaluation system and handling protocol. *Breast Cancer* 2006; 13: 232.
2. Hammond ME, Hayes DF, Dowsett M, et al. American Society of Clinical Oncology/College of American Pathologists guideline recommendations for immunohistochemical testing of estrogen and progesterone receptors in breast cancer (unabridged version). *Arch Pathol Lab Med* 2010; 134: e48-72.
3. Paik S, Shak S, Tang G, et al. A multigene assay to predict recurrence of tamoxifen-treated, node-negative breast cancer. *N Engl J Med* 2004; 351: 2817-26.
4. Xin L, Liu YH, Martin TA, Jiang WG. The era of multigene panels comes? The clinical utility of Oncotype DX and MammaPrint. *World J Oncol* 2017; 8: 34-40.
5. O'Connor SM, Beriwal S, Dabbs DJ, Bhargava R. Concordance between semiquantitative immunohistochemical assay and oncotype DX RT-PCR assay for estrogen and progesterone receptors. *Appl Immunohistochem Mol Morphol* 2010; 18: 268-72.
6. Badve SS, Baehner FL, Gray RP, et al. Estrogen- and progesterone-receptor status in ECOG 2197: comparison of immunohistochemistry by local and central laboratories and quantitative reverse transcription polymerase chain reaction by central laboratory. *J Clin Oncol* 2008; 26: 2473-81.
7. Kraus JA, Dabbs DJ, Beriwal S, Bhargava R. Semi-quantitative immunohistochemical assay versus oncotype DX((R)) qRT-PCR assay for estrogen and progesterone receptors: an independent quality assurance study. *Mod Pathol* 2012; 25: 869-76.
8. Bradshaw SH, Pidutti D, Gravel DH, Song X, Marginean EC, Robertson SJ. Predicting OncoDx recurrence scores with immunohistochemical markers. *Appl Immunohistochem Mol Morphol* 2013; 21: 490-6.
9. Park MM, Ebel JJ, Zhao W, Zynger DL. ER and PR immunohistochemistry and HER2 FISH versus oncotype DX: implications for breast cancer treatment. *Breast J* 2014; 20: 37-45.
10. Khoury T, Yan L, Liu S, Bshara W. Oncotype DX RT-qPCR assay

- for ER and PR correlation with IHC: a study of 3 different clones. *Appl Immunohistochem Mol Morphol* 2015; 23: 178-87.
11. Hanna MG, Bleiweiss IJ, Nayak A, Jaffer S. Correlation of Oncotype DX recurrence score with histomorphology and immunohistochemistry in over 500 patients. *Int J Breast Cancer* 2017; 2017: 1257078.
  12. Collins LC, Botero ML, Schnitt SJ. Bimodal frequency distribution of estrogen receptor immunohistochemical staining results in breast cancer: an analysis of 825 cases. *Am J Clin Pathol* 2005; 123: 16-20.
  13. Qureshi A, Pervez S. Allred scoring for ER reporting and its impact in clearly distinguishing ER negative from ER positive breast cancers. *J Pak Med Assoc* 2010; 60: 350-3.
  14. Allred DC, Mohsin SK. ER expression is not bimodal in breast cancer. *Am J Clin Pathol* 2005; 124: 474-5.
  15. Shousha S. Oestrogen receptor status of breast carcinoma: Allred/H score conversion table. *Histopathology* 2008; 53: 346-7.
  16. Madabhushi A, Lee G. Image analysis and machine learning in digital pathology: challenges and opportunities. *Med Image Anal* 2016; 33: 170-5.
  17. Veta M, Pluim JP, van Diest PJ, Viergever MA. Breast cancer histopathology image analysis: a review. *IEEE Trans Biomed Eng* 2014; 61: 1400-11.
  18. Mohammed ZM, Edwards J, Orange C, et al. Breast cancer outcomes by steroid hormone receptor status assessed visually and by computer image analysis. *Histopathology* 2012; 61: 283-92.
  19. Reisenbichler ES, Lester SC, Richardson AL, Dillon DA, Ly A, Brock JE. Interobserver concordance in implementing the 2010 ASCO/CAP recommendations for reporting ER in breast carcinomas: a demonstration of the difficulties of consistently reporting low levels of ER expression by manual quantification. *Am J Clin Pathol* 2013; 140: 487-94.
  20. Nassar A, Cohen C, Agersborg SS, et al. A new immunohistochemical ER/PR image analysis system: a multisite performance study. *Appl Immunohistochem Mol Morphol* 2011; 19: 195-202.
  21. Nadji M, Gomez-Fernandez C, Ganjei-Azar P, Morales AR. Immunohistochemistry of estrogen and progesterone receptors reconsidered: experience with 5,993 breast cancers. *Am J Clin Pathol* 2005; 123: 21-7.
  22. Iwamoto T, Booser D, Valero V, et al. Estrogen receptor (ER) mRNA and ER-related gene expression in breast cancers that are 1% to 10% ER-positive by immunohistochemistry. *J Clin Oncol* 2012; 30: 729-34.
  23. Troxell ML, Long T, Hornick JL, Ambaye AB, Jensen KC. Comparison of estrogen and progesterone receptor antibody reagents using proficiency testing data. *Arch Pathol Lab Med* 2017; 141: 1402-12.
  24. Zhang H, Han M, Varma KR, Clark BZ, Bhargava R, Dabbs DJ. High fidelity of breast biomarker metrics: a 10-year experience in a single, large academic institution. *Appl Immunohistochem Mol Morphol* 2018; 26: 697-700.

## Interobserver diagnostic reproducibility in advanced-stage endometrial carcinoma

Ho Jin Jung<sup>1</sup>, Soo Yeon Lee<sup>1</sup>, Jin Hwa Hong<sup>2</sup>, Yi Kyeong Chun<sup>1</sup>

Departments of <sup>1</sup>Pathology and <sup>2</sup>Obstetrics and Gynecology, Korea University Guro Hospital, Korea University College of Medicine, Seoul, Korea

**Background:** The accurate pathologic diagnosis and subtyping of high-grade endometrial carcinoma are often problematic, due to its atypical and overlapping histopathological features. **Methods:** Three pathologists reviewed 21 surgically resected cases of advanced-stage endometrial carcinoma. The primary diagnosis was based only on hematoxylin and eosin stained slides. When a discrepancy arose, a secondary diagnosis was made by additional review of immunohistochemical (IHC) stains. Finally, three pathologists discussed all cases and rendered a consensus diagnosis. **Results:** The primary diagnoses were identical in 13/21 cases (62%). The secondary diagnosis based on the addition of IHC results was concordant in four of eight discrepant cases. Among four cases with discrepancies occurring in this step, two cases subsequently reached a consensus diagnosis after a thorough discussion between three reviewers. Next-generation sequencing (NGS) study was performed in two cases in which it was difficult to distinguish between serous carcinoma and endometrioid carcinoma. Based on the sequencing results, a final diagnosis of serous carcinoma was rendered. The overall kappa for concordance between the original and consensus diagnosis was 0.566 (moderate agreement). **Conclusions:** We investigated step-wise changes in interobserver diagnostic reproducibility in advanced-stage endometrial carcinoma. We demonstrated the utility of IHC and NGS study results in the histopathological diagnosis of advanced-stage endometrial carcinoma.

**Key Words:** Endometrial neoplasms; Uterine neoplasm; Observer variation

Received: August 10, 2020 Revised: September 16, 2020 Accepted: October 4, 2020

**Corresponding Author:** Yi Kyeong Chun, MD, Department of Pathology, Korea University Guro Hospital, Korea University College of Medicine, 148 Gurodong-ro, Guro-gu, Seoul 08308, Korea

Tel: +82-2-2626-1472, Fax: +82-2-2626-1486, E-mail: ykcmd@naver.com

Endometrial carcinoma is the most common gynecological cancer in the Western world [1]. The annual incidence of endometrial cancer in South Korea has increased from 619 in 1999 to 2,263 in 2015 [2].

According to the 2014 WHO Classification of Tumors of Female Reproductive Organs [3], various histological subtypes of endometrial carcinoma include endometrioid carcinoma, serous carcinoma, clear cell carcinoma, carcinosarcoma, and undifferentiated/dedifferentiated carcinoma, among others. All subtypes except low-grade endometrioid carcinoma are high-grade malignancies, and are clinically more aggressive and exhibit poor prognoses [4,5]. Precise histological diagnosis of high-grade endometrial carcinoma can be challenging if histopathologic and immunohistochemical (IHC) characteristics are overlapping or atypical [6,7].

Several researchers have reported the utility of biomarker pan-

els and molecular profiling in endometrial carcinoma diagnosis. Han et al. [8] demonstrated that a seven-marker immunostaining panel (consisting of estrogen receptor [ER], progesterone receptor [PR], p16, p53, vimentin, PTEN, and IGF2BP3) could differentiate high-grade endometrioid carcinoma and serous carcinoma with 100% concordance. Nastic et al. [9] reported an increase in interobserver agreement rates after application of ER, PR, and p53 immunostaining and DNA ploidy studies. Molecular profiling can also aid in the differential diagnosis of endometrial carcinoma. For example, *TP53* mutations and *CCNE1* locus amplification are common in serous carcinoma, but rare in endometrioid carcinoma [10]. In contrast, most endometrioid carcinomas harbor *ARID1A* mutations, whereas serous carcinomas do not [10,11].

This study was designed to assess interobserver reproducibility in the subtype diagnosis of cases previously diagnosed as ad-



vanced-stage endometrial carcinoma in routine surgical pathology practice, under the assumption that there are more high-grade than low-grade carcinomas in cases diagnosed as advanced-stage endometrial carcinoma. Three pathologists with variable diagnostic experience reviewed the hematoxylin and eosin (H&E)-staining and IHC-stained slides. Through this study, we aimed to assess the diverse distribution of histological subtypes in advanced-stage endometrial carcinomas and evaluate the reproducibility of histological diagnosis among pathologists. We also investigated the utility and limitations of IHC staining and next-generation sequencing (NGS) analysis in the differential diagnosis of a few discordant cases and attempted to identify histological and IHC staining features that are useful in daily pathology practice.

## MATERIALS AND METHODS

### Patients and cases

Twenty-one patients with high International Federation of Gynecology and Obstetrics (FIGO) stage (stage III or IV) endometrial carcinoma who had undergone total hysterectomy in Korea University Guro Hospital (KUGH) between 2008 and 2017 were included in this study. A number of general pathologists performed the original diagnosis. Three pathologists (Y.K.C., S.Y.L., and H.J.J.) reviewed the cases; Y.K.C. is a gynecology specialty pathologist, S.Y.L. is a board-certified general pathologist, and H.J.J. is a fourth-year anatomic pathology resident.

### Three-step assessment of interobserver reproducibility

The diagnostic process proceeded as follows. First, three reviewers reached a primary diagnosis based on the H&E-stained slides. Each case was diagnosed based on the 2014 WHO Classification of Tumors of Female Reproductive Organs [3], and was categorized into one of the following entities: endometrioid carcinoma, serous carcinoma, mucinous carcinoma, clear cell carcinoma, undifferentiated/dedifferentiated carcinoma, carcinosarcoma, and mixed carcinoma. Cases diagnosed as endometrioid carcinoma were classified as low-grade (FIGO grade 1 and 2) or high-grade (FIGO grade 3).

In cases with discrepant original and primary diagnoses, reviewers reached a secondary diagnosis based on the H&E-stained and IHC-stained slides. Finally, all three pathologists conducted a discussion and reached a consensus diagnosis. If the discussion did not lead to a consensus diagnosis, NGS analysis was performed.

Concordance between the original and consensus diagnoses was calculated using the kappa statistics. A kappa value of 0.4

indicates poor agreement, 0.4–0.6 indicates moderate agreement, 0.6–0.8 indicates substantial/good agreement, and 0.8–1.0 indicates near perfect/ excellent agreement. The Windows version of IBM SPSS ver. 24.0 (IBM Corp., Armonk, NY, USA) was used for statistical analysis.

### IHC staining and interpretation

IHC staining was performed on whole slide sections using two automated staining systems, including a Bond-III autostainer (Leica Biosystems, Wetzlar, Germany) and a Bench-Mark ULTRA system (Ventana Medical Systems, Tucson, AZ, USA). In brief, 4- $\mu$ m-thick paraffin-embedded tissue sections were deparaffinized and rehydrated across a graded series of ethyl alcohol concentrations. Heat-induced antigen retrieval was carried out in citrate buffer. Sections were incubated with the primary antibody in an automated immunostainer. Counterstaining with hematoxylin was performed. The antibodies used were as follows: anti-p53 (1:200, DO-7, Novocastra, Newcastle, UK), anti-ER (Ready-To-Use [RTU], SP1, Roche, Basel, Switzerland), anti-PR (RTU, 1E2, Roche), anti-p16 (RTU, E6H4, Roche), anti-MLH1 (1:100, ES05, Novocastra), anti-MSH2 (1:400, G219-1129, Novocastra), anti-PMS2 (1:100, MRQ-28, Cell Marque, Rocklin, CA, USA), anti-MSH6 (1:200, 44, Cell Marque), anti-hepatocyte nuclear factor-1 $\beta$  (HNF-1 $\beta$ ; 1:200, polyclonal, Sigma-Aldrich, St. Louis, MO, USA), anti-napsin A (1:100, polyclonal, Cell Marque), anti-CD56 (1:200, 123 C3, DAKO, Glostrup, Denmark), anti-synaptophysin (1:200, polyclonal, Cell Marque), anti-chromogranin (1:500, Dak-A3, DAKO), anti-GATA3 (1:50, L50-823, Cell Marque), anti-CD10 (RTU, CC1, Roche), anti-thyroid transcription factor-1 (TTF-1; 1:200, 8G7G3/1, DAKO), anti-WT1 (1:200, 6F-H2, Cell Marque), anti-cytokeratin (CK; 1:200, AE1/AE3, DAKO), anti-vimentin (1:1000, Vim 384, DAKO), anti-Ki67 (1:100, MIB-1, DAKO), anti-PTEN (1:400, 6H2-1, DAKO), and anti-c-KIT (1:200, polyclonal, Novocastra).

Each reviewer independently assessed the results of IHC staining. When interpretation-associated discrepancies arose, all three reviewers conducted a discussion until a consensus was achieved. p53 immunostaining was interpreted as mutation type if the tumor exhibited: (1) diffuse strong nuclear positivity involving at least 80% of the tumor cells (aberrant pattern), (2) complete absence of staining with the presence of positive internal control staining of non-neoplastic cells such as lymphocytes (null pattern), or (3) unequivocal cytoplasmic staining accompanied by variable nuclear staining (cytoplasmic staining pattern). Cases were considered wild-type if any degree of non-diffuse nucle-

ar staining (<80%) of the tumor cells was present [12]. Immunostaining for ER and PR was scored based on the percentage of tumor cells exhibiting moderate to intense nuclear staining. p16 staining was interpreted as positive if  $\geq 90\%$  of tumor cells were stained. PTEN immunostaining was considered negative if there was a complete loss of expression in tumor cells. Immunostaining for MLH1, MSH2, MSH6, and PMS2 was considered negative (loss of expression pattern) if there was a complete absence of nuclear staining. Immunostaining for napsinA and WT1 was interpreted as positive if  $\geq 1\%$  of the tumor cells were stained, regardless of the staining intensity. HNF-1 $\beta$  immunostaining was interpreted as positive if there was positive staining in  $\geq 50\%$  of tumor cells. Immunostaining for neuroendocrine markers (CD56, synaptophysin, and chromogranin) was interpreted as positive if there was positive staining in  $\geq 10\%$  of tumor cells. Immunostaining for CK and vimentin was considered positive if there was diffuse staining in  $\geq 50\%$  of tumor cells. Immunostaining for CD10, GATA3, and TTF-1 was interpreted as positive if there was more than one area of focal staining. c-KIT immunostaining was considered positive if there was cytoplasmic staining in  $\geq 1\%$  of tumor cells. The Ki67 labeling index was measured by recording the tumor cell percentages that exhibited moderate to intense nuclear staining.

### Next-generation sequencing

Up to five 10- $\mu$ m-thick sections of formalin-fixed, paraffin-embedded tissue blocks were used for DNA and RNA sequencing analysis. Representative tumor areas were manually microdissected. DNA and RNA were extracted using the Invitrogen RecoverAll Total Nucleic Acid Isolation Kit (Invitrogen, Carlsbad, CA, USA). Massively parallel sequencing of cancer-related gene panels (Oncomine Comprehensive Assay v3, ThermoFisher Scientific Waltham, MA, USA) was performed using the Ion Chef and Ion Torrent sequencing platforms. Sequence data were aligned against the human reference genome (hg19 build). Bioinformatics data analysis was performed using Ion Reporter software (v.5.10.1.0) with the Oncomine Variants filter chain (v.5.6).

## RESULTS

### Interobserver diagnostic reproducibility

The original diagnoses in 21 cases were endometrioid carcinoma (n = 15), serous carcinoma (n = 5), and clear cell carcinoma (n = 1). Among the 15 cases of endometrioid carcinoma, five were low grade (G1, 2 cases; G2, three cases), and 10 cases were high grade (G3). The primary diagnoses made by the three reviewers

were identical in 13/21 cases (62%). These cases included endometrioid carcinoma (n = 9), serous carcinoma (n = 3), and clear cell carcinoma (n = 1). Table 1 showed a summary of the primary diagnosis.

Secondary diagnosis due to disagreement in primary diagnosis or diagnostic difficulty was performed in 8/21 cases (38%). Table 2 summarized the IHC staining result in eight discordant cases. The original diagnosis of eight cases with discrepancies was endometrioid carcinoma in six cases (one case of G1 and five cases of G3) and serous carcinoma in two cases. Secondary diagnosis based on H&E and IHC staining was concordant in four of eight discrepant cases. The secondary diagnosis of four concordant cases was mesonephric-like adenocarcinoma (case 1), carcinosarcoma (case 2), clear cell carcinoma (case 3), and large cell neuroendocrine carcinoma (LCNEC) (case 4). The four discordant cases were as follows: mixed carcinoma vs. LCNEC (case 5), G3 endometrioid vs. dedifferentiated carcinoma (case 6), and G3 endometrioid vs. serous carcinoma (cases 7 and 8).

Among four discordant cases, two cases reached a consensus diagnosis through review of all slides and discussion between three

**Table 1.** Original diagnosis and primary diagnosis of all cases

Case No.	Original diagnosis	Primary diagnosis		
		Reviewer 1	Reviewer 2	Reviewer 3
1	G1 EC	MesL	Low-grade EC	Low-grade EC
2	SC	SC vs. CS	SC	SC
3	G3 EC	G3 EC	CC	G3 EC
4	G3 EC	LCNEC	G3 EC	LCNEC
5	G3 EC	Mixed (G3 EC + CC + LCNEC)	G3 EC	SC
6	G3 EC	DD	DD	SC
7	G3 EC	G3 EC vs. SC	SC	G3 EC
8	SC	G3 EC vs. SC	SC	SC
9	G1 EC	Low-grade EC	Low-grade EC	Low-grade EC
10	G2 EC	Low-grade EC	Low-grade EC	Low-grade EC
11	G2 EC	Low-grade EC	Low-grade EC	Low-grade EC
12	G2 EC	Low-grade EC	Low-grade EC	Low-grade EC
13	G3 EC	G3 EC	G3 EC	G3 EC
14	G3 EC	G3 EC	G3 EC	G3 EC
15	G3 EC	G3 EC	G3 EC	G3 EC
16	G3 EC	G3 EC	G3 EC	G3 EC
17	G3 EC	G3 EC	G3 EC	G3 EC
18	SC	SC	SC	SC
19	SC	SC	SC	SC
20	SC	SC	SC	SC
21	CC	CC	CC	CC

G1, grade 1; G2, grade 2; G3, grade 3; EC, endometrioid carcinoma; MesL, mesonephric-like adenocarcinoma; SC, serous carcinoma; CS, carcinosarcoma; CC, clear cell carcinoma; LCNEC, large cell neuroendocrine carcinoma; Mixed, mixed cell adenocarcinoma; DD, dedifferentiated carcinoma.

pathologists. The consensus diagnosis was LCNEC (case 5) and dedifferentiated carcinoma (case 6). In two cases of G3 endometrioid vs. serous carcinoma (cases 7 and 8), NGS was performed because a consensus was not achieved even after discussion. Table 3 was a sequential diagnosis summary of eight discordant cases.

Through the above diagnostic process, three reviewers made a consensus diagnoses for 21 advanced-stage endometrial carcinoma cases. The final diagnoses included four cases of low-grade endometrioid carcinoma, five cases of high-grade (G3) endometrioid carcinoma, five cases of serous carcinoma, two cases of clear cell carcinoma, two cases of neuroendocrine carcinoma, one case of mesonephric-like adenocarcinoma, one case of carcinosarcoma, and one case of dedifferentiated carcinoma (Table 4). The overall kappa for concordance between the original diagnosis and consensus diagnosis was 0.566 (moderate agreement).

#### Cases with a consensus diagnosis from IHC staining

The original diagnosis of case 1 was G1 endometrioid carcinoma. Three pathologists' primary diagnosis were discordant, as

one pathologist diagnosed this case as mesonephric-like adenocarcinoma and two others diagnosed it as low-grade endometrioid carcinoma. The tumor exhibited diverse histological morphology such as papillary and ductal/glandular patterns with a low nuclear grade. Nuclear features of the cells included nuclear overlapping, nuclear grooves, and open, vesicular chromatin, similar to those of papillary thyroid carcinoma. Although the histopathological characteristics were consistent with those of mesonephric adenocarcinoma, mesonephric remnants and uterine cervical involvement were not identified. IHC staining showed positivity in GATA3 and TTF-1, negativity in CD10 and ER, and focal positivity in PR. Based on pathologic findings and IHC results, the consensus diagnosis was mesonephric-like adenocarcinoma (Fig. 1A, B).

In case 2, the original diagnosis was serous carcinoma. This primary diagnosis was discordant as two pathologists diagnosed this as serous carcinoma, while the remaining pathologist could not decide between serous carcinoma and carcinosarcoma. Microscopic findings showed serous and mesonephric carcinoma

**Table 2.** Immunohistochemical staining results of eight discordant cases

Case No.	Original diagnosis	p53	ER	PR	Others
1	G1 EC	Wild type	(-)	(+), 30%	GATA3 (+), TTF-1 (+), CD10 (-)
2	SC	Aberrant	(+), 10%	(+), 5%	p16 (+, diffuse in carcinoma) CK (+, diffuse in carcinoma, focal in sarcoma) Vimentin (+ in sarcoma) WT1 (+ in carcinoma)
3	G3 EC	Wild type	(-)	(-)	Napsin A (+), HNF-1 $\beta$ (-)
4	G3 EC	Wild type	(+), 30%	(-)	CD56 (+), chromogranin (+), synaptophysin (-)
5	G3 EC	Wild type	(+), 20%	(+), 15%	CD56 (+), synaptophysin (+), chromogranin (+, focal) PTEN (+), WT1 (-)
6	G3 EC	Wild type	(+), 10%	(+), 5%	pMMR
7	G3 EC	Null	(-)	(-)	p16 (+, diffuse), pMMR, WT1 (+), PTEN (+)
8	SC	Aberrant	(-)	(-)	p16 (+, diffuse), pMMR, WT1 (+, focal)

ER; estrogen receptor; PR, progesterone receptor; EC, endometrioid carcinoma; G1, grade 1; G3, grade 3; TTF-1, thyroid transcription factor-1; SC, serous carcinoma; CK, cytokeratin; pMMR, proficient mismatch repair.

**Table 3.** Sequential diagnosis of discordant cases

Case No.	Original diagnosis	Primary diagnosis			2nd diagnosis			Consensus diagnosis
		Reviewer 1	Reviewer 2	Reviewer 3	Reviewer 1	Reviewer 2	Reviewer 3	
1	G1 EC	MesL	Low-grade EC	Low-grade EC	MesL	MesL	MesL	MesL
2	SC	SC vs. CS	SC	SC	CS	CS	CS	CS
3	G3 EC	G3 EC	CC	G3 EC	CC	CC	CC	CC
4	G3 EC	LCNEC	G3 EC	LCNEC	LCNEC	LCNEC	LCNEC	LCNEC
5	G3 EC	Mixed (G3 EC + CC + LCNEC)	G3 EC	SC	LCNEC	LCNEC	Mixed (low-grade EC + LCNEC)	LCNEC
6	G3 EC	DD	DD	SC	DD	DD	G3 EC	DD
7	G3 EC	G3 EC vs. SC	SC	G3 EC	G3 EC vs. SC	SC	SC	SC <sup>a</sup>
8	SC	SC vs. G3 EC	SC	SC	G3 EC	SC	G3 EC	SC <sup>a</sup>

G1, grade 1; G2, grade 2; G3, grade 3; EC, endometrioid carcinoma; MesL, mesonephric-like adenocarcinoma; SC, serous carcinoma; CS, carcinosarcoma; LCNEC, large cell neuroendocrine carcinoma; Mixed, mixed cell adenocarcinoma; CC, clear cell carcinoma; DD, dedifferentiated carcinoma.

<sup>a</sup>Consensus diagnosis was made after next-generation sequencing analysis.



**Table 4.** Original diagnosis and consensus diagnosis of all reviewed cases

Case No.	Original diagnosis	Consensus diagnosis
1	G1 EC	MesL
2	SC	CS
3	G3 EC	CC
4	G3 EC	LCNEC
5	G3 EC	LCNEC
6	G3 EC	DD
7	G3 EC	SC
8	SC	SC
9	G1 EC	Low-grade EC
10	G2 EC	Low-grade EC
11	G2 EC	Low-grade EC
12	G2 EC	Low-grade EC
13	G3 EC	G3 EC
14	G3 EC	G3 EC
15	G3 EC	G3 EC
16	G3 EC	G3 EC
17	G3 EC	G3 EC
18	SC	SC
19	SC	SC
20	SC	SC
21	CC	CC

G1, grade 1; G2, grade 2; G3, grade 3; EC, endometrioid carcinoma; MesL, mesonephric-like adenocarcinoma; SC, serous carcinoma; CS, carcinosarcoma; CC, clear cell carcinoma; LCNEC, large cell neuroendocrine carcinoma; DD, dedifferentiated carcinoma.

components. Two small foci of atypical spindle and pleomorphic cell proliferation suggested the presence of a sarcomatous component. The spindle cell component exhibited strong vimentin positivity and aberrant p53 expression, while CK expression was focal and weak. After discussion, the three pathologists agreed upon the presence of a distinct sarcomatous component, and a consensus diagnosis of carcinosarcoma was made (Fig. 1C, D).

Case 3 showed solid or glandular proliferation patterns, and the tumor cells displayed severe nuclear atypia and abundant clear or eosinophilic cytoplasm. The primary diagnosis was discordant, with one diagnosis of clear cell carcinoma and two diagnoses of endometrioid carcinoma. On IHC stains, the tumor cells were p53 wild-type and negative for ER, PR, and HNF-1 $\beta$  with granular positivity for napsin A. The final consensus diagnosis was clear cell carcinoma (Fig. 1E, F).

In case 4, large polygonal cells with prominent nucleoli and abundant cytoplasm formed well-demarcated nests, which displayed peripheral palisading. Frequent mitotic figures were observed, and geographic tumor necrosis was identified. The primary diagnosis was discordant, with two diagnoses of neuroendocrine carcinoma and one diagnosis of G3 endometrioid carcinoma. The tumor cells revealed diffuse positivity to CD56 and chromogranin.

A consensus diagnosis of LCNEC was rendered (Fig. 1G, H).

### Cases confirmed by consensus discussion

For case 5, the primary diagnoses were mixed carcinoma (endometrioid carcinoma, clear cell carcinoma, and neuroendocrine carcinoma) vs. G3 endometrioid carcinoma vs. serous carcinoma. Histopathologic analysis showed that the tumor was composed of endometrioid carcinoma (50%), clear cell carcinoma (30%), and LCNEC (20%). The IHC staining revealed an LCNEC component showing diffuse positivity for CD56 and synaptophysin and focal positivity for chromogranin. Although the tumor consisted of various components, according to the criteria of the WHO Classification of Tumors of Female Reproductive Organs [3], case 5 was diagnosed as LCNEC (Fig. 2A, B).

In case 6, the primary diagnosis was divided into two diagnoses of dedifferentiated carcinoma and one diagnosis of serous carcinoma. The secondary diagnosis was also discordant, as two pathologists diagnosed the case as dedifferentiated carcinoma and the remaining pathologist's diagnosis was G3 endometrioid carcinoma. Microscopically, the tumor was composed of G1 endometrioid carcinoma and a poorly differentiated solid portion showing non-cohesive cells without readily visible gland formation. The three reviewers agreed that the solid portion was an undifferentiated carcinoma, not a high-grade endometrioid carcinoma component. A final consensus diagnosis of dedifferentiated carcinoma was reached (Fig. 2C, D).

### Cases that reached consensus diagnosis with NGS

The microscopic features of case 7 displayed columnar tumor cells with nuclear pseudostratification and pleomorphism. While the tumor's dominant pattern was solid proliferation, several foci showed complex papillary or glandular patterns. IHC staining revealed a complete loss of p53 staining, negativity for ER and PR, and positivity for p16, WT1, MLH1, PMS2, MSH2, and MSH6. NGS analysis was performed as histopathological features (suggestive of endometrioid carcinoma) and IHC features (suggestive of serous carcinoma) exhibited discrepancies (Fig. 2E, F). NGS revealed mutations in *TP53*, *PIK3CA*, and *NF1*, and copy number variations (CNVs) in *MYCL*, *FGFR3*, *CDK2*, *CDK4*, *ERBB2*, and *CCNE1*. As the molecular profile corresponded to a copy-number high group, the final diagnosis was rendered as serous carcinoma.

Case 8 presented with high-grade tumor cells with severe nuclear pleomorphism. The tumor showed complex glandular and solid patterns. In the solid portion, nuclear pleomorphism was less severe than that of typical serous carcinoma. The primary

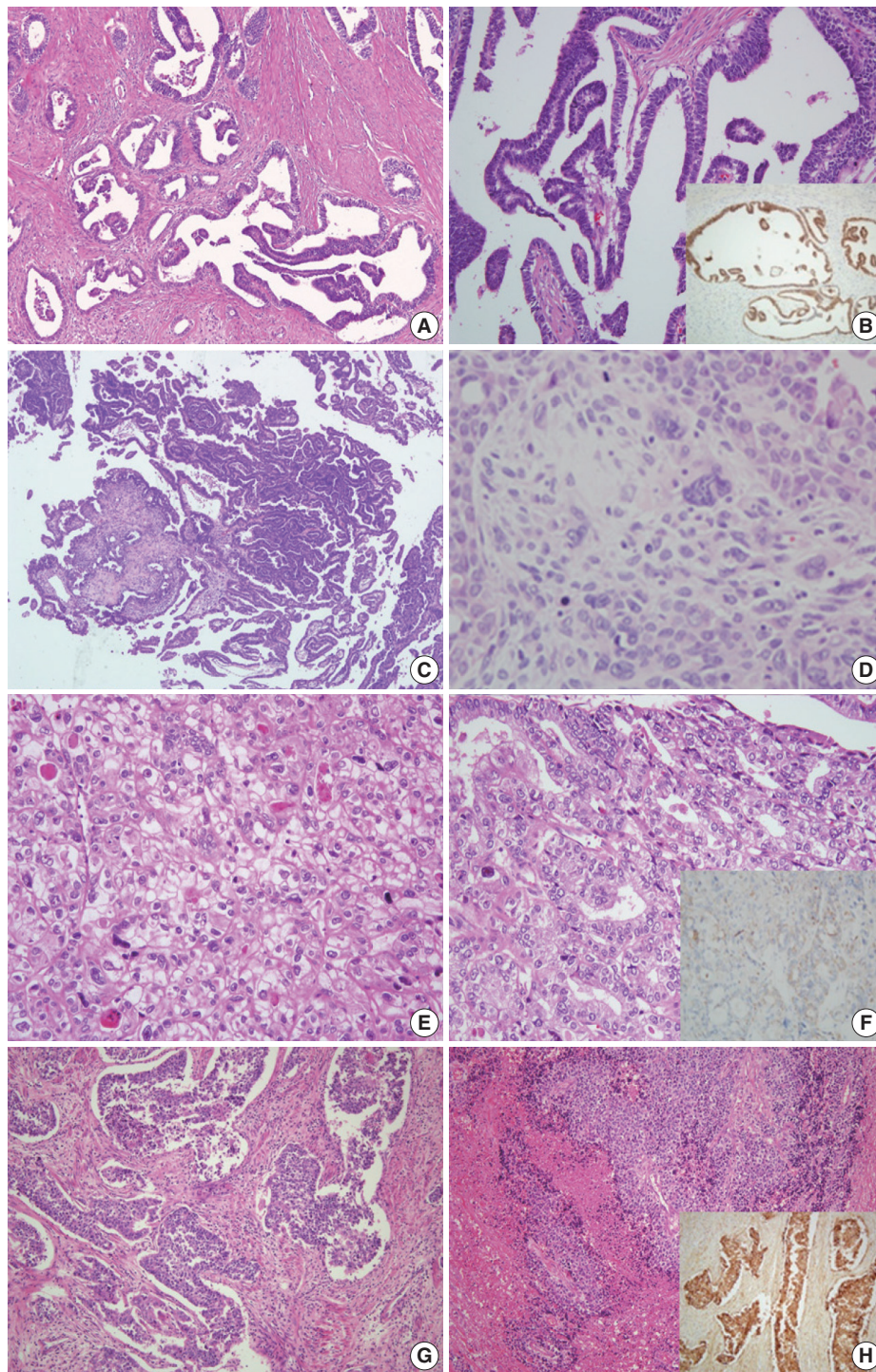


**Fig. 1.** Representative microscopic features of cases 1–4. (A) In case 1 (mesonephric-like adenocarcinoma), the tumor showed ductal/glandular and papillary patterns. (B) Nuclear features of tumor cells were similar to those of papillary thyroid carcinoma, showing nuclear overlapping and openness of vesicular chromatin. Immunohistochemical (IHC) staining showed positivity in GATA3 (inset). (C) In case 2 (carcinosarcoma), the tumor predominantly showed complex papillary components and small foci of hypercellular stromal lesions. (D) On higher magnification, this lesion consisted of atypical pleomorphic spindle cells with frequent mitosis. (E) In case 3 (clear cell carcinoma), the tumor mainly showed a solid pattern. The tumor cells had hyperchromatic nuclei with vesicular chromatin and eosinophilic or clear cytoplasm. (F) A portion of the tumor showed a glandular pattern with high-grade nuclear atypia. On IHC stains, the tumor cells exhibited granular positivity for napsin A (inset). (G) In case 4 (large cell neuroendocrine carcinoma), the tumor showed well-defined nests with peripheral palisading. (H) Geographic tumor necrosis and diffuse immunoreactivity to CD56 was seen (inset).



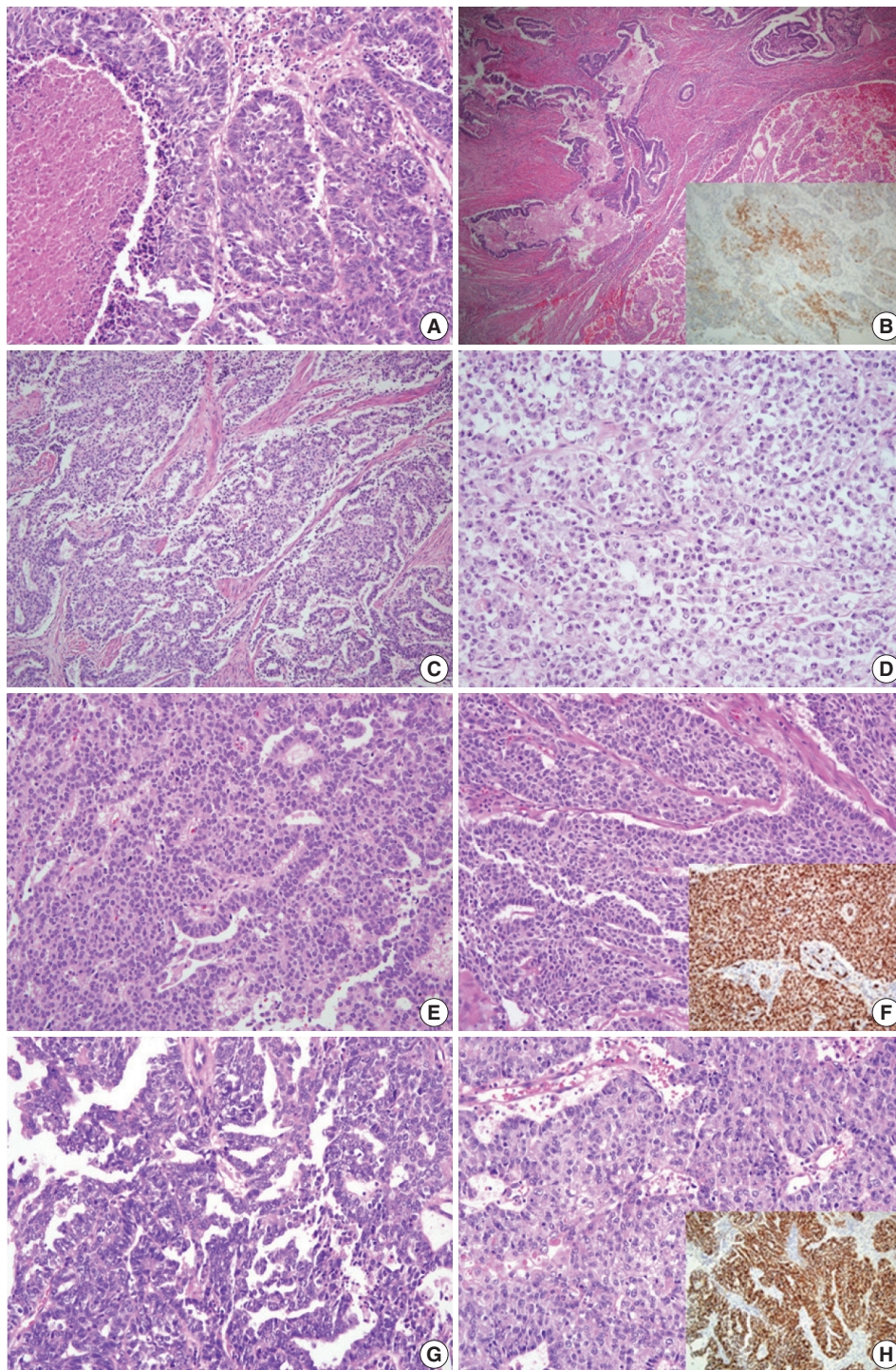


**Fig. 2.** Representative microscopic features of cases 5–8. (A) In case 5 (large cell neuroendocrine carcinoma), a portion of the tumor was composed of well-defined nests with peripheral palisading and geographic necrosis. (B) The tumor also partly showed complex glandular and papillary pattern. The Immunohistochemical (IHC) staining of tumor cells showed diffuse positivity for synaptophysin (inset). (C) In case 6 (dedifferentiated carcinoma), the tumor showed complex glandular architecture consisting of columnar cells. (D) The undifferentiated carcinoma component was composed of solid sheets of monotonous dyscohesive cells. (E) In case 7 (serous carcinoma), the tumor showed a focal complex glandular and papillary pattern. (F) It was mostly comprised of solid architecture with high-grade nuclei and diffuse positivity to WT1 (inset). (G) In case 8 (serous carcinoma), some areas of the tumor showed papillary and micropapillary architecture composed of columnar cells with prominent nucleoli and nuclear pleomorphism. (H) Most of the tumor showed a solid pattern with focal glandular differentiation with tumor cells showing mild nuclear atypia. On immunostaining, the tumor cells exhibited aberrant p53 expression (inset).



diagnoses were divided into G3 endometrioid carcinoma versus serous carcinoma. On immunostaining, the tumor cells exhibited aberrant p53 expression, negativity for PR, diffuse positivity for p16, MLH1, PMS2, MSH2, and MSH6, and focal positivity for WT1 and ER. While the immunoprofile suggested serous carcinoma, the diagnosis of G3 endometrioid carcinoma could not be entirely excluded for the histomorphological findings (Fig. 2G, H). NGS analysis revealed mutations in *TP53* and polymerase E (*POLE*) and CNVs involving *ALK*, *ERBB2*, *CCNE1*, *AKT2*, and *AXL*. Although *POLE* mutation was present, the total tumor mutation burden was not as high as that seen in the typical *POLE*-ultramutated type. Since a significant number of CNVs were detected, the case was assigned to the copy-number high group, and a final diagnosis of serous carcinoma was made.

## DISCUSSION

Diagnosis of high-grade endometrial carcinoma has been shown to be unreproducible, even among gynecologic pathology specialists. In several studies involving high-grade endometrial carcinoma, the consensus rate of cancer histotypes among the participating pathologists varied from 39% to 72% [7,8,13]. According to Gilks et al. [7], a diagnostic consensus among three reviewers about the exclusive or major subtype of high-grade endometrial carcinoma was reached in only 62.5% of cases. We studied diagnostic agreement in high-grade endometrial carcinoma cases to evaluate interobserver reproducibility, based on the assumption that advanced-stage endometrial carcinoma would predominantly consist of high-grade endometrial carcinomas.

Of the advanced-stage endometrial carcinomas included in this study, the original diagnosis and the primary diagnosis by three reviewers were identical in 13/21 cases (62%). These cases had typical histopathological features, and the diagnoses included nine cases of endometrioid carcinoma, three cases of serous carcinoma, and one case of clear cell carcinoma. Among the eight cases involving discordant primary diagnoses, six cases were initially diagnosed as endometrioid carcinoma and two cases were diagnosed as serous carcinoma. We attained diagnostic agreement for six of the eight cases based on characteristic histopathological features and IHC staining results. The cases in which meticulous histologic examination alone led to an agreed diagnosis were carcinosarcoma and dedifferentiated carcinoma. The diagnosis of LCNEC, mesonephric-like adenocarcinoma, and clear cell carcinoma were achieved by panel of IHC staining. The overall kappa for concordance between the original and consensus diagnosis was 0.566 (moderate agreement). Other studies

about interobserver reproducibility also show similar kappa values [8,13].

In cases 7 and 8, it was difficult to differentiate between serous carcinoma and G3 endometrioid carcinoma. Both cases exhibited papillary growth and marked nuclear atypia, and immunostaining findings suggested a diagnosis of serous carcinoma. However, the possibility of G3 endometrioid carcinoma could not be wholly excluded. Molecular profiling by NGS was performed to reach a final diagnosis. In a comprehensive genomic analysis of endometrioid and serous carcinoma based on the The Cancer Genome Atlas database, endometrioid and serous carcinomas were divided into four molecular subgroups [11], including *POLE* ultramutated, microsatellite instability-hypermutated, copy-number low, and copy-number high; serous carcinoma belongs only to the copy-number high group. Endometrioid carcinoma belongs to all four groups [14]. According to this molecular classification scheme, cases 7 and 8 were designated as copy-number high group and finally diagnosed as serous carcinoma.

In daily clinical practice settings, where molecular studies cannot be performed routinely, histopathological examination and IHC panel staining help to differentiate G3 endometrioid carcinoma from serous carcinoma. If the tumor shows papillary growth, cellular tufts, and diffuse high-grade nuclear atypia, a diagnosis of serous carcinoma is favored. When defining endometrioid features such as squamous or mucinous differentiation on a background of endometrial hyperplasia present, a diagnosis of endometrioid carcinoma can be rendered. The use of a panel of IHC stains can help to establish a confirmatory diagnosis when histomorphological findings are unclear or overlapping [6,9,15]. Biomarkers commonly used to distinguish between endometrioid and serous carcinomas are immunostaining for p53, p16, ER, PR, PTEN, and DNA mismatch repair proteins [6,9,12,16,17]. Tumors lacking aberrant p53 expression are unlikely to be serous carcinoma [17].

The final diagnosis of case 1 was mesonephric-like adenocarcinoma, whereas the original diagnosis was G1 endometrioid carcinoma. Mesonephric carcinoma exhibits diverse morphology, such as tubular, glandular, papillary, retiform, and glomeruloid patterns, and nuclei resembling those of papillary thyroid carcinoma, with dense focal eosinophilic intraluminal secretions [17,18]. Mesonephric-like adenocarcinoma can be differentiated from low-grade endometrioid carcinoma by immunostaining for ER and PR, as mesonephric-like adenocarcinoma rarely shows immunoreactivity to these antigens. As mesonephric-like adenocarcinoma shows aggressive clinical behavior with preponderance for pulmonary metastasis [18], accurate diagnosis of this

tumor is of critical importance.

Endometrial neuroendocrine carcinoma is a rare, highly aggressive tumor, and has a propensity for systemic spread and poor prognosis [19]. In this study, two LCNEC cases were originally diagnosed as G3 endometrioid carcinoma. Neuroendocrine carcinoma usually presents as pure neuroendocrine carcinoma or a mixture of other epithelial neoplasias, most commonly endometrioid carcinoma. The diagnosis of endometrial neuroendocrine carcinomas is challenging, due to its frequent association with low-grade endometrioid carcinoma. Awareness of these facts may help to avoid overdiagnosis or misdiagnosis of neuroendocrine carcinoma, especially in quantitatively limited samples [19].

The dedifferentiated carcinoma identified in this study (case 6) was composed of low-grade endometrioid carcinoma and undifferentiated carcinoma. Undifferentiated carcinoma is defined as a malignant epithelial neoplasm composed of small to intermediate-sized cells arranged in sheets, without any apparent glandular differentiation; it often exhibits a characteristically 'dyscohesive' pattern [6,17]. When combined with low-grade endometrioid carcinoma, it is often misinterpreted as a solid growth of endometrioid carcinoma. The original diagnosis of case 6 was G3 endometrioid carcinoma. While it is easy to overlook due to its rarity, diagnosis of undifferentiated/dedifferentiated carcinoma is essential, because it has a poorer prognosis than high-grade endometrioid carcinoma [20].

This study has a few limitations. First, the number of cases studied was small (a total of 21 cases) and the three reviewers produced diverse diagnoses, so there was no proper statistical method to calculate interobserver reproducibility. Second, only one of the three reviewers was an expert in gynecologic pathology. Since the two general pathologists were not familiar with the difficult histologic diagnosis of high-grade endometrial carcinoma, the interobserver discrepancy rate might have been measured higher than expected.

We investigated sequential changes in interobserver reproducibility in advanced-stage and high-grade endometrial carcinoma, with the stepwise addition of IHC results and molecular data. Accurate histological diagnosis of endometrial carcinoma subtypes is critical for patient management since several rare subtypes show unfavorable prognosis and require different treatment decisions. In conclusion, we demonstrated the utility of selected IHC markers and NGS molecular profiling in the diagnosis of advanced-stage endometrial carcinoma.

### Ethics Statement

This study was approved by the Institutional Review Board of KUGH (ac-

cession No. 2020GR0348). All the glass slides, paraffin blocks, and clinicopathological information were provided by the KUGH Biobank, which had collected patient samples and information with their informed consent.

### ORCID

Ho Jin Jung <https://orcid.org/0000-0002-5032-6178>  
 Soo Yeon Lee <https://orcid.org/0000-0003-0142-377X>  
 Jin Hwa Hong <https://orcid.org/0000-0002-6905-5363>  
 Yi Kyeong Chun <https://orcid.org/0000-0002-4235-9690>

### Author Contributions

Conceptualization: HJJ, SYL, JHH, YKC. Data curation: HJJ, SYL, YKC. Formal analysis: HJJ, SYL, YKC. Investigation: HJJ, SYL, YKC. Methodology: HJJ, JHH, YKC. Supervision: YKC. Validation: HJJ, SYL, JHH, YKC. Writing—original draft: HJJ, YKC. Writing—review & editing: HJJ, SYL, YKC. Approval of final manuscript: all authors.

### Conflicts of Interest

The authors declare that they have no potential conflicts of interest.

### Funding Statement

No funding to declare.

### References

1. Ferlay J, Soerjomataram I, Dikshit R, et al. Cancer incidence and mortality worldwide: sources, methods and major patterns in GLOBOCAN 2012. *Int J Cancer* 2015; 136: E359-86.
2. Lim MC, Won YJ, Ko MJ, et al. Incidence of cervical, endometrial, and ovarian cancer in Korea during 1999-2015. *J Gynecol Oncol* 2019; 30: e38.
3. Kurman RJ, Carcangiu ML, Herrington CS, Young RH. WHO classification of tumours of female reproductive organs. 4th ed. Lyon: IARC Press, 2014.
4. Bokhman JV. Two pathogenetic types of endometrial carcinoma. *Gynecol Oncol* 1983; 15: 10-7.
5. Wang J, Jia N, Li Q, et al. Analysis of recurrence and survival rates in grade 3 endometrioid endometrial carcinoma. *Oncol Lett* 2016; 12: 2860-7.
6. Murali R, Davidson B, Fadare O, et al. High-grade endometrial carcinomas: morphologic and immunohistochemical features, diagnostic challenges and recommendations. *Int J Gynecol Pathol* 2019; 38 Suppl 1: S40-63.
7. Gilks CB, Oliva E, Soslow RA. Poor interobserver reproducibility in the diagnosis of high-grade endometrial carcinoma. *Am J Surg Pathol* 2013; 37: 874-81.
8. Han G, Sidhu D, Duggan MA, et al. Reproducibility of histological cell type in high-grade endometrial carcinoma. *Mod Pathol* 2013; 26: 1594-604.
9. Nastic D, Shanwell E, Wallin KL, et al. A selective biomarker panel increases the reproducibility and the accuracy in endometrial biopsy diagnosis. *Int J Gynecol Pathol* 2017; 36: 339-47.
10. Yen TT, Wang TL, Fader AN, Shih IM, Gaillard S. Molecular classification and emerging targeted therapy in endometrial cancer. *Int J Gynecol Pathol* 2020; 39: 26-35.
11. Hussein YR, Soslow RA. Molecular insights into the classification of high-grade endometrial carcinoma. *Pathology* 2018; 50: 151-61.
12. Kobel M, Ronnett BM, Singh N, Soslow RA, Gilks CB, McCluggage WG. Interpretation of P53 immunohistochemistry in endo-

- metrial carcinomas: toward increased reproducibility. *Int J Gynecol Pathol* 2019; 38 Suppl 1: S123-31.
13. Hoang LN, Kinloch MA, Leo JM, et al. Interobserver agreement in endometrial carcinoma histotype diagnosis varies depending on The Cancer Genome Atlas (TCGA)-based molecular subgroup. *Am J Surg Pathol* 2017; 41: 245-52.
  14. Soslow RA, Tornos C, Park KJ, et al. Endometrial carcinoma diagnosis: use of FIGO grading and genomic subcategories in clinical practice: recommendations of the International Society of Gynecological Pathologists. *Int J Gynecol Pathol* 2019; 38 Suppl 1: S64-74.
  15. Hoang LN, McConechy MK, Kobel M, et al. Histotype-genotype correlation in 36 high-grade endometrial carcinomas. *Am J Surg Pathol* 2013; 37: 1421-32.
  16. Chen W, Husain A, Nelson GS, et al. Immunohistochemical profiling of endometrial serous carcinoma. *Int J Gynecol Pathol* 2017; 36: 128-39.
  17. Carlson JW, Nastic D. High-grade endometrial carcinomas: classification with molecular insights. *Surg Pathol Clin* 2019; 12: 343-62.
  18. Horn LC, Hohn AK, Krucken I, Stiller M, Obeck U, Brambs CE. Mesonephric-like adenocarcinomas of the uterine corpus: report of a case series and review of the literature indicating poor prognosis for this subtype of endometrial adenocarcinoma. *J Cancer Res Clin Oncol* 2020; 146: 971-83.
  19. Pocrnich CE, Ramalingam P, Euscher ED, Malpica A. Neuroendocrine carcinoma of the endometrium: a clinicopathologic study of 25 cases. *Am J Surg Pathol* 2016; 40: 577-86.
  20. Yokomizo R, Yamada K, Iida Y, et al. Dedifferentiated endometrial carcinoma: a report of three cases and review of the literature. *Mol Clin Oncol* 2017; 7: 1008-12.



# A comparative prognostic performance of definitions of Crohn-like lymphoid reaction in colorectal carcinoma

Younghoon Kim<sup>1,2,3</sup>, Jeong Mo Bae<sup>1,3</sup>, Jung Ho Kim<sup>1,3</sup>, Nam-Yun Cho<sup>1</sup>, Gyeong Hoon Kang<sup>1,2</sup>

<sup>1</sup>Laboratory of Epigenetics, Cancer Research Institute, Seoul National University College of Medicine, Seoul;

<sup>2</sup>Department of Pathology, Seoul National University College of Medicine, Seoul;

<sup>3</sup>Department of Pathology, Seoul National University Hospital, Seoul, Korea

**Background:** The prognostic potential of Crohn-like lymphoid reaction (CLR) in colorectal carcinoma (CRC) has been investigated through the assessment of different criteria. **Methods:** The prognostic impact of CLR was investigated in 636 CRC patients to compare methods from previously published articles. These methods included CLR measured by number of lymphoid aggregates (LAs) (CLR count), LA size greater than or equal to 1 mm (CLR size), CLR density with a cutoff value of 0.38, and subjective criteria as defined by intense CLR. **Results:** In univariate survival analysis, CLR-positive CRC as defined by the four aforementioned methods was associated with better overall survival (OS) (hazard ratio [HR], 0.463; 95% confidence interval [CI], 0.305 to 0.702;  $p < .001$ ; HR, 0.656; 95% CI, 0.411 to 1.046;  $p = .077$ ; HR, 0.363; 95% CI, 0.197 to 0.669;  $p = .001$ ; and HR, 0.433; 95% CI, 0.271 to 0.690;  $p < .001$ , respectively) and disease-free survival (DFS) (HR, 0.411; 95% CI, 0.304 to 0.639;  $p < .001$ ; HR, 0.528; 95% CI, 0.340 to 0.821;  $p = .004$ ; HR, 0.382; 95% CI, 0.226 to 0.645;  $p = .004$ ; and HR, 0.501; 95% CI, 0.339 to 0.741;  $p < .001$ , respectively) than CLR-negative CRC, regardless of criteria with the exception of OS for CLR density. In multivariate analysis, two objective criteria (CLR count and CLR density) and one subjective criterion (intense CLR) for defining CLR were considered independent prognostic factors of OS and DFS in CRC patients. **Conclusions:** CLR has similar traits regardless of criteria, but CLR-positivity should be defined by objective criteria for better reproducibility and prognostic value.

**Key Words:** Colorectal neoplasms; Crohn-like lymphoid reaction; Histology; Prognosis

Received: August 24, 2020 Revised: September 21, 2020 Accepted: October 6, 2020

Corresponding Author: Gyeong Hoon Kang, MD, PhD, Department of Pathology, Seoul National University College of Medicine, 103 Daehak-ro, Jongro-gu, Seoul 03080, Korea  
Tel: +82-2-740-8273, Fax: +82-2-765-5600, E-mail: ghkang@snu.ac.kr

Colorectal cancer (CRC) is the fourth most common cause of cancer death worldwide, and its incidence is increasing in young patients [1]. Although CRC is a heterogeneous cancer with various subtypes, a lymphoid reaction is known to represent the immune response to the tumor [2-4]. Among these reactions, the Crohn-like lymphoid reaction (CLR) consists of lymphoid aggregates (LAs), with or without germinal centers that are distributed within the bowel wall, that surpass the invasion front (IF) of the tumor and are mostly localized in the muscularis propria and the pericolic adipose tissue [5]. Like other lymphoid reactions within CRC, CLR has not only been described as a means of antitumor immune response but also as a prognostic factor in several individual studies [4,6-8].

In CRC, conditions that involve dense lymphocytic reactions, namely CLR, peritumoral reaction, intratumoral periglandular

reaction, and tumor-infiltrating lymphocytes, are strongly associated with molecular subtypes microsatellite instability (MSI) and the CpG island methylator phenotype (CIMP) [9-13]. Inflammatory bowel diseases (IBD) including ulcerative colitis and Crohn's disease could also be the reason for CLR in patients with CRC. Since certain molecular subtypes or preceding IBD could be associated with the prognosis, it would be possible to assume that these factors may act as confounding factors between CLR and patient prognosis [14-16]. However, previous studies have found that CLR is a prognostic indicator even within MSI-high or colitis-associated CRC populations [6,17]. Therefore, it has been acknowledged that a quantifying immune reaction could benefit in providing additional survival information in overall CRC patients [18].

Several different histological assessment systems have been

developed to determine the correlation between CLR and prognosis. Some of the criteria for identifying positive CLR have been categorized and applied to a single MSI-high CRC patient cohort [4-7]. However, a comparative analysis that assesses alternative criteria in a single CRC population regardless of molecular subtype or preceding disease conditions has been unavailable up to this point. In this study, we reviewed previous studies to investigate the methods that were used to measure CLR in CRC and categorized the criteria being used. Furthermore, we compared each criterion in a single CRC patient set to characterize different aspects of various CLR criteria including association with prognosis, age, sex, molecular subtype, and other histological characteristics. We attempted to clarify the prognostic value of CLR in CRC according to various assessment systems.

## MATERIALS AND METHODS

### Patients and specimens

We retrospectively analyzed 767 CRC patients who underwent tumor resection between January 2004 and December 2006. Among them, 636 patients whose whole section slide samples were available from the pathology archive at Seoul National University Hospital were selected. The available tissue samples were formalin-fixed, paraffin-embedded tissues that were obtained from CRC specimens resected during curative surgery. Patients exposed to chemotherapy or radiotherapy before resection were excluded. Patient information including age, sex, and other clinical or pathological data were collected from the electronic medical records.

### Analysis of molecular subtypes and *KRAS* and *BRAF* mutation status

MSI status was determined using five microsatellite markers (BAT25, BAT26, D2S123, D5S345, and D17S250). MSI-high was defined when instability was present in  $\geq 40\%$  of the mark-

ers. MSI-low and microsatellite stable (MSS) were defined as instability in one marker and none of the markers, respectively. CIMP status was determined by quantification of the DNA methylation levels in eight markers (*CACNA1G*, *CDKN2A*, *CRABP1*, *IGF2*, *MLH1*, *NEUROG1*, *RUNX3*, and *SOC1*) via bisulfate DNA modification and MethyLight as described previously [19]. CIMP was considered positive when more than four markers were methylated but negative otherwise. To evaluate mutations in *KRAS* and *BRAF*, microdissected tissues were manually collected and incubated in a mixture of lysis buffer and proteinase K at 55°C for 2 days. *KRAS* mutations were identified by direct sequencing of codons 12 and 13. *BRAF* mutations were identified by allele-specific polymerase chain reaction in codon 600 as described previously [20].

### Pathological assessment of CLR

Two pathologists (YK and JMB) assessed the CLR status of 636 CRC patient slides. Criteria used for assessments were obtained from the review of previous studies (Table 1) [4,6,7,9,17,21-23]. These criteria include (1) counting the number of three or more LAs, from Buckowitz et al. (Fig. 1A, CLR count), (2) size-based assessment of LA  $\geq 1$  mm, from Ueno et al. (Fig. 1B, CLR size), (3) criteria from the Väyrynen-Mäkinen group, which considers a density of CLR (the number of LAs divided by the length of the IF) greater than or equal to 0.38 to be high (Fig. 1C, CLR density), and (4) intense CLR (Fig. 1D), which represents less objective criteria such as transmural and intense CLR [4,7,21].

### Statistical analysis

R (ver. 3.3.1, R Foundation for Statistical Computing, Vienna, Austria) was used to analyze the CRC patient samples. To compare categorical variables, Fisher exact test was performed. For the univariate analysis, Kaplan-Meier analysis with a log-rank test was used to investigate the association between clinicopath-

**Table 1.** Characteristics of studies of the correlation between CLR and survival

Study	Stage	No.	Positive (%)	Subtype	Outcome	CLR criteria
Buckowitz et al. (2005) [21]	I-IV	118	35.6	-	OS	$\geq 3$ LAs
Ogino et al. (2009) [9]	I-IV	843	27.3	-	CSS, OS	Transmural CLR
Kim et al. (2015) [6]	I-IV	212	21.5-65.1	MSI-H	DFS	Intense CLR, LA $\geq 1$ mm, LA/IF $\geq 0.38$
Rozek et al. (2016) [22]	I-IV	1484	47.1	-	CSS, OS	$\geq 3$ LAs
Kakar et al. (2004) [23]	I-IV	248	41.1	Mucinous	OS	Intense CLR
Lewis et al. (2013) [17]	I-IV	89	56.2	Colitis-associated	PFS, OS	Transmural CLR
Ueno et al. (2013) [4]	I-IV	1354	73.3	-	DFS	LA $\geq 1$ mm
Väyrynen et al. (2014) [7]	I-IV	567	-	-	CSS	LA/IF $\geq 0.38$

CLR, Crohn-like lymphoid reaction; OS, overall survival; LA, lymphoid aggregate; CSS, cancer-specific survival; MSI-H, microsatellite instability-high; DFS, disease-free survival; IF, invasion front; PFS, progression-free survival.



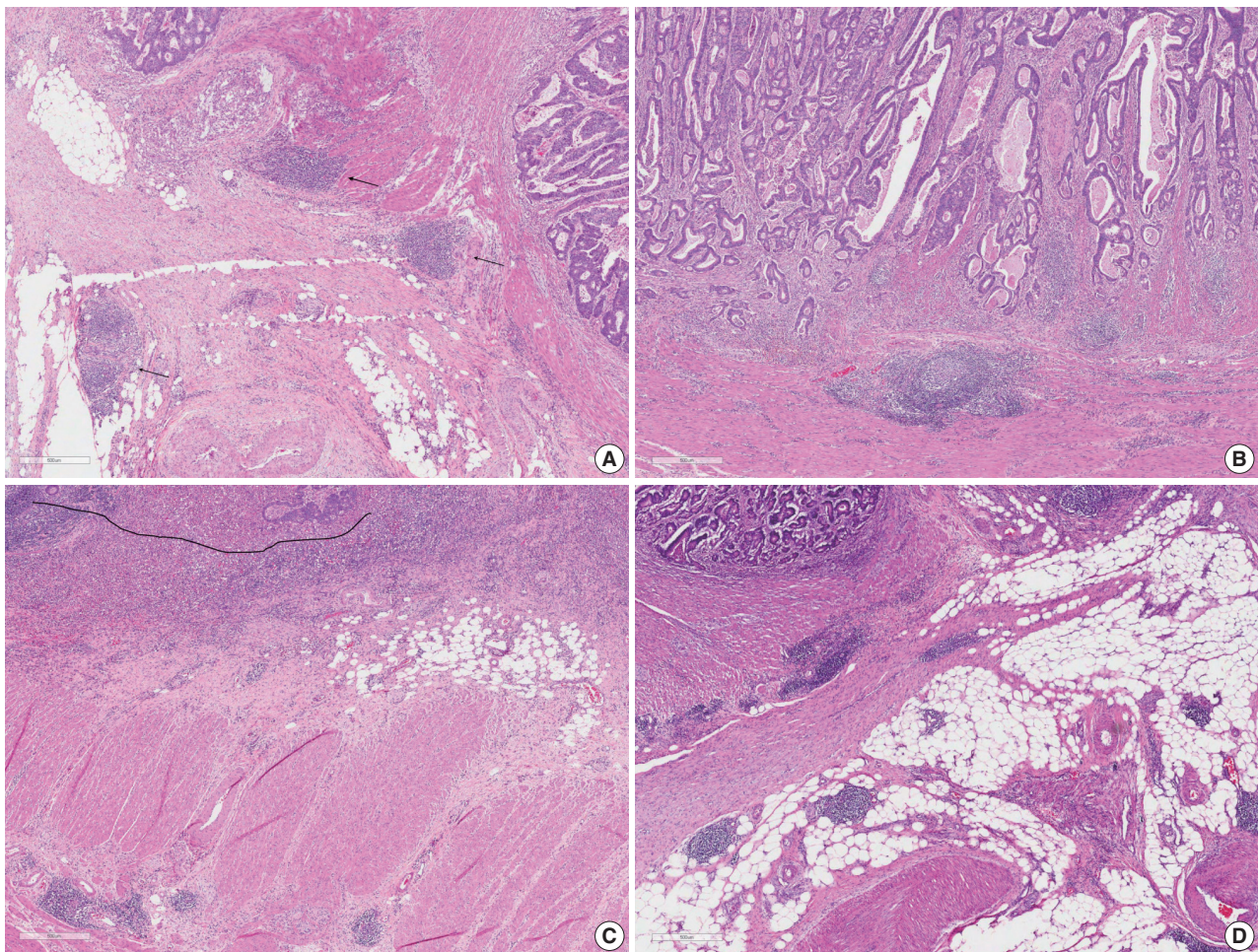


**Fig. 1.** Examples of Crohn-like lymphoid reaction (CLR)-positive cases according to each criterion. (A) At least three lymphoid aggregates (LAs) (arrow), positive according to CLR count. (B) A single LA, which is greater than or equal to 1 mm in diameter, positive by CLR size. (C) The number of LAs divided by the length of the invasion front (bold line) is greater than or equal to 0.38 (positive according to CLR density). (D) An intense LA in the proper muscle and subserosa.

ological parameters including CLR status and survival. Multivariate survival analysis, which was performed when the p-value was less than .05 in the univariate analysis for a given parameter, was conducted using the Cox proportional hazards regression model.

## RESULTS

### Association between clinicopathological parameters and CLR in CRC patients

The clinicopathological features of CRCs with CLR-positivity according to different CLR criteria are summarized in Table 2. CLR-positive CRCs, regardless of the CLR criteria used, were significantly associated with a lower pTNM stage. Lymphatic invasion demonstrated a significant inverse correlation with CLR-positive CRCs as defined by CLR count, CLR size, and intense

CLR ( $p = .002$ ,  $p = .005$ , and  $p = .021$ , respectively). CLR-positivity was positively correlated with MSI-high and demonstrated preference for the colon over the rectum and for the right-sided colon over the left-sided colon as the site of origin, regardless of criteria.

### Prognostic value of CLR according to different criteria in CRC patients

Univariate survival analysis revealed that CLR-positive CRC is associated with significantly better overall survival (OS) (hazard ratio [HR], 0.463; 95% confidence interval [CI], 0.305 to 0.702;  $p < .001$ ; HR, 0.363; 95% CI, 0.197 to 0.669;  $p = .001$ ; and HR, 0.433; 95% CI, 0.271 to 0.690;  $p < .001$ , respectively) and disease-free survival (DFS) (HR, 0.411; 95% CI, 0.304 to 0.639;  $p < .001$ ; HR, 0.382; 95% CI, 0.226 to 0.645;  $p = .004$ ; and HR, 0.501; 95% CI, 0.339 to 0.741;  $p < .001$ , respectively) than



**Table 2.** Clinicopathological parameters and CLR

Variable		CLR count (%)	p-value	CLR size (%)	p-value	CLR density (%)	p-value	Intense CLR (%)	p-value
Total	636	169 (26.6)		104 (16.4)		94 (14.8)		140 (22.0)	
Age			.470		.236		.736		.847
≥ 65	358	91 (25.4)		53 (14.8)		51 (14.2)		80 (22.3)	
< 65	278	78 (28.1)		51 (18.4)		43 (15.5)		60 (21.6)	
Sex			.583		.827		.670		.626
Male	383	105 (27.4)		64 (16.7)		65 (17.0)		87 (22.7)	
Female	253	64 (25.3)		40 (15.9)		29 (11.5)		53 (20.9)	
pTNM stage			.001		.041		.002		.005
I or II	306	100 (32.7)		60 (19.7)		59 (19.3)		82 (26.8)	
III or IV	330	69 (20.9)		44 (13.4)		35 (10.6)		58 (17.6)	
Lymphatic invasion			.002		.131		.005		.021
Absent	353	111 (31.4)		65 (18.5)		65 (18.4)		90 (25.5)	
Present	283	58 (20.5)		39 (13.8)		29 (10.2)		50 (17.7)	
Vascular invasion			.118		.214		.072		.486
Absent	549	152 (27.7)		94 (17.2)		87 (15.8)		124 (22.6)	
Present	87	17 (19.5)		10 (11.5)		7 (8.0)		16 (18.4)	
Perineural invasion			.141		.102		.065		.178
Absent	485	136 (28.0)		86 (17.8)		79 (16.3)		113 (23.3)	
Present	151	33 (21.9)		18 (11.9)		15 (9.9)		27 (17.9)	
MSI status			.002		.002		.001		.006
Low/stable	581	144 (24.8)		86 (14.8)		77 (13.3)		119 (20.5)	
High	55	25 (45.5)		18 (33.3)		17 (30.9)		21 (38.2)	
CIMP			.274		.510		.365		.438
Low	595	155 (26.1)		96 (16.2)		86 (14.5)		129 (21.7)	
High	41	14 (34.1)		8 (20.0)		8 (19.5)		11 (26.8)	
KRAS mutation			.839		.466		.704		> .99
Absent	470	124 (26.4)		74 (15.8)		68 (14.5)		104 (22.1)	
Present	166	45 (27.1)		30 (18.2)		26 (15.7)		36 (21.7)	
BRAF mutation			.429		.813		.619		.290
Absent	602	158 (26.2)		98 (16.3)		88 (14.6)		130 (21.6)	
Present	34	11 (32.4)		6 (17.6)		6 (17.6)		10 (29.4)	
Tumor location			.003		.001		.005		.005
Colon	451	135 (29.9)		87 (19.4)		78 (17.3)		78 (17.3)	
Rectum	185	34 (18.4)		17 (9.2)		16 (8.6)		16 (8.6)	
Tumor side			.005		.009		.002		.045
Left	461	60 (9.4)		39 (6.1)		38 (6.0)		47 (7.4)	
Right	175	109 (17.1)		65 (10.2)		56 (8.8)		93 (14.6)	

CLR, Crohn-like lymphoid reaction; MSI, microsatellite instability; CIMP, CpG island methylator phenotype.

CLR-negative CRC, when the criteria of CLR count, CLR density, and intense CLR were applied (Fig. 2). When CLR was assessed with the size criteria, it was significantly correlated only with improved DFS (HR, 0.528; 95% CI, 0.340 to 0.821;  $p = .004$ ), but not with better OS (HR, 0.656; 95% CI, 0.411 to 1.046;  $p = .077$ ). The correlation between survival and CLR showed identical significance when evaluating only MSI-low and MSS CRC patients (Supplementary Table S1). In the multivariate survival analysis, CLR-positivity based on CLR count, CLR density, and intense CLR were determined to be an independent prognostic factors after adjustment for lymphatic invasion, perineural invasion, venous invasion, and pTNM stage (Table 3). When ex-

cluding MSI-high CRC, CLR count and intense CLR were significantly associated with survival (Supplementary Table S2).

## DISCUSSION

Strong lymphocytic reactions have been suspected to predict favorable prognoses in CRC. Among the four entities of CLR, peritumoral reaction, intratumoral periglandular reaction, and tumor-infiltrating lymphocyte (TIL), TIL has been the target of most interest and the front-runner when evaluating the lymphatic reaction of CRC [13,24–28]. Therefore, the correlation between TIL and survival has been established in multiple large-

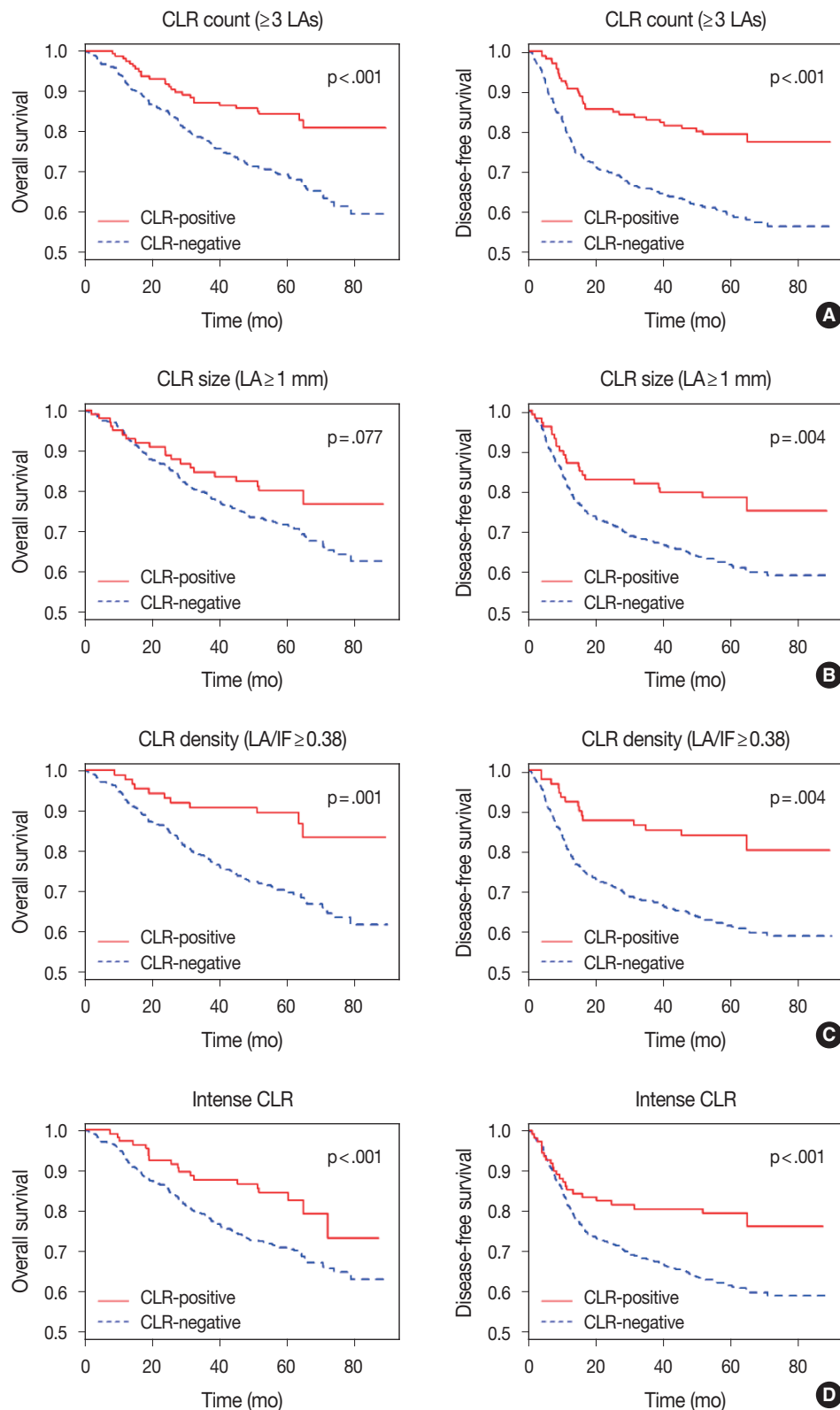


**Fig. 2.** Correlations between each Crohn-like lymphoid reaction (CLR) criterion and survival (overall survival and disease-free survival). (A) Kaplan-Meier curves for CLR count (at least three lymphoid aggregates [LAs]). (B) Kaplan-Meier curves for CLR size ( $LA \geq 1$  mm in diameter). (C) Kaplan-Meier curves for CLR density (the number of LAs divided by the length of the invasion front  $\geq 0.38$ ). (D) Kaplan-Meier curves for intense CLR.

**Table 3.** Multivariate analysis of CLR according to Cox proportional hazards regression model

Criteria	Overall survival			Disease-free survival		
	HR	95% CI	p-value	HR	95% CI	p-value
CLR count	0.595	0.390–0.907	.016	0.559	0.384–0.813	.002
CLR size				0.687	0.440–1.072	.098
CLR density	0.519	0.280–0.962	.037	0.558	0.328–0.949	.031
Intense CLR	0.610	0.378–0.984	.043	0.610	0.395–0.941	.025

Each variable was adjusted for lymphatic, perineural, and venous invasion and pTNM stage. One of the CLR criteria was included for each model. CLR, Crohn-like lymphoid reaction; HR, hazard ratio; CI, confidence interval.

scale studies [8,29,30]. Studies suggest that TIL should be considered as a superior predicting prognostic factor to other molecular markers, including MSI and the *KRAS* and *BRAF* mutations, and to the consensus molecular subtype from the CRC subtype consortium [8]. However, TIL has disadvantages when clinical applications are considered. Since a standardized area of interest has not been established, studies range from counting TILs in high power fields and single tissue microarray cores to whole slide sections [31,32]. Moreover, intratumoral epithelial and stromal regions, as well as subtypes of TILs according to immunohistochemical data, could also have differential or opposing influence on survival [33]. Unlike TIL, CLR has been uniformly addressed with whole section slides and could be considered a more reliable marker for evaluating the prognostic potential of the lymphatic reaction in CRC.

The role of CLR in CRC can be regarded as a tertiary lymphoid structure that is associated with the host immune response against tumor cells [4]. While some studies have reported CLR as a prognostic factor, the results are not always in agreement [6,9]. Furthermore, various methods used to evaluate CLR-positivity have been developed, but the effects of different assessment methods have not been completely elucidated and need to be reviewed in detail. In this study, we observed different aspects of CLR and survival by applying multiple criteria to a single cohort of CRC patients for the comparison of each criterion. According to univariate analysis, CLR was prognostic with any of the four criteria, but not all criteria could demonstrate CLR as an independent prognostic factor in multivariate analysis. However, we have previously reported that interobserver reproducibility is higher with objective criteria than with subjective criteria [6]. Therefore, in the present study, we defined CLR as positive when at least 3 LAs were present and when LA/IF greater than or equal to 0.38 was observed.

In this study, we limited our focus to criteria that dichotomized the CRC patients according to CLR, and therefore, semiquantitative three-tier grading by Graham and Appelman [5] was not included. Nevertheless, the findings from the previous studies

provided the basis of the criteria for this comparative analysis.

We clarified assessment methods for CLRs according to those presented in previous studies, analyzed 636 CRC cases for CLR according to four different criteria, and correlated CLR with clinicopathological features and prognoses. Findings of our study suggest that CLR should be considered as an independent prognostic marker, and for clinical practice, CLR-positivity should be defined with objective criteria such as at least 3 LAs or LA/IF greater than or equal to 0.38.

### Supplementary Information

The Data Supplement is available with this article at <https://doi.org/10.4132/jptm.2020.10.06>.

### Ethics Statement

This study was approved by the Ethics Committee of the Seoul National University Hospital, which waived the requirement to obtain informed consent (H-1313-050-542).

### ORCID

Younghoon Kim <https://orcid.org/0000-0003-4656-0188>  
 Jeong Mo Bae <https://orcid.org/0000-0003-0462-3072>  
 Jung Ho Kim <https://orcid.org/0000-0002-6031-3629>  
 Nam-Yun Cho <https://orcid.org/0000-0002-5736-2956>  
 Gyeong Hoon Kang <https://orcid.org/0000-0003-2380-6675>

### Author Contributions

Conceptualization: GHK. Data curation: YK, JMB. Formal analysis: YK, NYC. Funding acquisition: GHK. Investigation: YK, NYC. Methodology: YK. Resources: JMB. Software: YK. Supervision: GHK. Validation: GHK. Visualization: YK. Writing—original draft: YK. Writing—review & editing: JHK, GHK. Approval of final manuscript: all authors.

### Conflicts of Interest

GHK and JHK, contributing editors of the *Journal of Pathology and Translational Medicine*, were not involved in the editorial evaluation or decision to publish this article. All remaining authors have declared no conflicts of interest.

### Funding Statement

This work was supported by grants from the National Research Foundation (NRF) funded by the Korean Ministry of Science, ICT and Future Planning (2011-0030049 and 2016M3A9B6026921), a grant from the Korea Health Technology R&D Project through the Korea Health Industry



Development Institute funded by the Korean Ministry of Health and Welfare (HI14C1277), and a grant from the SNUH Research Fund (2320160090 (2016-1999)).

## References

1. Siegel RL, Miller KD, Jemal A. Cancer statistics, 2017. *CA Cancer J Clin* 2017; 67: 7-30.
2. Donehower LA, Creighton CJ, Schultz N, et al. *MLH1*-silenced and non-silenced subgroups of hypermutated colorectal carcinomas have distinct mutational landscapes. *J Pathol* 2013; 229: 99-110.
3. Guinney J, Dienstmann R, Wang X, et al. The consensus molecular subtypes of colorectal cancer. *Nat Med* 2015; 21: 1350-6.
4. Ueno H, Hashiguchi Y, Shimazaki H, et al. Objective criteria for crohn-like lymphoid reaction in colorectal cancer. *Am J Clin Pathol* 2013; 139: 434-41.
5. Graham DM, Appelman HD. Crohn's-like lymphoid reaction and colorectal carcinoma: a potential histologic prognosticator. *Mod Pathol* 1990; 3: 332-5.
6. Kim JH, Kim KJ, Bae JM, et al. Comparative validation of assessment criteria for Crohn-like lymphoid reaction in colorectal carcinoma. *J Clin Pathol* 2015; 68: 22-8.
7. Vayrynen JP, Sajanti SA, Klintrup K, et al. Characteristics and significance of colorectal cancer associated lymphoid reaction. *Int J Cancer* 2014; 134: 2126-35.
8. Williams DS, Mouradov D, Jorissen RN, et al. Lymphocytic response to tumour and deficient DNA mismatch repair identify subtypes of stage II/III colorectal cancer associated with patient outcomes. *Gut* 2019; 68: 465-74.
9. Ogino S, Noshio K, Irahara N, et al. Lymphocytic reaction to colorectal cancer is associated with longer survival, independent of lymph node count, microsatellite instability, and CpG island methylator phenotype. *Clin Cancer Res* 2009; 15: 6412-20.
10. Jass JR. HNPCC and sporadic MSI-H colorectal cancer: a review of the morphological similarities and differences. *Fam Cancer* 2004; 3: 93-100.
11. Alexander J, Watanabe T, Wu TT, Rashid A, Li S, Hamilton SR. Histopathological identification of colon cancer with microsatellite instability. *Am J Pathol* 2001; 158: 527-35.
12. Jass JR. Classification of colorectal cancer based on correlation of clinical, morphological and molecular features. *Histopathology* 2007; 50: 113-30.
13. Galon J, Costes A, Sanchez-Cabo F, et al. Type, density, and location of immune cells within human colorectal tumors predict clinical outcome. *Science* 2006; 313: 1960-4.
14. Juo YY, Johnston FM, Zhang DY, et al. Prognostic value of CpG island methylator phenotype among colorectal cancer patients: a systematic review and meta-analysis. *Ann Oncol* 2014; 25: 2314-27.
15. Ording AG, Horvath-Puho E, Erichsen R, et al. Five-year mortality in colorectal cancer patients with ulcerative colitis or Crohn's disease: a nationwide population-based cohort study. *Inflamm Bowel Dis* 2013; 19: 800-5.
16. Guastadisegni C, Colafranceschi M, Ottini L, Dogliotti E. Microsatellite instability as a marker of prognosis and response to therapy: a meta-analysis of colorectal cancer survival data. *Eur J Cancer* 2010; 46: 2788-98.
17. Lewis B, Lin J, Wu X, et al. Crohn's disease-like reaction predicts favorable prognosis in colitis-associated colorectal cancer. *Inflamm Bowel Dis* 2013; 19: 2190-8.
18. Ferris RL, Galon J. Additional support for the introduction of immune cell quantification in colorectal cancer classification. *J Natl Cancer Inst* 2016; 108: djw033.
19. Bae JM, Kim JH, Rhee YY, Cho NY, Kim TY, Kang GH. Annexin A10 expression in colorectal cancers with emphasis on the serrated neoplasia pathway. *World J Gastroenterol* 2015; 21: 9749-57.
20. Lee DW, Kim KJ, Han SW, et al. *KRAS* mutation is associated with worse prognosis in stage III or high-risk stage II colon cancer patients treated with adjuvant FOLFOX. *Ann Surg Oncol* 2015; 22: 187-94.
21. Buckowitz A, Knaebel HP, Benner A, et al. Microsatellite instability in colorectal cancer is associated with local lymphocyte infiltration and low frequency of distant metastases. *Br J Cancer* 2005; 92: 1746-53.
22. Rozek LS, Schmit SL, Greenson JK, et al. Tumor-infiltrating lymphocytes, Crohn's-like lymphoid reaction, and survival from colorectal cancer. *J Natl Cancer Inst* 2016; 108: djw027.
23. Kakar S, Aksoy S, Burgart LJ, Smyrk TC. Mucinous carcinoma of the colon: correlation of loss of mismatch repair enzymes with clinicopathologic features and survival. *Mod Pathol* 2004; 17: 696-700.
24. Titu LV, Monson JR, Greenman J. The role of CD8(+) T cells in immune responses to colorectal cancer. *Cancer Immunol Immunother* 2002; 51: 235-47.
25. Ling A, Edin S, Wikberg ML, Oberg A, Palmqvist R. The intratumoural subsite and relation of CD8(+) and FOXP3(+) T lymphocytes in colorectal cancer provide important prognostic clues. *Br J Cancer* 2014; 110: 2551-9.
26. Pages F, Berger A, Camus M, et al. Effector memory T cells, early metastasis, and survival in colorectal cancer. *N Engl J Med* 2005; 353: 2654-66.
27. Mei Z, Liu Y, Liu C, et al. Tumour-infiltrating inflammation and prognosis in colorectal cancer: systematic review and meta-analysis. *Br J Cancer* 2014; 110: 1595-605.
28. Kim Y, Bae JM, Li G, Cho NY, Kang GH. Image analyzer-based assessment of tumor-infiltrating T cell subsets and their prognostic values in colorectal carcinomas. *PLoS One* 2015; 10: e0122183.
29. Noshio K, Baba Y, Tanaka N, et al. Tumour-infiltrating T-cell subsets, molecular changes in colorectal cancer, and prognosis: cohort study and literature review. *J Pathol* 2010; 222: 350-66.
30. Frey DM, Drieser RA, Viehl CT, et al. High frequency of tumor-infiltrating FOXP3(+) regulatory T cells predicts improved survival in mismatch repair-proficient colorectal cancer patients. *Int J Cancer* 2010; 126: 2635-43.
31. Turksma AW, Coupe VM, Shamier MC, et al. Extent and location of tumor-infiltrating lymphocytes in microsatellite-stable colon cancer predict outcome to adjuvant active specific immunotherapy. *Clin Cancer Res* 2016; 22: 346-56.
32. Li Y, Liang L, Dai W, et al. Prognostic impact of programmed cell death-1 (PD-1) and PD-ligand 1 (PD-L1) expression in cancer cells and tumor infiltrating lymphocytes in colorectal cancer. *Mol Cancer* 2016; 15: 55.
33. Jakubowska K, Kisielewski W, Kanczuga-Koda L, Koda M, Famulski W. Stromal and intraepithelial tumor-infiltrating lymphocytes in colorectal carcinoma. *Oncol Lett* 2017; 14: 6421-32.

## Causes of necrotic features in fine-needle aspirates from cervical lymph nodes

Young Jin Seo<sup>1</sup>, Hyeongchan Shin<sup>1,2</sup>, Hye Won Lee<sup>1,2</sup>, Hye Ra Jung<sup>1,2</sup>

<sup>1</sup>Department of Pathology, Keimyung University Dongsan Hospital, Daegu;

<sup>2</sup>Department of Pathology, Keimyung University School of Medicine, Daegu, Korea

**Background:** Lymph node fine-needle aspiration (LN FNA) cytology indicates necrosis in various diseases. Dominant necrotic features make the diagnosis of underlying conditions very difficult. **Methods:** We retrospectively reviewed 460 patients who underwent cervical LN aspiration cytology that revealed necrotic findings at Keimyung University Dongsan Hospital in Daegu, Korea, from 2003–2017. Each specimen was evaluated and analyzed in association with the clinical findings, biopsy findings, and/or other ancillary tests, including acid-fast bacilli staining and molecular testing for *Mycobacterium tuberculosis*. **Results:** When necrotic features were noted upon cervical LN FNA cytology, the most common pathologic LN FNA category was necrosis alone (31.5%). The second most common category was granulomatous inflammation (31.3%), followed by Kikuchi disease (20.0%) and malignant neoplasm (8.7%). In cases where the cervical LN FNA revealed necrosis alone, the most common final diagnosis was tuberculosis. In young patients, Kikuchi disease should be considered as one cervical LN FNA category, while metastatic carcinoma should be suspected in older patients. **Conclusions:** Even when necrosis alone is observed in LN FNA cytology, it is important to determine the cause through further evaluation.

**Key Words:** Fine-needle aspiration; Lymph node; Necrosis; Tuberculosis; Kikuchi disease

**Received:** July 20, 2020 **Revised:** September 16, 2020 **Accepted:** September 28, 2020

**Corresponding Author:** Hye Ra Jung, MD, PhD, Department of Pathology, Keimyung University Dongsan Hospital, Department of Pathology, Keimyung University School of Medicine, 1095 Dalgubeol-daero, Dalseo-gu, Daegu 42601, Korea

Tel: +82-53-258-7395, Fax: +82-53-258-7382, E-mail: junghr0519@dsmc.or.kr

Fine-needle aspiration (FNA) is an excellent, minimally invasive diagnostic technique for evaluating a mass or lesion. In particular, FNA is commonly used for evaluating enlarged lymph nodes (LNs). In many cases, the aspirate can provide conclusive evidence for a diagnosis; sometimes, the cytology reveals only necrosis.

Necrosis of LNs is found in various diseases. Malignant neoplasms (including lymphomas and metastatic carcinomas) must first be excluded. In addition, numerous benign conditions, such as tuberculosis (TB) and Kikuchi disease, also cause LN necrosis. When necrosis is identified in an LN FNA cytology sample, pathologists should consider various entities and attempt to find clues that lead to a final diagnosis. However, LN FNA cytology sometimes reveals necrosis alone, and few studies have investigated this situation.

The aim of this study was to evaluate the causes of necrosis in FNA of enlarged LNs.

## MATERIALS AND METHODS

We searched the electronic medical record system of the Keimyung University Dongsan Hospital from 2003–2017 to find patients who underwent FNA on cervical LNs. We selected cases with a description of necrotic features on the pathology report. In addition, we also collected the clinical parameters of these cases, including patient age, sex, biopsy findings, other ancillary tests for *Mycobacterium tuberculosis* (MTB; including acid-fast bacilli staining), and molecular studies carried out using conventional polymerase chain reaction (PCR) or real-time PCR. We classified these cases into five categories: granulomatous inflammation, Kikuchi disease, suppurative inflammation, malignant neoplasm, and necrosis only. When granuloma was included in the microscopic description (e.g., granulomatous inflammation with caseous necrosis, granulomatous inflammation with a necrotic background, or necrosis with a vague granuloma), it was classi-

fied as granulomatous inflammation. When the LN FNA result contained content that indicated histiocytic necrotizing inflammation, we placed the patient into the Kikuchi disease category. Cases reported as suspicious for Kikuchi disease with various microscopic descriptions (e.g., necrotizing lymphadenitis, polymorphous lymphoid cells, and macrophages on a necrotic background) were classified as Kikuchi disease. Malignant neoplasms (e.g., metastatic carcinoma, metastatic sarcoma, metastatic melanoma, and malignant lymphoma) with a necrotic background were determined to be malignancies. Cases with suppurative inflammation on a necrotic background, acute inflammatory cells on a necrotic background, aspirated pus, or neutrophilic infiltration with necrotic material were classified as suppurative inflammation.

## RESULTS

### Clinical characteristics of the patients

We retrieved the electronic medical reports of 460 patients who underwent LN aspiration cytology at our hospital that revealed

necrotic features. The mean age of the patients was 42.5 years (range, 2 to 86 years; median, 40 years). The male-to-female ratio (M:F ratio) was 0.62. Except for cases of pure necrosis, the most common FNA category was granulomatous inflammation (31.3%), followed by Kikuchi lymphadenitis (20.0%), malignancy (8.7%), and suppurative lymphadenitis (6.5%) (Table 1).

### Granulomatous inflammation

Of the 460 patients, 144 were classified with granulomatous inflammation from among the LN FNA categories. The M:F ratio was 0.38. This type of inflammation was mainly distributed in people from 20–39 years of age (36.8%). Of the 144 patients with granulomatous inflammation, 117 underwent ancillary tests for MTB; 82 (70.0%) of these were diagnosed with TB. In addition, MTB testing was performed in 364 of the 460 total cases who underwent cervical LN FNA. Among these patients, 148 cases were MTB-positive, which represented 32% of all cervical LN FNA cases (Table 2).

**Table 1.** The age and sex distribution of cervical LN FNA categories according to the FNA diagnosis

FNA category	Mean age (yr)	Age range (yr)	Men (person)	Women (person)	Total (%)
Granulomatous inflammation (31.3%)	46.0	0–19	4	4	8
		20–39	14	39	53
		40–59	13	32	45
		<60	9	29	38
		Total	40	104	144
Kikuchi disease (20.0%)	26.4	0–19	15	16	31
		20–39	14	37	51
		40–59	1	8	9
		<60	0	1	1
		Total	30	62	92
Suppurative inflammation (6.5%)	40.8	0–19	0	5	5
		20–39	5	4	9
		40–59	4	7	11
		<60	3	2	5
		Total	12	18	30
Malignant neoplasm (8.7%)	61.9	0–19	0	0	0
		20–39	1	0	1
		40–59	8	6	14
		<60	24	1	25
		Total	33	7	40
Necrosis (31.5%)	44.0	0–19	5	6	11
		20–39	22	33	55
		40–59	13	36	49
		<60	15	15	30
		Total	55	90	145
Other (2.0%)	46.0	Total	5	4	9
Total	42.5		175	285	460

LN, lymph node; FNA, fine-needle aspiration.



### Kikuchi disease

Ninety-two patients who underwent LN FNA were determined to have Kikuchi disease. Of these 92 people, 89.1% were

young (< 40 years). The M:F ratio was approximately 1:2. Thirteen of these patients classified as having Kikuchi disease by LN FNA underwent ancillary tests for MTB. Among them, 11

**Table 2.** The results of ancillary tests for *Mycobacterium tuberculosis* in the granulomatous inflammation, Kikuchi disease, suppurative lymphadenitis, malignant neoplasm, and necrosis categories of cervical LN FNA findings

FNA category	Related Bx	MTB	Biopsy Dx	No. of cases
Granulomatous inflammation	Present	Positive	ND	3
		Negative	Granulomatous inflammation	7
			Kikuchi disease	2
			Lymphoma	2
			Metastatic squamous cell carcinoma	1
	Absent	ND	ND	79
		Positive	ND	24
		Negative	ND	26
		ND	ND	0
		Positive	Preauricular pit	1
Kikuchi disease	Present	Negative	Kikuchi disease	1
		ND	ND	1
		Positive	ND	2
	Absent	Negative	ND	10
		ND	ND	78
		Positive	Granulomatous inflammation	1
Suppurative lymphadenitis	Present	Negative	Metastatic carcinoma	1
			Warthin's tumor	1
			Metastatic carcinoma	1
		ND	ND	11
		Positive	ND	7
	Absent	Negative	ND	8
		ND	Adenocarcinoma	1
			Adenocarcinoma	4
			Diffuse large B-cell lymphoma	2
			Malignant tumor, unclassified	1
Malignant neoplasm	Present	Negative	Other metastatic carcinoma	2
		ND	Small cell carcinoma	7
			Squamous cell carcinoma	23
			ND	4
		Positive	Granulomatous inflammation	4
	Absent	Negative	Infarct	1
			Kikuchi disease	3
			Lymphoma	2
			Other mimickers	5
		ND	Granulomatous inflammation	1
Necrosis	Present	Positive	infarct	1
		Negative	Kikuchi	1
			Lymphoma	2
			Other mimickers	3
		ND	ND	49
	Absent	Positive	ND	28
		Negative	ND	41
		ND	Reactive hyperplasia	1
			Granulomatous inflammation	1
		ND	ND	1
Others	Present	Negative	ND	6
		ND	ND	
	Absent	Negative	ND	
		ND	ND	

LN, lymph node; FNA, fine-needle aspiration; Related Bx, presence or absence of biopsy on related site of fine needle biopsy; MTB, result of ancillary tests including acid-fast bacillus stain, polymerase chain reaction or reverse transcription polymerase chain reaction for *Mycobacterium tuberculosis*; Biopsy Dx, diagnosis by related site biopsy; ND, not done.

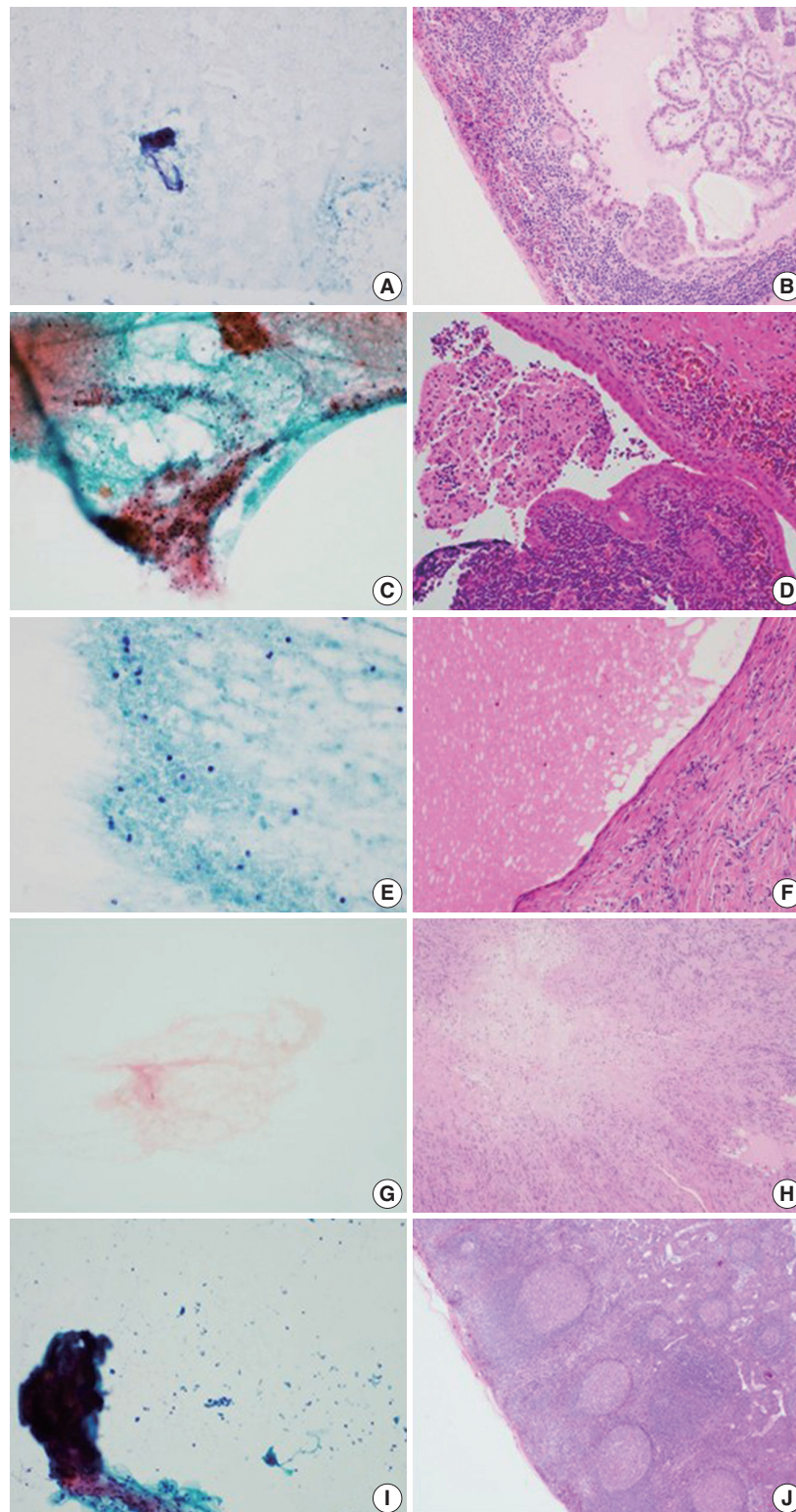


**Fig. 1.** Smear and biopsy findings of the neck lesion diagnosed as necrosis on aspiration but changed diagnosis by biopsy (A, B). (A) Fine needle aspiration (FNA) shows colloid material. (B) Lymph node (LN) excision specimen was diagnosed as metastatic papillary carcinoma. (C, D) Case 2. (C) FNA shows pinkish amorphous material. (D) LN excision specimen was diagnosed as Warthin tumor. (E, F) Case 3. (E) FNA shows cystic fluid material. (F) LN excision specimen was diagnosed as salivary duct cyst. (G, H) Case 4. (G) FNA shows myxoid stroma. (H) LN excision specimen was diagnosed as schwannoma. (I, J) Case 5. (I) FNA shows red blood cells and fibrin material. (J) LN excision specimen was diagnosed as reactive hyperplasia.

patients were negative, but the remaining two patients had positive results. Therefore, the final diagnosis of 11 patients was TB.

### Suppurative lymphadenitis

Of the 460 total patients, 30 (6.7%) were classified with suppurative lymphadenitis. Twenty-five patients (83.3%) were <60 years of age. The M:F ratio was 0.67. Among these 30 patients, 21 underwent ancillary tests for MTB. Eleven patients received a final diagnosis of TB. Four of the 10 patients who were negative for MTB underwent LN biopsy and were finally diagnosed with granulomatous inflammation, Warthin tumor, and metastatic carcinoma (Table 2).

### Malignant neoplasm

In 40 patients, malignant neoplasms were classified into distinct LN FNA categories. The average patient age was 61.9 years. The M:F ratio was 4:7. All 40 patients underwent LN biopsies in the same region. Metastatic carcinoma accounted for 92.5% of cases. Among these cases, the incidence of squamous cell carcinoma was 62.2%. Two cases of malignant lymphoma were diffuse large B-cell lymphomas. In young patients, many cases were diagnosed as TB, while some older patients had metastatic carcinoma.

### Necrosis alone

Of the 460 cases, 145 were classified as having necrosis alone; 94 cases underwent ancillary testing for MTB, and 53 patients (56.4%) were diagnosed with TB. In addition, 27 patients received an LN biopsy. These remaining cases were finally diagnosed with granuloma, Kikuchi disease, necrosis, lymphomas, and other disorders (Table 2). Seven other mimickers included reactive hyperplasia (n = 2), metastatic papillary carcinoma (n = 1), Warthin tumor (n = 1), salivary duct cyst (n = 1), schwannoma (n = 1), and spindle cell tumor (n = 1) (Fig. 1).

## DISCUSSION

FNA is frequently performed as a minimally invasive procedure in patients with mass lesions of superficial organs. It is also a very useful test for clinicians to use when deciding on a treatment. However, the FNA cytology slides may offer no diagnostic clues. In some cases, the cellularity is too low and reveals only necrotic material. In these situations, the pathologist faces difficulties in arriving at a diagnosis. Necrosis is common in benign inflammatory lesions as well as in metastatic malignancies. Extensive necrosis is known to accompany not only metastatic ma-

lignancy, but also acute inflammation or granulomatous inflammation. In addition, focal necrosis is seen in LNs associated with systemic lupus erythematosus, infectious mononucleosis, and brucellosis [1].

We reviewed the literature on LN FNAs that reveal necrotic features. The most common reports were on TB [2-11], followed by studies on lymphoma [12-19] and metastatic lesions [20-23] (Table 3). However, most of these studies were case reports. There have been very few systematic reports of cases where necrosis is observed or certain diseases must be considered to be more important based on the patient age.

In this study, we analyzed 460 patients who underwent cervical LN FNA cytology that revealed necrotic features. The most common causative disease was TB. Of the 460 patients, 247 underwent ancillary testing for MTB, and 148 (59.9%) were finally diagnosed with TB. Typically, the most characteristic cytologic findings of TB are nodular collections of epithelioid histiocytes with Langhans giant cells and caseous necrosis. However, either end of the cytologic spectrum may be seen, especially necrosis without granulomas [24]. Kumar et al. [5] reported that the presence of acute lymphadenitis does not completely exclude TB. They clinically suspected TB in 263 cases with a cytologic picture that demonstrated acute suppurative inflammation. LN FNA should be repeated in all FNA cases that show acute suppurative inflammation without granulomas. It has been reported that a repeat LN FNA helps to detect more than 55% of additional TB cases [25]. In this study, among the patients classified with suppurative lymphadenitis according to FNA cytology, 36.7% were finally diagnosed with TB following ancillary tests. Therefore, it is important to rule out TB when necrotic features are noted on LN FNA cytology.

Necrotic features may also be characteristic of the Kikuchi disease category in cervical LN FNA. The FNA findings in Kikuchi disease typically reveal a polymorphous lymphoid population, crescentic histiocytes, extensive apoptotic bodies, and necrosis. The combination of crescentic histiocytes and karyorrhectic debris suggests the diagnosis of Kikuchi disease. However, some cases show only karyorrhexis and necrosis, which is not specific for Kikuchi disease. For example, infectious mononucleosis may rarely demonstrate extensive necrosis. Infectious mononucleosis is a self-limited viral disease that frequently involves the cervical LNs of young patients who present with fever and pharyngitis. In infectious mononucleosis, a polymorphous infiltrate with atypical large lymphoid cells is usually noted. The patient's clinical history is helpful in arriving at a differential diagnosis in these cases [26].



Another important cause of necrotic features in cervical LN FNA cytology is malignant neoplasm. Among our 460 cases, 49 were finally confirmed as malignancies (including metastatic carcinoma) by tissue biopsy. The mean age of these patients was 62 years. Forty cases were metastatic carcinoma. Among these cases, the most common malignancy was squamous cell carcinoma (62.5%). This trend was consistent with the findings of previous reports. In squamous cell carcinoma, metastatic LNs of the head and neck are often the first signs of malignancy in the inconspicuous organs of this region [1]. Additionally, cystic changes are often observed in metastatic LNs in squamous cell carcinoma [27]. Necrotic material may also be identified in the cyst spaces; therefore, pathologists should be mindful during their microscopic examinations. In our study, most cases were diagnosed as

malignant neoplasms by FNA alone; the remaining nine cases were diagnosed as suppurative lymphadenitis ( $n = 1$ ), granuloma ( $n = 3$ ), and necrosis ( $n = 5$ ) of the LNs. Therefore, when necrotic features are seen in the cervical LN FNA cytology in older patients, pathologists should consider the possibility of malignancy and carefully correlate their findings with the clinical history of the patient to ensure the proper evaluation is recommended to clinicians, even though there may be a paucity of cells on the smeared slides.

In this study, we identified misdiagnosed cases of cervical LN necrosis on FNA. Following an excision biopsy, these cases were diagnosed as reactive hyperplasia, salivary duct cysts, Warthin tumors, schwannomas, and spindle cell tumors. As demonstrated by these cases, fibrinoid material that is present due to excessive

**Table 3.** Previously published reports with the keywords “FNA,” “necrosis,” and “lymph node”

Category	Diagnosis	Journal	First author	Publication Year
Infection ( $n = 17$ )	Cat scratch disease ( $n = 1$ )	Am J Clin Pathol	Choi AH [28]	2015
	Histoplasmosis ( $n = 1$ )	Cancer Cytopathol	Gailey MP [29]	2013
	Infection ( $n = 1$ )	J Thorac Oncol	Aerts JG [30]	2008
	Tuberculosis ( $n = 11$ )	Diagn Cytopathol	Das DK [3]	1992
		Am J Clin Pathol	Lapuerta P [31]	1997
		Cytopathology	Ersoz C [4]	1998
		Cytopathology	Kumar N [5]	1998
		World J Gastroenterol	Xia F [7]	2003
		Cytopathology	Aljafari AS [2]	2004
		Southeast Asian J Trop Med Public Health	Chantranuwat C [6]	2006
		J Gastroenterol	Itaba S [9]	2007
		Int J Tuberc Lung Dis	Berzosa M [8]	2010
		Diagn Cytopathol	Mittal P [10]	2011
		Ann Thorac Surg	Sun J [11]	2013
	Tularemia ( $n = 3$ )	Infection	Ulu-Kilic A [32]	2013
		APMIS	Tuncer E [33]	2014
		Acta Cytol	Markoc F [34]	2014
Kikuchi disease ( $n = 2$ )	Kikuchi disease ( $n = 2$ )	Diagn Cytopathol	Hsueh EJ [35]	1993
		Diagn Cytopathol	Viguer JM [36]	2001
Lymphoma ( $n = 8$ )	Hodgkin lymphoma ( $n = 2$ )	Diagn Cytopathol	Florentine BD [12]	2014
		J Clin Exp Hematop	Okuni M [13]	2018
	Langerhans cell histiocytosis ( $n = 1$ )	Cytopathology	Phulware RH [14]	2019
	Non-Hodgkin lymphoma ( $n = 5$ )	Acta Cytol	Tani E [16]	1989
		Acta Cytol	Sneige N [15]	1990
		Leuk Lymphoma	Dao TH [17]	1991
		Diagn Cytopathol	Dunphy CH [18]	1997
		Indian J Pathol Microbiol	Handa U [19]	2005
Metastatic lesion ( $n = 4$ )	Squamous cell carcinoma ( $n = 4$ )	Diagn Cytopathol	Allison DB [22]	2016
		Cytojournal	Lastra RR [21]	2013
		Diagn Cytopathol	Banet N [20]	2016
		Cytopathology	Rollo F [23]	2018
Other ( $n = 3$ )	Paraganglioma ( $n = 1$ )	Diagn Cytopathol	Fite JJ [37]	2018
	Sarcoidosis ( $n = 2$ )	Eur Respir J	Annema JT [38]	2005
		Coll Antropol	Vrbica Z [39]	2010

hemorrhaging, amorphous material of tumor components, or hypocellular myxoid stroma could be confused with a necrotic background.

An accurate diagnosis on cervical LN FNA cytology is important to determine the most appropriate treatment and to prevent unnecessary surgery. This study was conducted in the Republic of Korea, and we found that the most common cause of necrosis in cervical LN FNA cytology was TB. When there are necrotizing features in the FNA of the cervical lymph nodes in young patients, Kikuchi disease should be considered first. Metastatic carcinoma should always be suspected in older patients, even if they do not have any previous history of malignancy. In addition, when necrotizing features are noted in the FNA of the cervical lymph nodes of patients in any age group, MTB testing should be performed in parallel to exclude TB, which has a high prevalence in the Republic of Korea.

### Ethics Statement

This study was approved by the Institutional Review Board of the Keimyung University Dongsan Hospital with a waiver of informed consent (DSMC 2020-03-069-002) and performed in accordance with the principles of the Declaration of Helsinki.

### ORCID

Young Jin Seo <https://orcid.org/0000-0002-9048-0903>  
 Hyeonchan Shin <https://orcid.org/0000-0002-3716-7678>  
 Hye Won Lee <https://orcid.org/0000-0001-8540-524X>  
 Hye Ra Jung <https://orcid.org/0000-0002-1477-6606>

### Author Contributions

Conceptualization: HRJ. Data curation: YJS, HS. Formal analysis: YJS, HRJ. Methodology: YJS, HRJ. Supervision: HRJ. Visualization: YJS, HWL. Writing—original draft: YJS, HRJ. Writing—review & editing: YJS, HS, HWL, HRJ. Approval of final manuscript: all authors.

### Conflicts of Interest

The authors declare that they have no potential conflicts of interest.

### Funding Statement

No funding to declare.

### References

- van Schaik JE, Muller Kobold AC, van der Laan B, van der Vegt B, van Hemel BM, Plaat BEC. Squamous cell carcinoma antigen concentration in fine needle aspiration samples: a new method to detect cervical lymph node metastases of head and neck squamous cell carcinoma. *Head Neck* 2019; 41: 2561-5.
- Aljafari AS, Khalil EA, Elsiddig KE, et al. Diagnosis of tuberculous lymphadenitis by FNAC, microbiological methods and PCR: a comparative study. *Cytopathology* 2004; 15: 44-8.
- Das DK, Bhambhani S, Pant JN, et al. Superficial and deep-seated tuberculous lesions: fine-needle aspiration cytology diagnosis of 574 cases. *Diagn Cytopathol* 1992; 8: 211-5.
- Ersoz C, Polat A, Serin MS, Soylu I, Demircan O. Fine needle aspiration (FNA) cytology in tuberculous lymphadenitis. *Cytopathology* 1998; 9: 201-7.
- Kumar N, Tiwari MC, Verma K. AFB staining in cytodagnosis of tuberculosis without classical features: a comparison of Ziehl-Neelsen and fluorescent methods. *Cytopathology* 1998; 9: 208-14.
- Chantranuwat C, Assanasen T, Shuangshoti S, Sampatanukul P. Polymerase chain reaction for detection of *Mycobacterium tuberculosis* in papanicolaou-stained fine needle aspirated smears for diagnosis of cervical tuberculous lymphadenitis. *Southeast Asian J Trop Med Public Health* 2006; 37: 940-7.
- Xia F, Poon RT, Wang SG, Bie P, Huang XQ, Dong JH. Tuberculosis of pancreas and peripancreatic lymph nodes in immunocompetent patients: experience from China. *World J Gastroenterol* 2003; 9: 1361-4.
- Berzosa M, Tsukayama DT, Davies SF, et al. Endoscopic ultrasound-guided fine-needle aspiration for the diagnosis of extra-pulmonary tuberculosis. *Int J Tuberc Lung Dis* 2010; 14: 578-84.
- Itaba S, Yoshinaga S, Nakamura K, et al. Endoscopic ultrasound-guided fine-needle aspiration for the diagnosis of peripancreatic tuberculous lymphadenitis. *J Gastroenterol* 2007; 42: 83-6.
- Mittal P, Handa U, Mohan H, Gupta V. Comparative evaluation of fine needle aspiration cytology, culture, and PCR in diagnosis of tuberculous lymphadenitis. *Diagn Cytopathol* 2011; 39: 822-6.
- Sun J, Teng J, Yang H, et al. Endobronchial ultrasound-guided transbronchial needle aspiration in diagnosing intrathoracic tuberculosis. *Ann Thorac Surg* 2013; 96: 2021-7.
- Florentine BD, Cohen AN. Nodular sclerosing classical Hodgkin lymphoma masquerading as acute suppurative-necrotizing lymphadenitis. *Diagn Cytopathol* 2014; 42: 238-41.
- Okuni M, Yakushijin K, Sakai Y, et al. A case of classical Hodgkin lymphoma with total lymph node infarction. *J Clin Exp Hematop* 2018; 58: 24-6.
- Phulware RH, Guleria P, Iyer VK, et al. Cytological diagnosis of Langerhans cell histiocytosis: a series of 47 cases. *Cytopathology* 2019; 30: 413-8.
- Sneige N, Dekmezian RH, Katz RL, et al. Morphologic and immunocytochemical evaluation of 220 fine needle aspirates of malignant lymphoma and lymphoid hyperplasia. *Acta Cytol* 1990; 34: 311-22.
- Tani E, Liliemark J, Svedmyr E, Mellstedt H, Biberfeld P, Skoog L. Cytomorphology and immunocytochemistry of fine needle aspirates from blastic non-Hodgkin's lymphomas. *Acta Cytol* 1989; 33: 363-71.
- Dao TH, Fleury-Feith J, Haioun C, et al. Percutaneous fine needle aspiration cytology and biopsy in the diagnosis and classification of lymphoma: clinical evaluation. *Leuk Lymphoma* 1991; 5: 237-42.
- Dunphy CH, Ramos R. Combining fine-needle aspiration and flow cytometric immunophenotyping in evaluation of nodal and extranodal sites for possible lymphoma: a retrospective review. *Diagn Cytopathol* 1997; 16: 200-6.
- Handa U, Mohan H, Punia RS, Nada R. FNAC in a case of NHL presenting initially as nodal infarction. *Indian J Pathol Microbiol* 2005; 48: 510-2.
- Banet N, Rooper LM, Maleki Z. Metastatic HPV-related head and neck squamous cell carcinoma to the lung and mediastinal lymph nodes in aspirated cytology material: a diagnostic pitfall. *Diagn Cytopathol* 2016; 44: 206-14.
- Lastra RR, Pramick MR, Nakashima MO, et al. Adequacy of fine-

- needle aspiration specimens for human papillomavirus infection molecular testing in head and neck squamous cell carcinoma. *Cytojournal* 2013; 10: 21.
22. Allison DB, Bishop JA, Ali SZ. Cytopathologic characteristics of SMARCB1 (INI-1) deficient sinonasal carcinoma: a potential diagnostic pitfall. *Diagn Cytopathol* 2016; 44: 700-3.
  23. Rollo F, Dona MG, Pellini R, et al. Cytology and direct human papillomavirus testing on fine needle aspirates from cervical lymph node metastases of patients with oropharyngeal squamous cell carcinoma or occult primary. *Cytopathology* 2018; 29: 449-54.
  24. Mac DeMay R. The art and science of cytopathology. Chicago: American Society for Clinical Pathology, 2012.
  25. Kumar N, Jain S, Murthy NS. Utility of repeat fine needle aspiration in acute suppurative lesions: follow-up of 263 cases. *Acta Cytol* 2004; 48: 337-40.
  26. Tong TR, Chan OW, Lee KC. Diagnosing Kikuchi disease on fine needle aspiration biopsy: a retrospective study of 44 cases diagnosed by cytology and 8 by histopathology. *Acta Cytol* 2001; 45: 953-7.
  27. Mokhtari S. Mechanisms of cyst formation in metastatic lymph nodes of head and neck squamous cell carcinoma. *Diagn Pathol* 2012; 7: 6.
  28. Choi AH, Bolaris M, Nguyen DK, Panosyan EH, Lasky JL 3rd, Duane GB. Clinicocytopathologic correlation in an atypical presentation of lymphadenopathy with review of literature. *Am J Clin Pathol* 2015; 143: 749-54.
  29. Gailey MP, Klutts JS, Jensen CS. Fine-needle aspiration of histoplasmosis in the era of endoscopic ultrasound and endobronchial ultrasound: cytomorphic features and correlation with clinical laboratory testing. *Cancer Cytopathol* 2013; 121: 508-17.
  30. Aerts JG, Kloover J, Los J, van der Heijden O, Janssens A, Tournoy KG. EUS-FNA of enlarged necrotic lymph nodes may cause infectious mediastinitis. *J Thorac Oncol* 2008; 3: 1191-3.
  31. Lapuerta P, Martin SE, Ellison E. Fine-needle aspiration of peripheral lymph nodes in patients with tuberculosis and HIV. *Am J Clin Pathol* 1997; 107: 317-20.
  32. Ulu-Kilic A, Gulen G, Sezen F, Kilic S, Sencan I. Tularemia in central Anatolia. *Infection* 2013; 41: 391-9.
  33. Tuncer E, Onal B, Simsek G, et al. Tularemia: potential role of cytopathology in differential diagnosis of cervical lymphadenitis: multi-center experience in 53 cases and literature review. *APMIS* 2014; 122: 236-42.
  34. Markoc F, Koseoglu RD, Koc S, Gurbuzler L. Tularemia in differential diagnosis of cervical lymphadenopathy: cytologic features of tularemia lymphadenitis. *Acta Cytol* 2014; 58: 23-8.
  35. Hsueh EJ, Ko WS, Hwang WS, Yam LT. Fine-needle aspiration of histiocytic necrotizing lymphadenitis (Kikuchi's disease). *Diagn Cytopathol* 1993; 9: 448-52.
  36. Viguer JM, Jimenez-Heffernan JA, Perez P, Lopez-Ferrer P, Gonzalez-Peramato P, Vicandi B. Fine-needle aspiration cytology of Kikuchi's lymphadenitis: a report of ten cases. *Diagn Cytopathol* 2001; 25: 220-4.
  37. Fite JJ, Maleki Z. Paraganglioma: cytomorphic features, radiologic and clinical findings in 12 cases. *Diagn Cytopathol* 2018; 46: 473-81.
  38. Annema JT, Veselic M, Rabe KF. Endoscopic ultrasound-guided fine-needle aspiration for the diagnosis of sarcoidosis. *Eur Respir J* 2005; 25: 405-9.
  39. Vrbica Z, Boras Z, Rakusic N, et al. Necrotising sarcoid granulomatosis of the spinal cord: case report. *Coll Antropol* 2010; 34: 713-7.



## A case of cribriform carcinoma of the skin: a newly described rare condition

Hyun Lee<sup>1</sup>, Chong-Hyun Won<sup>2</sup>, Chan-Sik Park<sup>1</sup>

Departments of <sup>1</sup>Pathology and <sup>2</sup>Dermatology, Asan Medical Center, University of Ulsan College of Medicine, Seoul, Korea

Primary cribriform carcinoma of the skin is an indolent, rare, adnexal tumor. Although its malignant potential remains uncertain, no recurrence or metastasis has been reported. A 33-year-old man presented with a solitary, erythematous, subcutaneous nodule on the right knee. The clinical impression was epidermal cyst, and the resected tumor demonstrated a well-circumscribed mass in the dermis and subcutis. The tumor was composed of two regions: a solid component and a cribriform component. The solid component (90%) showed multiple solid nests of epithelial cells. Individual cells had large, oval-to-round, hyperchromatic, pleomorphic nuclei with a nuclear groove. The cribriform component (10%) showed similar neoplastic cells with many prominent lumina. Some lumina had an eosinophilic substance that exhibited a positive periodic acid-Schiff reaction. No recurrence or metastasis was observed within a follow-up period of eight months after excision. In conclusion, we report the first case of primary cribriform carcinoma of the skin in Korea.

**Key Words:** Cribriform carcinoma; Apocrine tumor; Skin tumor

**Received:** August 10, 2020 **Revised:** September 13, 2020 **Accepted:** October 5, 2020

**Corresponding Author:** Chan-Sik Park, MD, PhD, Department of Pathology, Asan Medical Center, University of Ulsan College of Medicine, 88 Olympic-ro 43-gil, Songpa-gu, Seoul 05505, Korea  
Tel: +82-2-3010-5838, Fax: +82-2-472-7898, E-mail: csikpark@amc.seoul.kr

Cribriform carcinoma of the skin (primary cutaneous cribriform carcinoma [PCCC]) is an indolent, rare, adnexal tumor with a presumed apocrine lineage. The first global case was described in 1998 [1], and the most recent (4th) World Health Organization (WHO) classification for skin now includes this condition. Currently, only 42 cases have been reported in the English literature (Table 1) [1–7]. The female-to-male ratio is 2:1, with a median age of 47 years (range, 20 to 77 years). Most cases involve the extremities (85%). Although its malignant potential remains uncertain, no recurrence or metastasis has been reported.

Herein, we report the first Korean case of primary cribriform carcinoma of the skin.

### CASE REPORT

A 33-year-old man presented with a solitary, erythematous, subcutaneous nodule on the right knee (Fig. 1A), which had developed a few months prior. The clinical impression was epidermal cyst. His past medical history comprised intracranial hemorrhage due to arteriovenous malformation 10 years previous.

After the patient underwent systemic evaluation, including positron emission tomography–computed tomography (PET-CT) and gastric endoscopy, the mass was confirmed as a primary skin tumor, and resection was performed. The resected tumor was a well-circumscribed, yellowish-white, fibrotic, firm, 2.0 × 1.2 × 0.7-cm mass (Fig. 1B).

Histologically, the tumor was a well-circumscribed mass of the dermis and subcutis. The tumor was composed of (Fig. 2A) a predominantly solid component (90%) and a predominantly cribriform component (10%). The solid component showed multiple solid nests of epithelial cells. Individual cells had large, oval-to-round, hyperchromatic, pleomorphic nuclei with a nuclear groove (Fig. 2B). The cytoplasm was eosinophilic and scant. The cribriform component showed similar neoplastic cells with many prominent lumina, giving rise to a cribriform pattern with a thin, thread-like, intraluminal bridge (Fig. 2C). Some lumina had an eosinophilic substance that exhibited a positive periodic acid–Schiff reaction (Fig. 2D). At the periphery of the tumor, multifocal lymphoid aggregates (Fig. 2E), desmoplastic reaction, and some infiltrative tumor cell clusters were present (Fig. 2F).

Table 1. Summary of reported cases

Case No.	Study	Year	Age (yr)	Sex	Site	Clinical diagnosis	Size (cm)	Treatment	F/U period	Prognosis	Positive IHC	Negative IHC	Comments
1	Current case	2020	33	M	Lower extremity (Rt. knee)	Epidermal cyst	2.0	Excision	8 mo	NROMD	S100 (diffuse, luminal component; patchy, solid component), EMA (diffuse, solid component), CK7, CK5/6 (patchy), CD117 (patchy), EpCAM (patchy), CEA (intra-luminal), p63 (rare)	CK20, GCDPF-15, ER, calponin, SMA	History of intracranial hemorrhage due to arteriovenous malformation No evidence of other malignancies
2	Requena et al. [1]	1998	NA	NA	Lower extremity	NA	NA	Excision	NA	NA	NA	NA	First description Reported as mainly women with a mean age of 44 years (range, 20 to 55) Two cases of recurrent tumor after incomplete excision
3			NA	NA	Lower extremity	NA	NA	Excision	NA	NA	NA	NA	
4			NA	NA	Lower extremity	NA	NA	Excision	NA	NA	NA	NA	
5			NA	NA	Upper extremity	NA	NA	Excision	NA	NA	NA	NA	
6			NA	NA	Pubis	NA	NA	Excision	NA	NA	NA	NA	
7	Adamski et al. [5]	2005	37	M	Lower extremity (Lt. popliteal fossa)	NA	2.0	Excision	2 yr	NROMD	CK7	CK20, GCDPF-15, S100	-
8	Fernandez-Flores et al. [4]	2007	62	F	Lower extremity (Lt. popliteal fossa)	NA	0.8	Excision	NA	NROMD	CK AE1/AE3, CAM 5.2, CK7, EMA, ER (2+, 1%-5% cells), c-erbB-2 (2+, 50%-75% cells), p53 (1+, 1%-5% cells), S100 (2+, 50%-75% cells)	CK20, CEA, PR, GCDPF-15, CD15, SMA	-
9	Rutten et al. [2]	2009	48	M	Lower extremity (Rt. thigh)	Dermatofibroma (histiocytoma)	-	Excision	18 yr	NROMD	CK MNF116, CK AE1/AE3, CAM 5.2, CK7, CEA (more prominent in the ductal structures), EMA (more prominent in the ductal structures)	CK20, GCDPF-15, S100, α-SMA, MSA, calponin, CD68, vimentin	-
10			51	F	Upper extremity (Rt. forearm)	Cyst	-	Excision	NA	NA			-
11			44	F	Back	Dermatofibroma (histiocytoma)	-	Excision	13 yr	NROMD			-
12			77	F	Neck	NA	-	Excision	NA	NA			Recurrent tumor after incomplete excision
13			32	F	Lower extremity (Rt. thigh)	Dermatofibroma (histiocytoma)	-	Excision	9 yr	NROMD			-
14			42	F	Lower extremity (Rt. thigh)	Dermatofibroma (histiocytoma)	-	Excision	NA	NA			-
15			34	F	Upper extremity (Rt. arm)	Dermatofibroma (histiocytoma)	-	Excision	11 yr	NROMD			-
16			40	M	Upper extremity (Lt. forearm)	Dermatofibroma (histiocytoma)	-	Excision	NA	NA			-
17			23	M	Lower extremity (Lt. calf)	NA	-	Excision	NA	NA			-
18			20	F	Rt. buttock	Cyst	-	Excision	NA	NA			No evidence of other malignancies
19			67	F	Lt. preauricular area	BCC vs. adnexal tumor	-	Excision	8 yr	NROMD			-
20			60	M	Lower extremity (Rt. foot dorsum)	Dermatofibroma (histiocytoma)	-	Excision	4 yr	NROMD			-
21			54	F	Upper extremity (acral)	NA	-	Excision	NA	NA			-

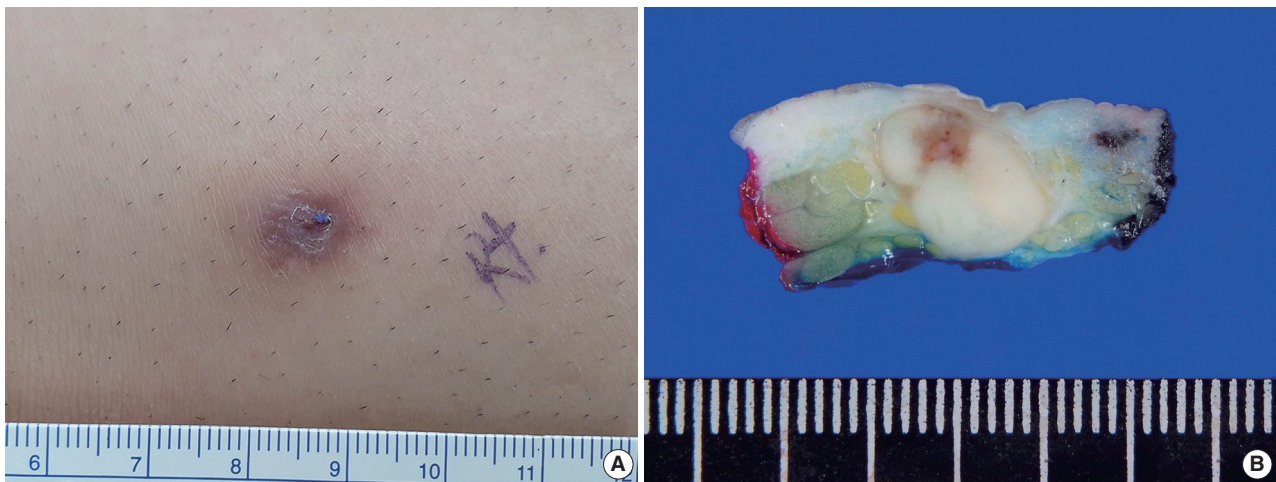
(Continued to the next page)

Table 1. Continued

Case No.	Study	Year	Age (yr)	Sex	Site	Clinical diagnosis	Size (cm)	Treatment	F/U period	Prognosis	Positive IHC	Negative IHC	Comments
22			49	F	Lower extremity (Lt. thigh)	Dermatofibroma (histiocytoma)	-	Excision	4 yr	NROMD			-
23			59	F	Lt. shoulder	Dermatofibroma (histiocytoma)	-	Excision	NA	NA			-
24			28	M	Lower extremity (Rt. lower leg)	NA	-	Excision	NA	NA			-
25			54	M	Upper extremity (Rt. hand)	NA	-	Excision	NA	NA			-
26			50	F	Upper extremity (Rt. hand)	NA	-	Excision	NA	NA			-
27			70	M	Rt. trunk	Long-standing lesion	-	Excision	6 yr	NROMD			-
28			64	F	NA	Dermatofibroma (histiocytoma)	-	Excision	5 yr	NROMD			-
29			40	F	Lower extremity (Lower arm)	NA	-	Excision	5 yr	NROMD			-
30			64	M	Upper back	Dermatofibroma (histiocytoma) or cyst	-	Excision	3 yr	NROMD			-
31			54	M	Lower extremity (Lower arm)	NA	-	Excision	3 yr	NROMD			-
32			44	F	Upper extremity (Lt. thumb)	NA	-	Excision	2 yr	NROMD			-
33			36	F	Lower extremity (Lt. anterior thigh)	Dermatofibroma (histiocytoma)	-	Excision	NA	NA			-
34			26	F	Lower extremity (Lt. posterior leg)	Fibroma	-	Excision	NA	NA			-
35	Aps et al. [3]	2015	41	F	Lower extremity (leg)	Epidermal inclusion cyst	0.6	Excision	NA	NROMD	S100 (diffuse in three cases, patchy in one case), CD117 (diffuse in two cases, patchy in one case), CK5/6, CK7, EpCAM, CEA (luminal), EMA (luminal), p63 (rare)	CK20, GCDFP-15, ER, PR, calponin, SMA	-
36			32	F	Upper extremity (elbow)	NA	0.5	Excision	NA	NA			-
37			35	M	Lower extremity (leg)	NA	0.5	Excision	NA	NROMD			-
38			59	F	Upper extremity (arm)	NA	0.4	Excision	NA	NA			-
39			61	M	Upper extremity (arm)	Mobile nodule	0.7	Excision	NA	NA			-
40			31	M	Lower extremity (leg)	Dermatofibroma	1.2	Excision	NA	NA			-
41	Yokota et al. [7]	2017	39	F	Upper extremity (Rt. forearm)	NA	0.5 (clinical)	Excision	15 mo	NROMD	CK5/6, CK7, CA15-3, CA125, CD117, S100 (partial), p63 (partial), p63 (partial)	CK20, calponin, GCDFP-15, mammaglobulin, MUC1, ER, AR, D2-40	Stable in size for more than 10 years, no evidence of other malignancies
42	Bogner et al. [6]	2018	65	M	Lt. lateral neck	NA	0.6 (clinical)	Excision	3 mo	NROMD	CK7 (strong), EMA (strong), CAM 5.2 (strong), EpCAM (lesser degree), CEA (in some of the lumina), p63, p40	CK20, D2-40, TTF-1, CDX-2, hepatocyte antigen, PSA, PSAP, calponin, S100	No evidence of other malignancies

F/U, follow up; IHC, immunohistochemical staining; Rt., right; Lt., left; NROMD, no recurrence or metastatic disease; EMA, epithelial membrane antigen; CK, cytokeratin; EpCAM, epithelial cell adhesion molecule; CEA, carcinoembryonic antigen; GCDFP-15, gross cystic disease fluid protein-15; ER, estrogen receptor; SMA, smooth muscle actin; MSA, muscle specific antigen; NA, data not available; S100, S-100 protein; PR, progesterone receptor; BOC, basal cell carcinoma; MUC1, mucin1; AR, androgen receptor; TTF-1, thyroid transcription factor 1; PSA, prostate-specific antigen; PSAP, prostatic acid phosphatase; +, >50% of tumor cells are positive; patchy, 25%–50% of tumor cells are positive; rare, < 1% of tumor cells are positive.





**Fig. 1.** Gross appearance of the mass. (A) A solitary, erythematous, subcutaneous nodule on the right knee. (B) The cut surface of the mass is well-circumscribed, yellowish-white, fibrotic, and firm.

The epidermis was neither involved with nor connected to the tumor.

The two components of the tumor displayed distinctive immunohistochemical staining patterns for epithelial membrane antigen (EMA) (Fig. 3A) and S-100 protein (Fig. 3B). The predominantly solid component exhibited diffuse immunopositivity for EMA and focal immunopositivity for S100 protein, while the predominantly luminal component exhibited focal immunopositivity for EMA and diffuse immunopositivity for S-100 protein.

Given its histopathologic features, the mass was diagnosed as PCCC. No recurrence or metastasis was observed within a follow-up period of 8 months after excision.

## DISCUSSION

PCCC is a rare, newly described, unique, adnexal neoplasm with an indolent clinical course. Currently, no recurrence or metastasis has been reported. In few cases, remnants have been reported after incomplete excision [1,3]. Accurate diagnosis and exclusion of metastasis are important for avoiding over-treatment.

In cases of primary skin neoplasms, the differential diagnosis should include tumors that can show a cribriform pattern: adenoid cystic carcinoma, secretory carcinoma, and tubular adenoma (eccrine papillary adenoma). The histopathologic features for differential diagnoses are listed in Table 2. Adenoid cystic carcinoma can be distinguished by the presence of basaloid epithelial cells with more uniform nuclei surrounding the pseudolumina. The presence of frequent perineural invasion and small true ducts with myoepithelial cell differentiation are points of

differential diagnosis. Secretory carcinoma exhibits tubules and microcysts with conspicuous intraluminal secretions, but back-to-back proliferation and cuboidal neoplastic cells are characteristic compared with PCCC. Tubular adenoma can show dilated cystic spaces with attenuated epithelium, micro-papillae, and focal intraluminal bridging, mimicking PCCC. However, this condition lacks cytologic atypia and mitotic activity and involves accumulation of basal/myoepithelial cells.

Histopathologically, metastatic tumors that show a cribriform pattern should be excluded. A cribriform pattern can be seen in cancers of various organs, including the breast (adenoid cystic carcinoma and cribriform adenocarcinoma), prostate (ductal carcinoma and acinar carcinoma), stomach, colon, lung, thyroid (cribriform-morular variant of papillary thyroid carcinoma), uterine endometrium, and salivary gland [8-10]. To exclude metastasis, imaging studies, such as PET-CT and CT, and immunohistochemical staining are required.

Immunohistochemical staining results are listed in Table 1. Although decapitation secretion in the luminal border supports apocrine differentiation, gross cystic disease fluid protein-15, a marker for the apocrine gland, was negative in previous reports [1-7] and in our case. The S-100 protein, a marker for the eccrine gland, demonstrated variable results (diffuse positive, focal positive, and negative) in previous reports [1-7]. Our case showed more prominent S-100 protein in the luminal component. EMA was positive in previous reports [1-7]. Rutten et al. [2] reported more prominent EMA in the luminal structures, while our case showed more prominent EMA in the solid component.

The relatively mutually exclusive immunohistochemical staining patterns of EMA and S-100 protein may be associated with



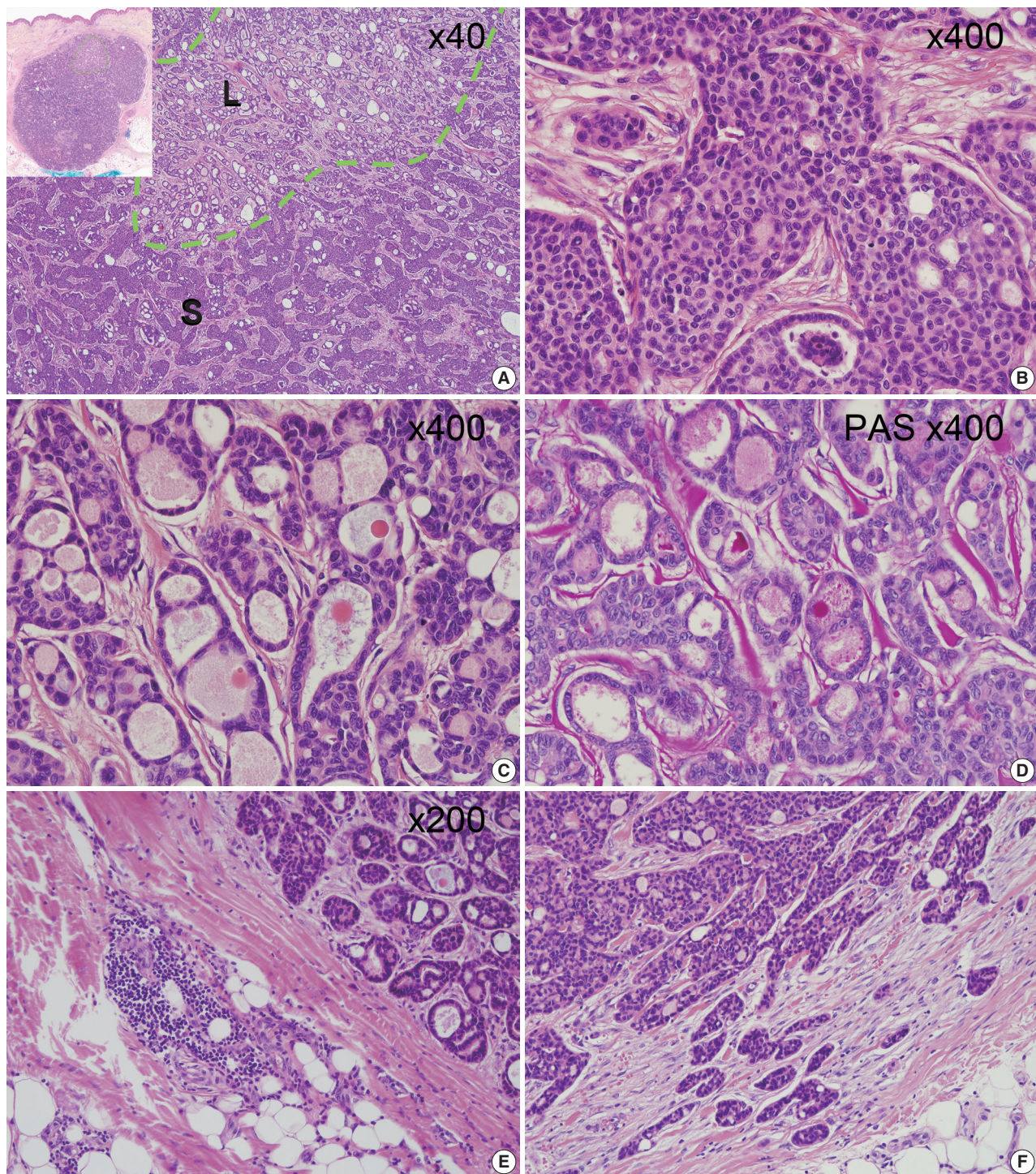


**Fig. 2.** Histopathologic features of the mass. (A) The mass exhibited a predominantly solid component (90%) and a predominantly cribriform component (10%, inside the green line). (B) The predominantly solid component revealed pleomorphic nuclei. (C) The predominantly cribriform component had similar cytologic features to those of the solid component and demonstrated many prominent small lumina with a thin thread-like intraluminal bridge (cribriform pattern) along with an occasional eosinophilic substance. (D) The intraluminal eosinophilic substance with periodic acid–Schiff reaction. (E) Multifocal lymphoid aggregates at the periphery. (F) Infiltrative tumor clusters at the periphery. S, predominantly solid component; L, predominantly luminal component.



architectural differentiation, and further research is needed.

In conclusion, we report the first case of cribriform carcinoma

of the skin in Korea. Pathologists should be aware of cribriform carcinoma of the skin to avoid over-treatment.

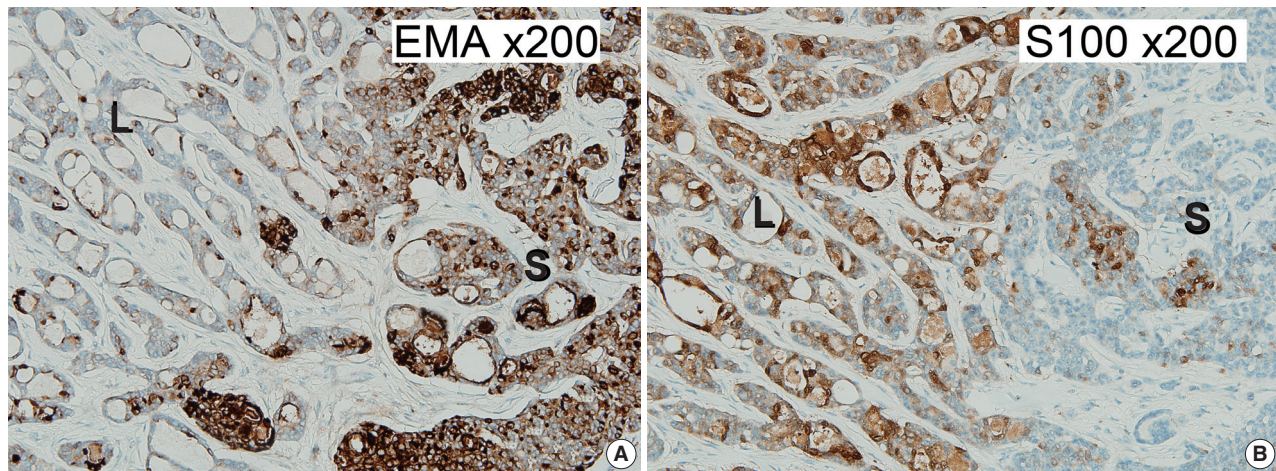


**Fig. 3.** Results of immunohistochemical (IHC) staining. (A) IHC for epithelial membrane antigen: diffuse immunopositivity for the predominantly solid component (on the right) and focal immunopositivity for the predominantly luminal component (on the left). (B) IHC for S-100 protein: diffuse immunopositivity for the predominantly luminal component (on the left) and focal immunopositivity for the predominantly solid component (on the right). S, predominantly solid component; L, predominantly luminal component.

**Table 2.** Histopathologic characteristics of cribriform carcinoma and similar tumors

	Cribriform carcinoma	Adenoid cystic carcinoma	Secretory carcinoma	Tubular adenoma
Architecture	Usually well-circumscribed Mixed variable portion of solid and cribriform  No back-to-back appearance  No cuboidal cells Desmoplastic stroma	Poorly circumscribed Composed of lobules, islands, and cords of basaloid cells with numerous cystic and ductular spaces	Intradermal, circumscribed Back-to-back proliferation of tubules and microcysts  Cuboidal cells  Sclerotic stroma	Well circumscribed Variable sized tubules with attenuated epithelium  Micro-papillae, and focal intraluminal bridging Paucicellular fibrous stroma Recognition of myoepithelial layer Eosinophilic proteinaceous material
Intra-(pseudo) luminal substance	Eosinophilic substance with PAS reaction	Mucin or basement membrane material that stains with mucicarmine, Alcian blue, and colloidal iron	Conspicuous intraluminal secretions	
Nuclei	Pleomorphic	Uniform	Mildly pleomorphic	Uniform
Mitosis	Rare	Rare	Rare to few	Absent
Perineural invasion	Absent	Present, frequent	Absent	Absent
Immunohistochemical staining	Variable CK (MNFI16, AE1/AE3, CAM5.2, and CK7)  EpCAM  CD117, S100, and p63: variable CEA, EMA: highlight ductal component	EMA and monoclonal CEA  S100, p63, GFAP, SMA, MSA and calponin: often stain peripheral cells (myoepithelial differentiation)	S100 protein, mammaglobin and STAT5A  NTRK3: variable	HMFG-1 and GCDPF-15  EMA and CEA: luminal cells  S100 and SMA: myoepithelial cells
Reference	[11,12]	[12,13]	[12,14]	[3,12,13]

PAS, periodic acid-Schiff; CK, cytokeratin; EMA, epithelial membrane antigen; CEA, carcinoembryonic antigen; S100, S-100 protein; GCDPF-15, gross cystic disease fluid protein-15; EpCAM, epithelial cell adhesion molecule; GFAP, glial fibrillary acidic protein; SMA, smooth muscle actin; MSA, muscle specific antigen.



## Ethics Statement

This study was approved by the Institutional Review Board of Asan Medical Center (IRB 2020-0364). Formal written informed consent was not required, with a waiver from the appropriate Institutional Review Board.

## ORCID

Hyun Lee <https://orcid.org/0000-0001-7005-8142>  
 Chong-Hyun Won <https://orcid.org/0000-0003-1997-2240>  
 Chan-Sik Park <https://orcid.org/0000-0001-9783-4498>

## Author Contributions

Conceptualization: CSP. Data curation: HL. Formal analysis: HL. Funding acquisition: CSP. Investigation: CSP. Methodology: HL. Resources: WCH. Supervision: CSP. Validation: CSP, HL. Writing—original draft: HL. Writing—review & editing: CSP. Approval of final manuscript: all authors.

## Conflicts of Interest

CSP, a contributing editor of the *Journal of Pathology and Translational Medicine*, was not involved in the editorial evaluation or decision to publish this article. All remaining authors have declared no conflicts of interest.

## Funding Statement

No funding to declare.

## References

1. Requena L, Kiryu H, Ackerman AB. Neoplasms with apocrine differentiation. Philadelphia: Lippincott-Raven, 1988; 879-905.
2. Rutten A, Kutzner H, Mentzel T, et al. Primary cutaneous cribriform apocrine carcinoma: a clinicopathologic and immunohistochemical study of 26 cases of an under-recognized cutaneous adnexal neoplasm. *J Am Acad Dermatol* 2009; 61: 644-51.
3. Arps DP, Chan MP, Patel RM, Andea AA. Primary cutaneous cribriform carcinoma: report of six cases with clinicopathologic data and immunohistochemical profile. *J Cutan Pathol* 2015; 42: 379-87.
4. Fernandez-Flores A, Pol A, Juanes F, Crespo LG. Immunohistochemical phenotype of cutaneous cribriform carcinoma with a panel of 15 antibodies. *Med Mol Morphol* 2007; 40: 212-7.
5. Adamski H, Le Lan J, Chevrier S, Cribier B, Watier E, Chevrant-Breton J. Primary cutaneous cribriform carcinoma: a rare apocrine tumour. *J Cutan Pathol* 2005; 32: 577-80.
6. Bogner R, Brown T, Fearneyhough P, Gataky G. Primary cutaneous cribriform carcinoma treated with mohs micrographic surgery. *Dermatol Surg* 2018; 44: 583-5.
7. Yokota K, Kono M, Mori S, Shimizu K, Matsumoto T, Akiyama M. A solid variant of primary cutaneous cribriform carcinoma: a small, stable, long-term lesion. *Eur J Dermatol* 2017; 27: 419-21.
8. Branca G, Ieni A, Barresi V, Tuccari G, Caruso RA. An updated review of cribriform carcinomas with emphasis on histopathological diagnosis and prognostic significance. *Oncol Rev* 2017; 11: 317.
9. Page DL, Dixon JM, Anderson TJ, Lee D, Stewart HJ. Invasive cribriform carcinoma of the breast. *Histopathology* 1983; 7: 525-36.
10. McNeal JE, Reese JH, Redwine EA, Freiha FS, Stamey TA. Cribriform adenocarcinoma of the prostate. *Cancer* 1986; 58: 1714-9.
11. Requena L, Sanguenza O. Cribriform carcinoma. In: Requena L, Sanguenza O, eds. *Cutaneous adnexal neoplasms*. Cham: Springer, 2017; 313-20.
12. Elder DE, Massi D, Scolyer RA, Willemze R. WHO classification of skin tumours. Lyon: IARC Press, 2018.
13. Cassario D. Diagnostic pathology: neoplastic dermatopathology. Salt Lake City: Amirsys Publishing Inc., 2012.
14. Llamas-Velasco M, Mentzel T, Rutten A. Primary cutaneous secretory carcinoma: a previously overlooked low-grade sweat gland carcinoma. *J Cutan Pathol* 2018; 45: 240-5.

# Fibrocartilaginous mesenchymoma with an unusual location in the rib

Sun-Ju Oh

Department of Pathology, Kosin University Gospel Hospital, Busan, Korea

Fibrocartilaginous mesenchymoma is a rare bone tumor, with fewer than 35 cases reported in the literature since 1984. This tumor usually occurs in the long bones of children and adolescents. In the current case, the tumor affected a rib. A 17-year-old boy presented with a mass in the right fifth rib. Radiologic findings revealed an osteolytic mass with cortical destruction and calcification; en bloc resection was performed. The tumor showed three distinct histologic features: bland spindle cell proliferation, benign cartilage nodules, and epiphyseal plate-like enchondral ossification. The pathologic diagnosis was fibrocartilaginous mesenchymoma. The patient remains free of disease 1 year after the surgery. Pathological diagnosis of fibrocartilaginous mesenchymoma can be challenging, especially when the tumor occurs in an unusual site. When any fibro-osseous lesion with a cartilaginous component is encountered, the possibility of fibrocartilaginous mesenchymoma should be considered because of its locally aggressive behavior.

**Key Words:** Fibrocartilaginous mesenchymoma; Fibrocartilaginous dysplasia; Enchondral ossification

**Received:** August 10, 2020 **Revised:** September 15, 2020 **Accepted:** October 8, 2020

**Corresponding Author:** Sun-Ju Oh, MD, Department of Pathology, Kosin University Gospel Hospital, 262 Gamcheon-ro, Seo-gu, Busan 49267, Korea  
Tel: +82-51-990-6744, Fax: +82-51-990-3080, E-mail: 10highpowerfield@gmail.com

Fibrocartilaginous mesenchymoma (FM) is a rare, locally aggressive bone tumor, with fewer than 35 cases reported in the literature since 1984 when it was first reported by Dahlin et al. [1-3]. FM predominantly affects young patients with a median age of 13 years. This tumor principally occurs in long tubular bones and, infrequently, in the axial skeleton such as the iliac-pubic bones and vertebrae. Rib is an unusual location for FM, with only one published report [4]. Herein, we present a second case of FM arising in the rare anatomic site of the rib.

## CASE REPORT

A 17-year-old boy was referred to the thoracic surgery department due to a mass located on the right side of the back. The patient had experienced intermittent pain and discomfort for several months at the time of admission, and localized swelling was noted on his back during physical examination. A chest radiograph showed a radiolucent lesion with cortical disruption in the posterolateral aspect of the right 5th rib. A computed tomography scan performed at the local clinic revealed an osteolytic mass with a juxtacortical extension (Fig. 1). Focal calcification was identified, but no periosteal reaction was observed. Overall

radiologic findings suggested a benign tumor, including fibrous dysplasia (FD). En bloc resection was performed without a prior biopsy.

The surgical specimen revealed a 3.1-cm-sized, ill-defined, eccentrically located, hard mass. The resected tumor was confined to the rib without expansion to the surrounding soft tissue, although the cortex had been partly destroyed. The cut surface of the tumor showed spotty areas of cartilaginous tissue (Fig. 2A). Histologically, the tumor was predominantly composed of hyaline cartilage nodules juxtaposed with hypocellular fibrous tissue (Fig. 2B). The cartilage islands throughout the tumor revealed low to intermediate cellularity but did not have any cytologic features of malignancy, such as nuclear atypia, multinucleation, mitosis, or myxoid changes (Fig. 2C). The hypocellular fibrotic area measured 1 cm in size, accounted for about 20% of the lesion, and consisted of benign spindle-to-stellate cells in a collagenous stroma without nuclear atypia or mitotic figures, suggesting low-grade sarcoma (Fig. 2D). The tumor was characterized by enchondral ossification at the periphery of the cartilage deposits, reminiscent of the epiphyseal growth plate or the cartilage cap of an osteochondroma (Fig. 2C). Newly formed bone was present and appeared as well-formed long and short trabec-

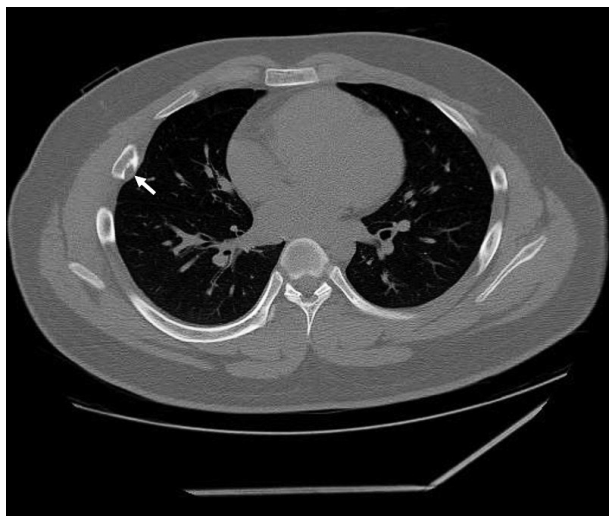


**Fig. 1.** Computed tomography shows an osteolytic lesion (arrow) with calcification and juxtacortical extension at the posterolateral side of the right 5th rib.

ulae with prominent osteoblastic rimming. Multinucleated giant cells were not observed. Because the tumor was characterized as a fibro-osseous lesion with abundant cartilage nodules, the possibility of low-grade osteosarcoma, chondrosarcoma, and fibrocartilaginous dysplasia (FCD), a variant of FD, were considered. Immunohistochemical stains for murine double minute 2 (MDM2) and cyclin-dependent kinase 4 (CDK4) were negative in the spindle cells, excluding the possibility of low-grade osteosarcoma. Chondrosarcoma was unlikely because the cartilage islands were composed of benign chondrocytes without atypia, as described earlier. In addition, the lesion showed well-formed bone trabeculae and did not feature the characteristic, irregular, curvilinear trabeculae of woven bone without the osteoblastic rimming of FD or FCD. Epiphyseal growth plate-like enchondral ossification was another distinguishing feature, distinguishing it from FCD. A final diagnosis of FM was rendered based on the overall histologic findings. The patient was regularly followed every 3 months and is doing well 1 year after resection.

## DISCUSSION

A rare neoplasm, FM was initially described as “a fibrocartilaginous mesenchymoma with low-grade malignancy” in 1984 by Dahlin et al. [1], who found unique lesions originally diagnosed as FCD but with different clinical, radiographic, and morphologic features. Since then, there have been debates in the literature regarding FM as a separate neoplasm or one that coincides with FCD [5-7]. However, several studies, particular-

ly molecular analyses, have demonstrated that FM is not genetically related to FCD, which has a characteristic *GNAS* (guanine nucleotide-binding protein  $\alpha$ -stimulating polypeptide) mutation [2]. Accordingly, the 5th edition of the World Health Organization classification of bone tumors newly listed FM as an independent tumor entity [8].

FM predominantly affects long bones, including the femur, tibia, and humerus; a few cases have been reported in rare locations, such as metatarsus, iliac–pubic bones, vertebrae, and ribs [2]. FM tends to affect young patients aged 3 months to 27 years (median age of 13 years), with a slight predominance of male patients. Radiologically, FM appears as an expansile osteolytic lesion with cartilaginous calcification and cortical destruction, and extension to soft tissue is not uncommon.

Histologically, FM is characterized by spindle cell proliferation in association with bland cartilage nodules and epiphyseal growth plate-like enchondral ossification. The morphology of spindle cells varies with respect to cellularity, nuclear pleomorphism, and mitotic figures, but it usually mimics low-grade spindle cell sarcoma. The occasional presence of multinucleated giant cells can be observed. Pathologic diagnosis can be challenging, particularly in small biopsies in which various fibro-osseous lesions with new bone formation must be considered.

The differential diagnoses include FCD, low-grade osteosarcoma, dedifferentiated chondrosarcoma, desmoplastic fibroma, and chondromesenchymal hamartoma of the chest wall when the tumor occurs in the ribs, as in the current case. FCD is a variant of FD and contains nodules of benign hyaline cartilage. Rare cases of FCD demonstrate enchondral ossification as in FM; however, FCD principally consists of bland spindle cells and characteristic, irregular, curvilinear trabeculae of woven bone, lacking osteoblastic rimming. Furthermore, *GNAS* mutations are detected in many cases of FCD, whereas no specific molecular aberrations have been found in FM [2]. Although the *GNAS* mutation was not tested in the present case, differentiation from FCD was not difficult due to the tumor’s overall histological characteristics. Finally, in contrast to FCD, FM is characterized clinically by a high propensity for local recurrence. The presence of epiphyseal plate-like cartilage is used to differentiate FM from desmoplastic fibroma and low-grade osteosarcoma. A molecular test for *MDM2* amplification can be helpful to differentiate low-grade osteosarcoma from FM. Dedifferentiated chondrosarcoma is characterized by a low-grade cartilaginous tumor juxtaposed with a high-grade sarcoma. Cartilaginous nodules in dedifferentiated chondrosarcoma do not feature the epiphyseal growth plate-like appearance characteristic of FM. Moreover, dediffer-



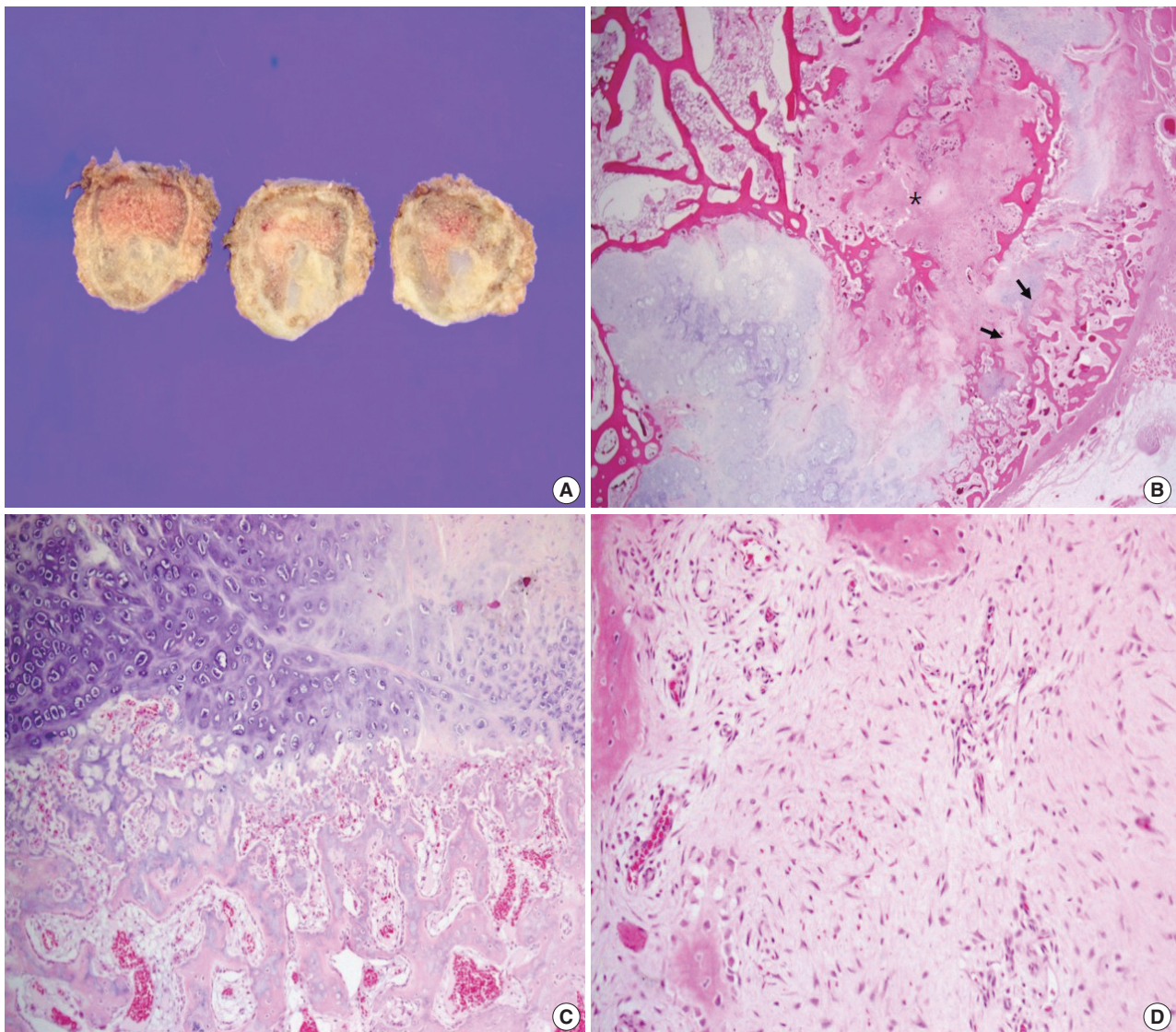


**Fig. 2.** Histologic findings. (A) Gross examination reveals an ill-defined, eccentrically-located, hard mass with multifocal glistening bluish grey nodules corresponding to cartilage tissue. The cortex had been partially destroyed. (B) The tumor consists of multiple cartilage islands with a fibrocollagenous area (asterisk) and well-formed new bone trabeculae (arrows). (C) Epiphyseal plate-like enchondral ossification is observed at the periphery of the cytologically bland cartilage nodules. (D) A hypocellular fibrocollagenous lesion consisting of spindle and stellate cells without nuclear pleomorphism or mitosis is noted. Reactive woven bone formation with osteoblastic rimming is observed.

entiated chondrosarcoma always shows high-grade sarcoma, whereas the spindle cells in FM commonly have a benign appearance. Chondromesenchymal hamartoma of the chest wall is histologically similar to FM in terms of a varying admixture of spindle cells, cartilage, and foci of epiphyseal growth plate-like enchondral ossification. However, chondromesenchymal hamartoma of the chest wall is a tumor of early infancy and occurs only in the rib; moreover, it has a prominent, aneurysmal, bone cyst-like appearance that is not a feature of FM.

FM is a locally aggressive tumor with no distant metastasis reported thus far. Local recurrence occurs only in cases of incom-

plete removal, such as curettage or intralesional excision. Complete surgical excision with adequate margins is the treatment of choice for FM.

FM is a rare bone tumor that affects young patients and has a propensity for long tubular bones. We report a case of FM with an unusual location in the rib, which was successfully treated by en bloc resection. In cases of bone tumors that show characteristic histologic features of bland spindle cells, benign cartilage nodules, and epiphyseal plate-like enchondral ossification, physicians should consider the possibility of FM. Finally, FM is locally aggressive, so marginal resection or close follow-up for incomplete

removal is required.

### Ethics Statement

This study was approved by the institutional review board (IRB) of Kosin University Gospel Hospital with a waiver of informed consent (IRB No. 2019-07-037).

### ORCID

Sun-Ju Oh <https://orcid.org/0000-0001-6013-8579>

### Conflicts of Interest

The authors declare that they have no potential conflicts of interest.

### Funding Statement

No funding to declare.

### References

1. Dahlin DC, Bertoni F, Beabout JW, Campanacci M. Fibrocartilaginous mesenchymoma with low-grade malignancy. *Skeletal Radiol* 1984; 12: 263-9.
2. Gambarotti M, Righi A, Vanel D, et al. Fibrocartilaginous mesenchymoma of bone: a single-institution experience with molecular investigations and a review of the literature. *Histopathology* 2017; 71: 134-42.
3. Saito T, Motoi T, Suehara Y, et al. Fibrocartilaginous mesenchymoma of the tibia with predominant microcystic features: a case report and literature review. *Hum Pathol Case Rep* 2019;16:100288.
4. Bulychova IV, Unni KK, Bertoni F, Beabout JW. Fibrocartilaginous mesenchymoma of bone. *Am J Surg Pathol* 1993; 17: 830-6.
5. Czerniak B. Dorfman and Czerniak's bone tumors. 2nd ed. Philadelphia: Elsevier Saunders, 2016; 606-14.
6. Bhaduri A, Deshpande RB. Fibrocartilaginous mesenchymoma versus fibrocartilagenous dysplasia: are these a single entity? *Am J Surg Pathol* 1995; 19: 1447-8.
7. Lin J, Shulman SC, Steelman CK, et al. Fibrocartilaginous mesenchymoma, a unique osseous lesion: case report with review of the literature. *Skeletal Radiol* 2011; 40: 1495-9.
8. Fletcher CD. WHO classification of tumours of soft tissue and bone tumours. 5th ed. Lyon: IARC Press, 2020; 470-1.

## ***EGFR*-mutated pulmonary adenocarcinoma with concurrent *PIK3CA* mutation, and with acquired *RET* fusion and *EGFR* T790M mutation after afatinib therapy**

Minhye Kim<sup>1</sup>, Ji Min Na<sup>1</sup>, Gyeong-Won Lee<sup>2</sup>, Seung Jun Lee<sup>3</sup>, Jong Duk Kim<sup>4</sup>, Jung Wook Yang<sup>5</sup>

<sup>1</sup>Department of Pathology, Gyeongsang National University Hospital, Jinju;

<sup>2</sup>Division of Hematology-Oncology, Department of Internal Medicine,

<sup>3</sup>Division of Pulmonology and Allergy, Department of Internal Medicine, Gyeongsang National University Hospital, Gyeongsang National University College of Medicine, Jinju;

<sup>4</sup>Department of Cardiothoracic Surgery, Gyeongsang National University Hospital, Jinju;

<sup>5</sup>Department of Pathology, Gyeongsang National University Hospital, Gyeongsang National University College of Medicine, Jinju, Korea

Generally, receptor tyrosine kinase (*RTK*) fusions are mutually exclusive of epidermal growth factor receptor (*EGFR*) mutations in non-small cell lung cancer (NSCLC). However, *RTK* fusions have recently emerged as mechanisms of actionable resistance to *EGFR*–tyrosine kinase inhibitors (TKIs) in *EGFR*-mutated NSCLC [1]. More than half of the acquired *RET* fusions following *EGFR*-TKI therapy occur in response to osimertinib (third-generation) treatment. To the best of our knowledge, only one case of NSCLC with acquired *RET* fusion following afatinib (second-generation) therapy has been reported in the English literature. Phosphatidylinositol-4,5-bisphosphate 3-kinase catalytic subunit alpha (*PIK3CA*) mutations are found infrequently (approximately 7%) in pulmonary adenocarcinoma [2]. Although other oncogenic driver mutations in NSCLC are mutually exclusive, *PIK3CA* mutations frequently coexist with other mutations [2,3]. Here, we report a rare case of *EGFR*-mutated pulmonary adenocarcinoma with concurrent *PIK3CA* mutation, displaying acquired *RET* fusion and *EGFR* T790M mutation following afatinib therapy.

### **CASE REPORT**

A 64-year-old man without a known underlying disease was

transferred with dyspnea and pleural effusion. He was a smoker with a 30 pack-year history. The clinical course is shown in Fig. 1. The cytological examination of the pleural fluid confirmed the diagnosis as metastatic adenocarcinoma of the lung (Fig. 1A). Chest computed tomography (CT) (Fig. 2A) suggested lung malignancy with pleural and lymph node metastases. Positron emission tomography showed a 3-cm-sized hypermetabolic mass in the right upper lobe of the lung. CT-guided needle biopsy was performed on the mass in the right upper lobe, and adenocarcinoma was diagnosed (Fig. 1B). The *EGFR* mutation status was tested using real-time polymerase chain reaction clamping method on the pleural fluid and our results revealed exon 19 deletion. The patient received afatinib treatment, and as a result, the size of the lung mass and amount of pleural fluid were found to be decreased on chest CT after 3 months (Fig. 2B). However, the disease was stable for 6 months, and next-generation sequencing (NGS) was performed on the previous needle biopsy specimen of the lung on an Ion Torrent S5 sequencer (Thermo Fisher Scientific, Waltham, MA, USA) using a commercially available targeted gene panel (Oncomine Comprehensive Assay v3, Thermo Fisher Scientific). The NGS results showed exon 19 deletion of *EGFR* and *PIK3CA* G118D mutation. The disease progressed in 7.5 months (Fig. 2C) and afatinib had to be discontinued. Video-assisted thoracoscopic wedge resection was performed on the right upper lobe of the lung, and the status of the *EGFR* mutation was re-evaluated. Microscopic examination of the specimen showed tumor heterogeneity with solid and cribriform components (Fig. 1C), and acinar and papillary components (Fig. 1D). A second *EGFR* mutation test showed T790M

Received: September 1, 2020 Revised: October 21, 2020

Accepted: November 2, 2020

Corresponding Author: Jung Wook Yang, MD, PhD

Department of Pathology, Gyeongsang National University Hospital, Gyeongsang National University College of Medicine, 79 Gangnam-ro, Jinju 52727, Korea  
Tel: +82-55-772-8065, Fax: +82-55-759-7952, E-mail: woogi1982@gmail.com



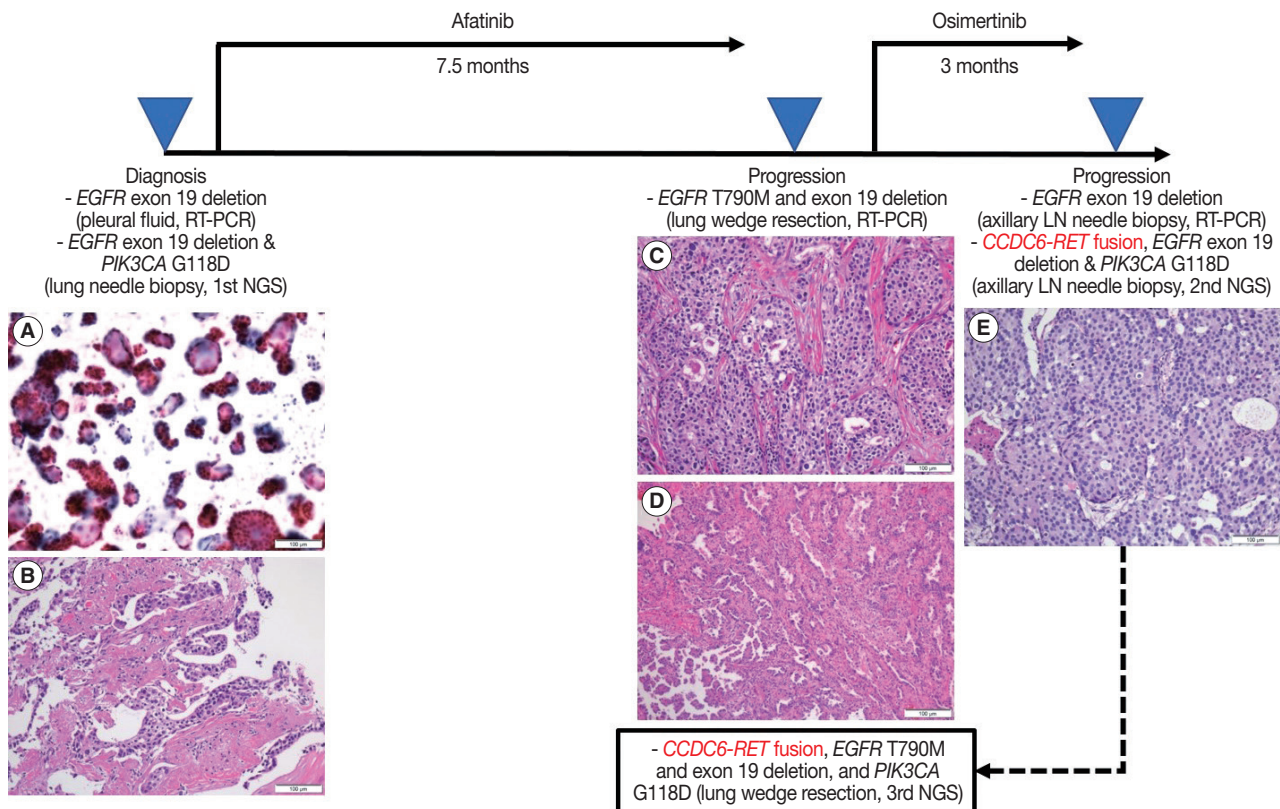


**Fig. 1.** Clinical course and pathological diagnosis of the patient. Adenocarcinoma was diagnosed using pleural fluid (A), and lung needle biopsy (B). Lung wedge resection specimen showed tumor heterogeneity; solid and cribriform components (C), and acinar and papillary components (D). (E) Metastatic adenocarcinoma was observed in the axillary LN. *EGFR*, epidermal growth factor receptor; *PIK3CA*, phosphatidylinositol-4,5-bisphosphate 3-kinase catalytic subunit alpha; NGS, next-generation sequencing; RT-PCR, reverse transcription; LN, lymph node.

mutation and exon 19 deletion. The patient was prescribed with osimertinib, but the disease progressed in 3 months (Fig. 2D). Needle biopsy of the right axillary lymph node was performed for further molecular evaluation of the cancer. Metastatic adenocarcinoma with a solid and cribriform pattern was observed in the lymph node (Fig. 1E). The third *EGFR* mutation test showed exon 19 deletion but not T790M mutation. The second NGS test on axillary lymph node specimens revealed a new *CCDC6-RET* fusion in addition to exon 19 deletion of *EGFR* and *PIK3CA* G118D mutation. Additionally, a third NGS test was performed on the wedge resection specimen (second biopsy), which showed *CCDC6-RET* fusion with T790M mutation and exon 19 deletion of *EGFR* and *PIK3CA* G118D.

## DISCUSSION

Viola et al. analyzed 86 cases of *RTK* fusions as acquired resistance in *EGFR*-mutated NSCLC [1]. The acquired *RTK* fusions occurred most frequently (57%) after the third generation *EGFR*-TKI therapy (first, 24%; second, 12%). The most fre-

quently reported acquired *RTK* fusion in *EGFR*-TKI-resistant NSCLC was *RET* fusion, whereas *CCDC6-RET* fusion was the most common variant. Combined *EGFR* and *RET* inhibition with osimertinib and BLU-667 may be an effective therapeutic strategy in *EGFR*-TKI-resistant NSCLC with acquired *RTK* fusion [4]. The concurrent *PIK3CA* mutation is a known poor prognostic and predictive marker for *EGFR*-TKI therapy in pulmonary adenocarcinomas [2]. *CCDC6-RET* fusion and *PIK3CA* G118D mutation are not the most common variants in NSCLC with a single oncogenic driver mutation [1,5,6].

In this case, considering the third NGS result, the *CCDC6-RET* fusion probably occurred with *EGFR* T790M mutation after afatinib treatment. In lung wedge specimens resected after afatinib treatment, we observed tumor heterogeneity (Fig. 1C, D). We could not confirm which tumor population had *CCDC6-RET* fusion or *EGFR* T790M mutation or both. Considering morphological features (Fig. 1C, E), we assumed that tumor population with solid and cribriform patterns (Fig. 1C) had *CCDC6-RET* fusion.

In conclusion, we report a rare case of *EGFR*-mutated pul-

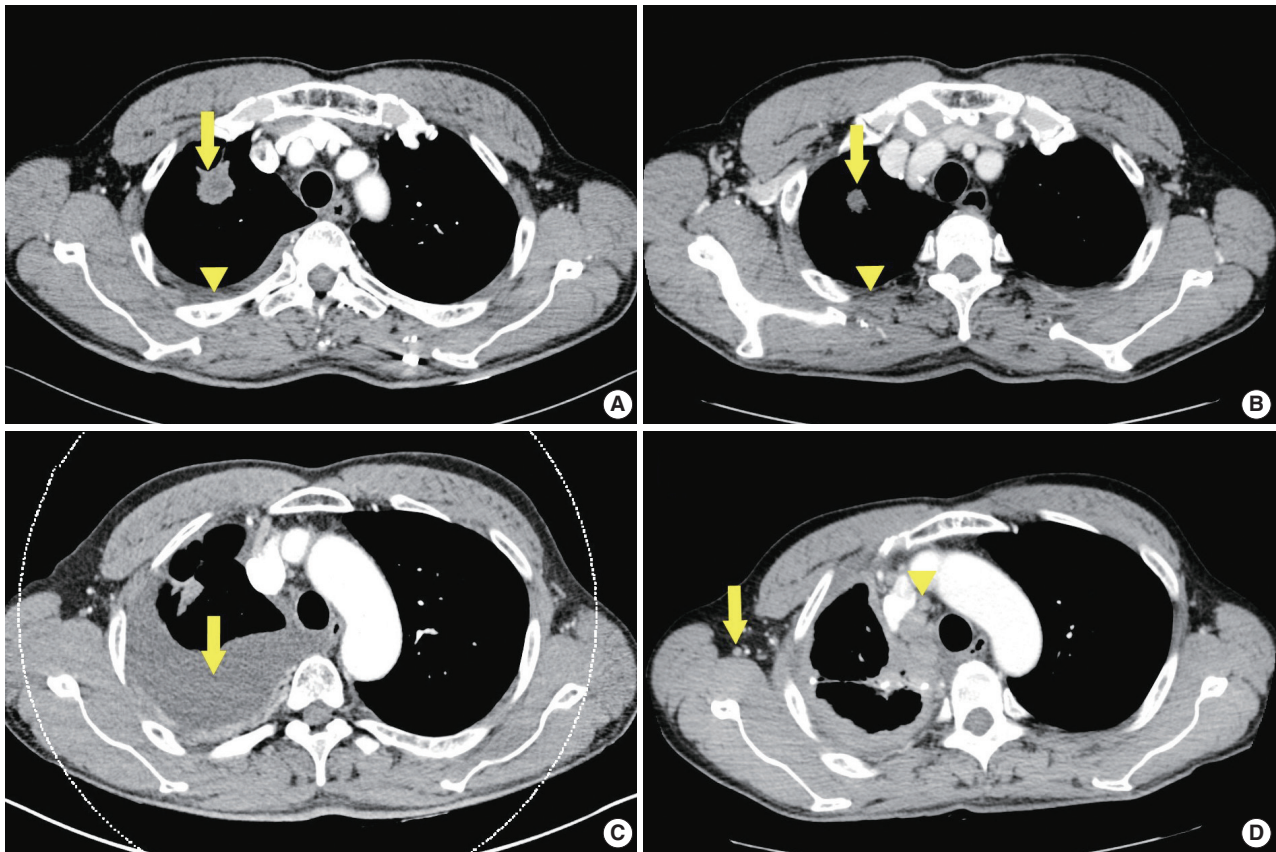


**Fig. 2.** Chest computed tomography. (A) Lung mass (arrow) in right upper lobe with pleural fluid (arrowhead) at diagnosis. (B) Decreased size of lung mass (arrow) and amount of pleural fluid (arrowhead) after 3 months of afatinib therapy. (C) Increased amount of pleural fluid (arrow) after 7.5 months with afatinib therapy. (D) Increased size of axillary (arrow) and mediastinal (arrowhead) lymph nodes after 3 months with osimertinib therapy.

monary adenocarcinoma with concurrent *PIK3CA* mutation, and acquired *RET* fusion and *EGFR* T790M mutation after *EGFR*-TKI therapy. Since NSCLC has a number of well-known oncogenic driver mutations, we believe that NGS is currently one of the best methods to determine the treatment of NSCLC, especially adenocarcinoma.

#### Ethics Statement

This study was approved by the Institutional Review Board of Gyeongsang National University Hospital, and informed consent was waived (IRB No. GNUH 2020-08-005).

#### ORCID

Minhye Kim <https://orcid.org/0000-0002-8631-5104>  
 Ji Min Na <https://orcid.org/0000-0003-4330-6598>  
 Gyeong-Won Lee <https://orcid.org/0000-0002-1781-2262>  
 Seung Jun Lee <https://orcid.org/0000-0002-1849-5086>  
 Jong Duk Kim <https://orcid.org/0000-0003-0268-1674>  
 Jung Wook Yang <https://orcid.org/0000-0002-9698-3667>

#### Author Contributions

Conceptualization: JWY. Data Curation: MK, JWY. Investigation: MK, JMN, JWY. Resources: GWL, SJL, JDK. Supervision: JWY. Visualization: MK, JWY. Writing—original draft preparation: MK, JWY. Writing—review and editing: MK, JWY. Approval of final manuscript: all authors.

#### Conflicts of Interest

The authors declare that they have no potential conflicts of interest.

#### Funding Statement

No funding to declare.

#### References

1. Zhu VW, Klempner SJ, Ou SI. Receptor tyrosine kinase fusions as an actionable resistance mechanism to EGFR TKIs in *EGFR*-mutant non-small-cell lung cancer. *Trends Cancer* 2019; 5: 677-92.
2. Eng J, Woo KM, Sima CS, et al. Impact of concurrent *PIK3CA* mutations on response to EGFR tyrosine kinase inhibition in *EGFR*-mutant lung cancers and on prognosis in oncogene-driven lung adenocarcinomas. *J Thorac Oncol* 2015; 10: 1713-9.
3. Wang L, Hu H, Pan Y, et al. *PIK3CA* mutations frequently coexist with *EGFR/KRAS* mutations in non-small cell lung cancer and sug-

- gest poor prognosis in *EGFR/KRAS* wildtype subgroup. PLoS One 2014; 9: e88291.
4. Piotrowska Z, Isozaki H, Lennerz JK, et al. Landscape of acquired resistance to osimertinib in *EGFR*-mutant NSCLC and clinical validation of combined *EGFR* and *RET* inhibition with osimertinib and BLU-667 for acquired *RET* fusion. Cancer Discov 2018; 8: 1529-39.
  5. Scheffler M, Bos M, Gardizi M, et al. *PIK3CA* mutations in non-small cell lung cancer (NSCLC): genetic heterogeneity, prognostic impact and incidence of prior malignancies. Oncotarget 2015; 6: 1315-26.
  6. Ahn JW, Kim HS, Yoon JK, et al. Identification of somatic mutations in *EGFR/KRAS/ALK*-negative lung adenocarcinoma in never-smokers. Genome Med 2014; 6: 18.



